RWTH Aachen University

Institute of Jet Propulsion and Turbomachinery

DLR - German Aerospace Center

Institute of Space Propulsion

Optimization of a Reusable Launch Vehicle using Genetic Algorithms

A thesis submitted for the degree of

M.Sc. Aerospace Engineering

by

Simon Jentzsch

June 20, 2020

Advisor:	Felix Wrede, M.Sc.
External Advisors:	Kai Dresia, M.Sc.
	Dr. Günther Waxenegger-Wilfing
Examiner:	Prof. Dr. Michael Oschwald

Statutory Declaration in Lieu of an Oath

I hereby declare in lieu of an oath that I have completed the present Master thesis entitled *'Optimization of a Reusable Launch Vehicle using Genetic Algorithms'* independently and without illegitimate assistance from third parties. I have used no other than the specified sources and aids. In case that the thesis is additionally submitted in an electronic format, I declare that the written and electronic versions are fully identical. The thesis has not been submitted to any examination body in this, or similar, form.

City, Date, Signature

Abstract

SpaceX has demonstrated that reusing the first stage of a rocket implies a significant cost reduction potential. In order to maximize cost savings, the identification of optimum rocket configurations is of paramount importance. Yet, the complexity of launch systems, which is further increased by the requirement of a vertical landing reusable first stage, impedes the prediction of launch vehicle characteristics.
Therefore, in this thesis, a multidisciplinary system design optimization approach is applied to develop an optimization platform which is able to model a reusable launch vehicle with a large variety of variables and to optimize it according to a predefined launch mission and optimization objective. An integration of NASA's CEA program, detailed mass estimations as well as reverse engineering of Falcon 9's retropropulsive landing first stage are used to virtually build launch vehicles for a given set of rocket parameters, payload mass and target orbit. Due to the enormous amount of possible parameter combinations, a genetic algorithm is applied to identify optimized launch vehicle configurations fast and accurately.
Validating the model with Falcon 9 as reference vehicle demonstrated the ability of the optimizer to predict the gross lift-off weight of a rocket with a maximum deviation of 3.6%. Extensive testing of the optimization program showcased its vast potential in rocket design and indicated that methane is a viable rocket fuel alternative for future launch vehicles.

Contents

List of Figures

List of Tables

List of Acronyms

ACS	Attitude Control System
BC	Ballistic Coefficient
CEA	Chemical Equilibrium with Applications
CFD	Computational Fluid Dynamics
DEAP	Distributed Evolutionary Algorithms in Python
DLR	Deutsches Zentrum für Luft- und Raumfahrt e. V.
GA	Genetic Algorithm
GEO	Geostationary Orbit
GLOW	Gross Lift-Off Weight
GTO	Geostationary Transfer Orbit
ISS	International Space Station
LCH4	Liquid Methane
LEO	Low Earth Orbit
LH2	Liquid Hydrogen
LOX	Liquid Oxygen
MECO	Main Engine Cut-Off
MEO	Medium Earth Orbit
MMH	Monomethylhydrazine
NASA	National Aeronautics and Space Administration
NTO	Dinitrogen Tetroxide
ROF	Mixture Ratio

RP-1	Rocket Propellant-1
SI	Structural Index
SSME	Space Shuttle Main Engine
SSO	Sun Synchronous Orbit
SSTO	Single-Stage-To-Orbit
TSTO	Two-Stage-To-Orbit
TVC	Thrust Vector Control

Chapter 1

Introduction

With the success of SpaceX's partially reusable Falcon 9 rocket, the international market of launch services gained a promising competitor to the traditional expendable launch vehicles. Refurbishing and reusing the rocket's first stage after landing it by means of retropropulsion allows SpaceX to offer their service at a significantly lower price than other launch service providers. Because of private companies, e.g. SpaceX and Blue Origin, disrupting the market, reducing costs became the driving design factor in today's space transport economy. This led to rocket reusability once again being discussed in Europe.

With this paradigm shift from building high-performance expendable launch vehicles to low-cost reusable rockets, the choice of propellants also needs to be reevaluated. Due to its thermodynamic properties and availability, cryogenic liquid methane (LCH4) is promising to be a more economical fuel alternative to the widely used cryogenic liquid hydrogen (LH2) and kerosene (e.g. RP-1). While the six times higher density and 90 K higher evaporation temperature of LCH4 facilitate a simpler and more compact launch vehicle as well as propulsion system design in comparison with LH2, its higher specific impulse (I_{sp}), preferable coking temperature limits and cooling characteristics offer advantages in performance, regenerative engine cooling and reusability in contrast to RP-1. However, as of yet no operational launch vehicle using LCH4 has been built, which is why its impact on the overall launch vehicle configuration needs to be assessed to enable a comparison with other propellants on launch system level.

1.1 Motivation

Finding the optimal design of a launch vehicle is challenging because of the inherent complexity of the launch system which comprises multiple interconnected subsystems. For a particular mission, various rocket parameters need to be optimized. Trade-off studies are used to determine, for example, the number of stages in the

vehicle, their dimensions, the number of engines in each stage, the utilized engine cycle, propellant combination and mixture ratio as well as combustion chamber pressure and nozzle area expansion ratio. The optimum configuration depends on the mission and the optimization objective, i.e. highest performance, highest reliability or lowest cost. Especially the rocket propulsion system features various design parameters that determine the characteristics of the launch vehicle, which is why considerable time and effort are spent in evaluation and development of suitable methods for quantitative comparison when selecting the propulsion system for a new multiyear high-cost project [15].

The requirement of a vertical landing reusable first stage increases the complexity and the interdependencies between the subsystems furthermore. To find the optimum delta-v and therefore propellant mass allocation onto the stages, tools such as the Lagrange multiplier and Newton-Raphson method are usually used for expendable launch vehicles. However, part of the first stage propellant mass is reserved for the landing maneuvers and greatly depends on the staging configuration, hence traditional optimization methods cannot be applied.

In order to overcome this intricacy, a multidisciplinary system design optimization approach is necessary [9]. Therefore, the first objective of this thesis is to develop an optimization platform which is able to model a reusable launch vehicle with a large variety of variables and to optimize it according to a particular launch mission and optimization objective. An optimization program for expendable launch vehicles that was developed in the scope of a prior thesis is used as a basis to build upon [12]. An integration of NASA's Chemical Equilibrium with Applications (CEA) program is used to obtain generic engine performance data, which are compared to currently operational and historical engines for validation. Furthermore, a trajectory simulation is implemented to account for the changing I_{sp} of the engines during ascent. Reverse engineering of the Falcon 9 vehicle enables the propellant mass calculation for the landing maneuvers. Detailed mass estimations for all subsystems facilitate the realistic modelling of the launch vehicle. As the multiplicity of rocket parameters results in an enormous amount of possible combinations, a suitable algorithm to navigate the search space is necessary. Here, genetic algorithms (GAs) have proven to be a robust method for estimating a series of unknown parameters within a model of a physical system in an optimization problem [10]. In this work, the Distributed Evolutionary Algorithms in Python (DEAP) computation framework is used and adapted to the problem at hand. The GA generates random parameter combinations, each representing a potential launch vehicle, and mimics natural selection and natural genetics to identify optimized launch vehicle solutions. To limit computation time, sensible parameter boundaries are implemented. The possibility of fixing parameters allows the investigation of particular parameter sets in the optimization program.

The second focus of this work is the application of the optimization program to study the influence of propellant combination, staging configuration and high-level rocket engine parameters on the performance of a two-stage-to-orbit (TSTO)

launch vehicle with reusable vertical landing first stage for various mission configurations. The rocket's gross lift-off weight (GLOW) is used as the parameter to be minimized by the GA, as without implementing cost functions the preliminary goal is to find the parameter set that represents the lightest launch vehicle. In general, heavier launchers entail higher costs, which is why a weight optimization indirectly leads to a cost optimization. The main emphasis is laid on the comparison of the two currently most used liquid rocket fuels, hydrogen and kerosene, with methane, which is increasingly being researched and promises properties that improve the engine's reusability. As reusable launch vehicles are the topic of multiple current research studies, the results of the XTRAS [19], AKIRA [20], ENTRAIN [22] and RETALT [23] studies are compared to the output of the optimization program. Various sensitivity analyses reveal the influences of the I_{sp}, delta-v budget and the structural efficiency on the launch vehicle performance and thus indicate the robustness of the optimized launch vehicle solutions. Using the structure mass of a launch vehicle as a cost measure, the application of the total structure mass as well as the expendable mass as alternative optimization objectives reveals the influence of different reuse-cases on launch vehicle design.

1.2 Structure of this Thesis

In this thesis, genetic algorithms are used to develop an optimization program for reusable launch vehicles. At first, chapter 2 deals with the fundamental tools for rocket performance and mission requirement calculation. In addition, rocket propulsion systems and their characteristics, engine performance parameter calculation, as well as the concept of rocket staging and its optimization are described in detail. Furthermore, suitable mass estimations for each launch vehicle subsystem are given and the functional principle of genetic algorithms is explained. Next, chapter 3 outlines the implementation of the aforementioned into the optimization program, depicts its workflow and identifies necessary input parameters. Subsequently, the launch vehicle model in the optimizer is validated with SpaceX's Falcon 9 as reference vehicle in chapter 4. In order to obtain the optimum settings of the genetic algorithm for the following calculations, a hyperparameter tuning is conducted in chapter 5. Afterwards, chapter 6 presents an extensive comparison of optimized launch vehicles with regard to their propellant combination and staging configuration. Moreover, assumptions of various current launch vehicle research studies are applied to compare the results and multiple sensitivity analyses are performed to examine different influences on launch vehicle performance. At the end, the use of alternative optimization objectives is explored. Chapter 7 concludes this thesis and gives an outlook on future work.

Chapter 2

Theoretical Background

This chapter deals with the theoretical background applied to the software that was developed in the course of this thesis. It encompasses the basics of rocket propulsion, the optimization of launch vehicle configurations as well as mass estimations for important subsystems. Furthermore, genetic algorithms and their use in launch vehicle optimization are presented.

2.1 Basic Rocket Equations and Definitions

The following section briefly describes the equations and definitions necessary to understand the basics of rocket design and performance calculation.

2.1.1 Tsiolkovsky Rocket Equation

Named after Russian scientist Konstantin Tsiolkovsky who derived it in 1903, the Tsiolkovsky equation describes the motion of vehicles that generate thrust by ejecting part of their mass at high velocity and thus accelerate due to the conservation of linear momentum. Assuming a constant effective exhaust velocity c_e and no other forces, such as aerodynamic or gravitational forces, acting upon the rocket, the Tsiolkovsky rocket equation is given as:

$$\Delta v = c_e \cdot ln\left(\frac{m_0}{m_f}\right) \tag{2.1}$$

where Δv is delta-v, the maximum attainable flight velocity increment of the vehicle, m_0 the initial mass of the rocket before the launch and m_f the final mass at burnout. Even though the delta-v is measured in meters per second, it is not equivalent to the physical change of velocity as this is only the case in a gravity-free vacuum and acceleration in direction of the velocity vector. Retropropulsion leads to a

decrease in velocity but an increase in delta-v. It is an important measure as it allows comparison of one propulsion system or launch vehicle with another as well as one flight mission with another and it can show the impact of upgrades and design improvements on the overall system performance [15].

2.1.2 Thrust and Specific Impulse

The thrust produced by a rocket propulsion system acting upon the vehicle consists of the momentum thrust term and the pressure thrust term and it is given as [15]:

$$F = \dot{m} \cdot u_e + (p_e - p_a) \cdot A_e \tag{2.2}$$

where F is the thrust, $\dot{m}$ the propellant mass flow, u_e its exhaust velocity relative to the vehicle, A_e the cross-sectional area at the nozzle exit, p_e the exhaust gas pressure at the nozzle exit and p_a the ambient fluid pressure [15].

To maximize thrust, the exhaust gas velocity at the nozzle exit u_e needs to be maximized. According to [15] it can be calculated as follows:

$$u_e = \sqrt{\frac{2\gamma}{\gamma - 1} \frac{RT_0}{M} \left(1 - \left(\frac{p_e}{p_0}\right)^{\frac{\gamma-1}{\gamma}}\right)} \tag{2.3}$$

where γ is the heat capacity ratio, R the universal gas constant, T_0 the total temperature inside the combustion chamber, M the average molar mass, p_e the pressure at the exit of the nozzle and p_0 the pressure inside the combustion chamber. Maximizing the exhaust velocity u_e requires maximization of T_0, minimization of M and minimization of the pressure ratio p_e/p_0.

Dividing the thrust by the propellant mass flow yields the effective exhaust velocity c_e used in the Tsiolkovsky equation (Eq. 2.1):

$$c_e = \frac{F}{\dot{m}} = u_e + \frac{(p_e - p_a) \cdot A_e}{\dot{m}} \tag{2.4}$$

According to the Tsiolkovsky equation, the effective exhaust velocity and the propellant mass fraction of the initial mass determine the possible velocity gain and hence the performance of the rocket. Therefore, the efficiency with which propellant mass is converted into thrust is the key indicator for the performance of the rocket engine and propellant combination [3]. Dividing the effective exhaust velocity by standard gravity g_0 yields the specific impulse I_{sp} as the key measure for the efficiency of the propulsion system. It is defined as the thrust per sea-level weight rate (per second) of propellant consumption. The unit of the specific impulse is seconds [7].

$$I_{sp} = \frac{c_e}{g_0} = \frac{F}{\dot{m} \cdot g_0} \tag{2.5}$$

For the same amount of thrust or delta-v, an engine with a higher I_{sp} consumes less propellant than an engine with a lower I_{sp}. Using Eq. 2.5 the Tsiolkovsky equation (Eq. 2.1) can be rewritten as follows:

$$\Delta v = I_{sp} \cdot g_0 \cdot ln\left(\frac{m_0}{m_f}\right) \tag{2.6}$$

2.1.3 Orbits

Depending on the objective of the mission, the payload that is transported by the launch vehicle is placed into a certain orbit or onto an interplanetary trajectory. In most cases the payload consists of a satellite, whose purpose determines its target orbit altitude. Below, an incomplete variety of potential orbits is presented.

LEO
Objects in low earth orbit (LEO) circle earth at an altitude of 200-1000 km. Because of its proximity to earth's surface, this orbit is commonly used by earth observation satellites as well as space stations, such as the ISS. To stay in orbit, objects need to travel at a speed of around 7.8 km/s. It is the most used of all orbits [1].

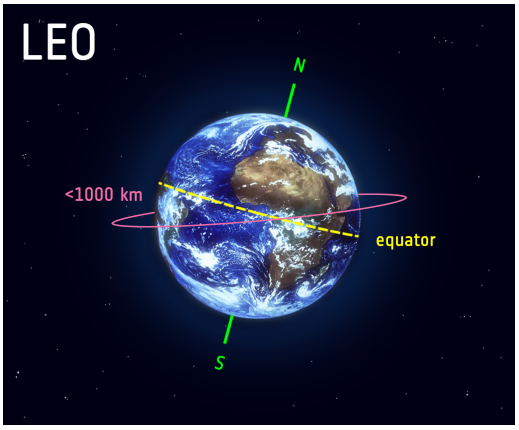

Figure 2.1: Low Earth Orbit [1]

MEO
Medium earth orbits (MEO) comprise a large range of orbits with altitudes between LEO and GEO. It is similar to LEO in that it allows for different orbit inclinations and does not dictate a specific path around earth. It is often used by navigation satellites, like the European Galileo system (see Figure 2.2) [1].

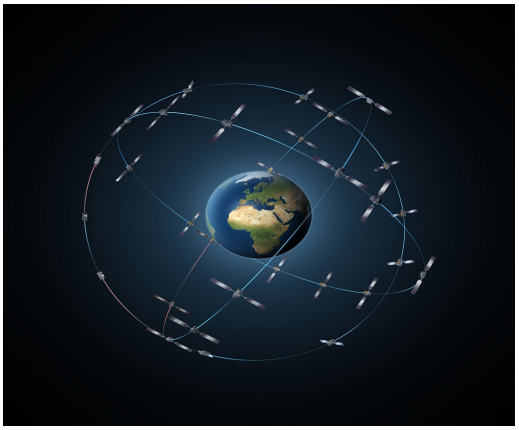

Figure 2.2: Medium Earth Orbit [1]

GEO
Satellites in geostationary orbit (GEO) circle earth in the equatorial plane at an altitude of 35786 km with a velocity of around 3 km/s to match earth's rotation. This makes them appear to be stationary over a fixed position on earth's surface. Satellites in GEO are typically telecommunication satellites. The inclination of a GEO needs to be 0° [1].

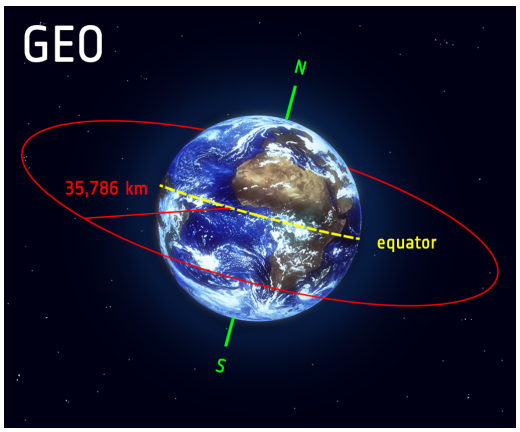

Figure 2.3: Geostationary Orbit [1]

GTO
The geostationary transfer orbit (GTO) is a highly eccentric orbit in which payload is placed whose target orbit is a GEO. GTOs have a perigee (point closest to earth) of 200 km and an apogee (point farthest away from earth) of 35786 km. When the satellite reaches the apogee it needs to fire its engines to rise the perigee and reach the GEO [1].

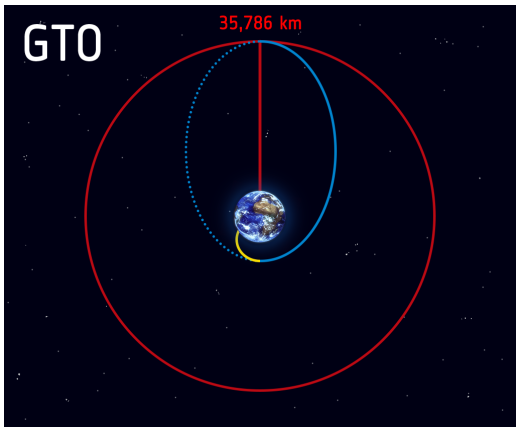

Figure 2.4: Geost. Transfer Orbit [1]

SSO
Sun synchronous orbits (SSO) are a type of LEO with inclinations greater than 95°. Due to earth not being a perfect sphere and the resulting deviation of its gravitational field, the plane of a SSO rotates. A rotation of 360° per year can be achieved resulting in the satellite passing a certain point on earth always at the same time of day. SSOs are predominantly used by weather and earth observation satellites [1].

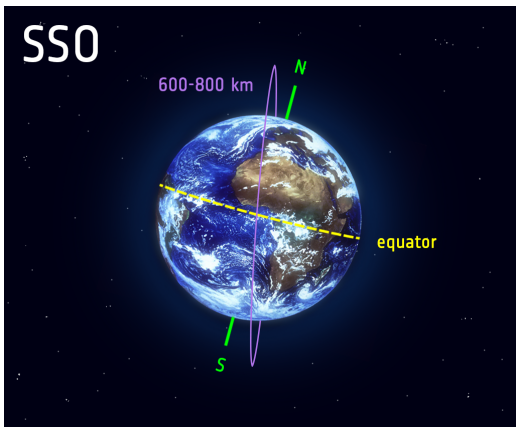

Figure 2.5: Sun Synchronous Orbit [1]

2.1.4 Delta-v Budget Calculation

After choosing the target orbit, the mission's delta-v budget can be calculated. The delta-v budget or mission velocity is the sum of all flight velocity increments needed to accomplish the mission objective and it is a convenient way to describe the magnitude of the energy requirement of the space mission [15].

Energy Budget
The total energy required to put an object from earth's surface into orbit consists of its kinetic energy in orbit as well as the potential energy that is needed to move the object in earth's gravitational field from its position on the surface to its orbital altitude (Eq. 2.7).

$$\Delta E_{tot} = \Delta E_{kin} + \Delta E_{pot} \tag{2.7}$$

The ideal velocity increment or delta-v equivalent to ΔE_{tot} is calculated as follows:

$$\Delta v_{id} = \sqrt{\Delta v_o^2 + \Delta v_g^2} \tag{2.8}$$

where Δv_o represents the orbital velocity of the object and Δv_g the velocity equivalent to the required potential energy. Δv_o can be calculated using the vis-viva equation, which links local velocity and current position of an object in an elliptical Keplerian orbit around a dominating celestial body (Eq. 2.9) [15]:

$$\Delta v_o = \sqrt{2\mu \left(\frac{1}{r} - \frac{1}{2a} \right)} \tag{2.9}$$

with μ being the standard gravitational parameter, which is the product of the gravitational constant γ and the mass M of the celestial body (for earth: $\mu = 3.98600 \cdot 10^{14}$ m^3/s^2 [15]), r the distance between the object in orbit and the center of the celestial body and a the semi-major axis of the elliptical orbit. In the case of a satellite orbiting earth is $r = R_E + h$, with R_E being the earth radius ($R_E = 6371$ km) and h the altitude of the current satellite position over earth's surface. The semi-major axis is $a = (r_{perigee} + r_{apogee})/2$.

In order to obtain Δv_g, the gravitational force needs to be integrated over the altitude change of the object and, due to energy conservation, set equal to its equivalent kinetic energy. This yields in our case of a satellite orbiting earth [15]:

$$\Delta v_g = \sqrt{2 \int_{R_E}^{R_E - h} g(r) dr} = \sqrt{2 \int_{R_E}^{R_E - h} g_0 \frac{R_E^2}{r^2} dr} \tag{2.10}$$

with $g(r)$ being the acceleration due to gravity as a function of the distance to earth's

center point, assuming earth being a point mass [7]. Solving (Eq. 2.10) yields:

$$\Delta v_g = \sqrt{2 g_0 R_E \left(1 - \frac{R_E}{R_E - h}\right)} \tag{2.11}$$

Corrections to the Energy Budget
Because of gravity losses, aerodynamic drag, maneuvers and safety margins, the actually required mission velocity is higher than previously calculated. The formulas to calculate these losses cannot be computed since drag, acceleration of gravity and flight path angle are unknown functions of time. Experience and data from previous missions provide a basis for choosing conservative values for these losses [7]. Furthermore, the rocket gains a velocity increment during launch due to earth's rotational speed. This effect depends on the latitude of the launch site and can be maximally taken advantage of at the equator. A list of typical values for velocity gains and losses is given in Table 2.1.

Correction	**Magnitude**
Gravity losses	1000 - 1500 m/s
Aerodynamic drag losses	100 - 150 m/s
Maneuvers	10 - 15 m/s
Safety margin	1 - 2 %
Earth rotation (Kourou)	-460 m/s
Earth rotation (Kennedy Space Center)	-408 m/s

Table 2.1: Velocity gains and losses [14]

Inclination Changes
The inclination i of an orbit is the angle between the equatorial plane and the plane of the orbiting satellite. It is subject to the launch azimuth, which is the flight direction at orbit insertion. For a launch direction directly eastward the inclination becomes minimal and equal to the launch site latitude, otherwise it will always be greater. An inclination smaller than launch latitude cannot be achieved as the plane of orbit must contain the center of the earth (the focus of the ellipse) as well as the point at which the satellite is inserted into orbit. This is why an inclination change is necessary when a GEO satellite is placed into orbit as long as the launch site is not located along the equator [7], giving launch sites at small latitudes an advantage for these missions.

Optimal orbital plane changes requiring minimum delta-v are a complicated matter and often require two or more impulses (firings of the engines). The following

formula, used to calculate the delta-v requirement Δv_i for an inclination change only, requires the old and the new orbit to intersect, which allows a single impulse maneuver, and to have the same form, meaning that no orbital speed change occurs [7]:

$$\Delta v_i = v_o \cdot 2sin\frac{\Delta i}{2} \tag{2.12}$$

where v_o is the orbital velocity at the time of the maneuver and Δi the angle between the old and the new orbital plane. It is apparent that large Δi and inclination changes at high orbital velocities need to be avoided, as they impose very high delta-v and therefore propellant mass requirements. For example, an inclination change of $\Delta i = 60°$ results in a delta-v requirement equal to the current orbital velocity. Therefore, changes to the orbital plane are best to be performed at the apogee. As geostationary satellites themselves are mostly responsible for orbit insertion from GTO to GEO, they also need to perform the necessary inclination changes [24, 16]. Hence, delta-v due to inclination changes will not appear in the delta-v budget used in this thesis.

Delta-v Budget in the Optimization Program

Using Eq. 2.8 to Eq. 2.11 and applying conservative amounts of losses as well as gains, the following rounded delta-v budgets for a GTO and a LEO mission can be obtained and are used throughout this thesis. Losses are assumed to be equal for both missions, as they occur primarily during ascent of the launch vehicle. During the flight phase of a GTO mission that differs from a LEO mission, the magnitude of losses is negligible in the context of this thesis. The following table gives an overview over calculated values for Δv_o, Δv_g, the resulting Δv_{id} and finally a rounded value for Δv with losses, gains and a safety margin for both missions that is used hereafter (see Table 2.2). In the end, the total velocity gain supplied by the propulsion system of the launch vehicle must be equal to or greater than the required delta-v budget of the mission.

Parameter	**GTO (200 x 35786 km)**	**LEO (200 x 200 km)**
Δv_o at perigee	10245 m/s	7788 m/s
Δv_g at perigee	1950 m/s	1950 m/s
Δv_{id}	10429 m/s	8028 m/s
Δv	**12000** m/s	**9500** m/s

Table 2.2: Delta-v calculation

2.2 Rocket Propulsion Systems

The propulsion system, being the reason for distinction of rockets from other forms of transportation, is one of the most if not the most crucial subsystem of a rocket. Although all subsystems are necessary for successful operation, the propulsion system has the largest single influence on performance. With its mass and specific impulse as measure for efficiency, it has a double influence in the Tsiolkovsky equation (Eq. 2.6). A Vulcain engine delivers up to 4 GW of thermal power, which is equivalent to the output of a large nuclear power plant in the small volume of its combustion chamber [3]. Handling these levels of thermal and mechanical loads is a major challenge resulting in highly complex architecture, making the propulsion system the most expensive part of the launch vehicle. A cost breakdown for the first stage of an Atlas V (401) rocket is shown in Fig. 2.6 a). Due to large thermal gradients, high heat fluxes, thermal and mechanical stresses as well as cyclic loads, the rocket propulsion system is responsible for more than 50% of all failed launch missions (see Fig. 2.6 b)). Therefore, reliability and durability are paramount in the design of a rocket engine, especially for reusable engines.

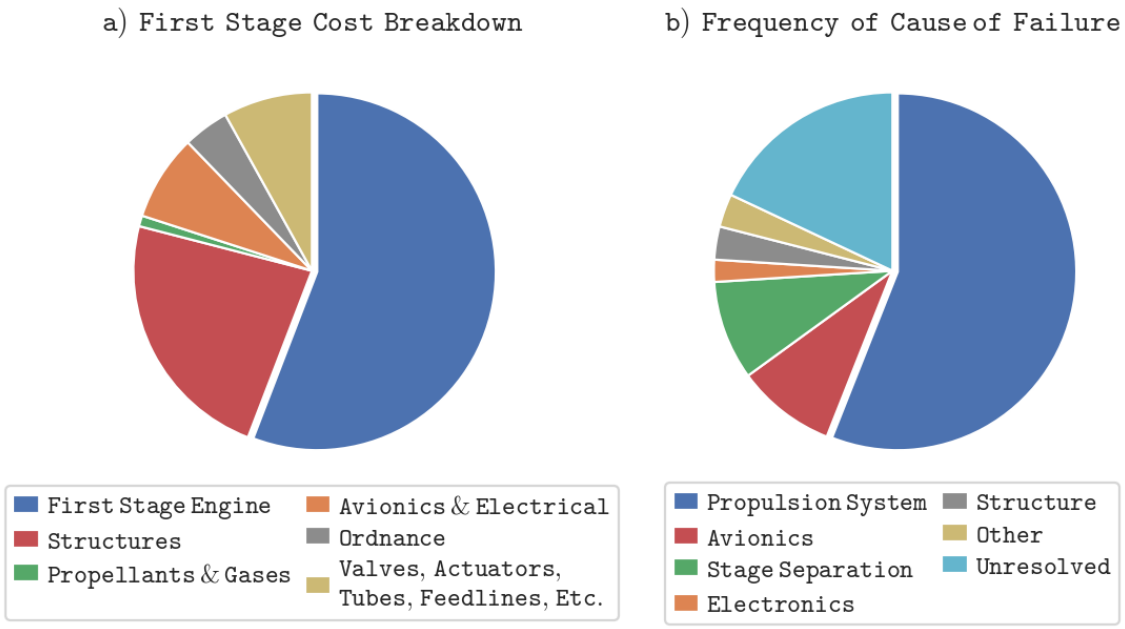

Figure 2.6: First stage cost breakdown (a)) [2] and frequency of cause of failure of launch systems (b)) [3]

Classification

One way to classify rocket propulsion systems is the physical concept by which energy is added to the ejected propellant mass. Fig. 2.7 gives an overview over different types of propulsion systems for space vehicles. As only chemical and nuclear engines are capable of delivering high levels of thrust, they are the only propulsion methods qualified for space launch applications. Failure always being a possibility,

nuclear engines have not yet been used in launch vehicles to avoid the devastating consequences of radioactive fallout.

In chemical rocket propulsion the energy from a high-pressure combustion reaction of propellant chemicals allows the heating of reaction product gases to very high temperatures (up to 4100 °C). The subsequent thermodynamic expansion of these gases in a nozzle accelerates them to high velocities (up to 4300 m/s) [15]. Chemical propulsion systems can be further divided depending on the state of matter of the used propellants. Rocket engines using liquid or solid propellants constitute the majority of the used chemical propulsion systems and are therefore described in more detail hereafter.

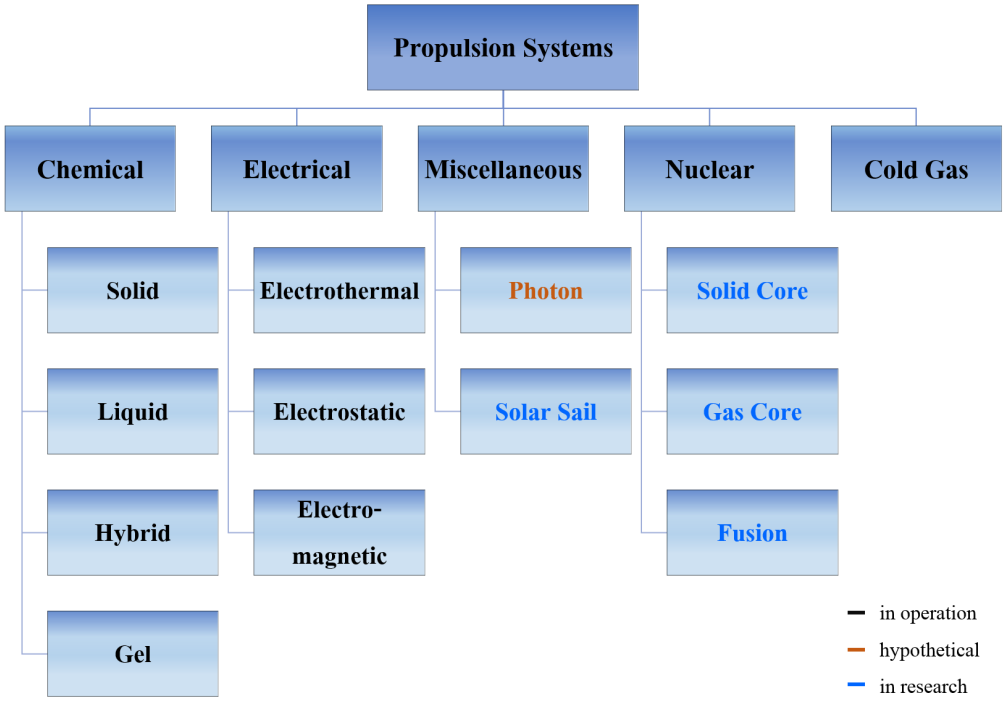

Figure 2.7: Classification of space propulsion systems [3]

Comparison of Solid and Liquid Propellants

Liquid and solid propellants each have advantages and disadvantages that determine their fields of application. A comparison of some of their properties is given in Table 2.3. A clear statement whether one or the other is better can only be made in the context of a specific use case. Because of instant readiness, good storability and reliability due to their simple architecture, solid propellant motors are preferred for military missiles [15]. In space launch applications, the high power density of solid propellants make them useful for booster stages that support the main stage's engine(s) during ascent, delivering high levels of thrust whilst keeping compactness (e.g. Ariane 5, Space Shuttle). Liquid propellant rocket engines have the advantages of a high specific impulse as well as throttling and restart capabilities, making them the preferred propulsion system for main and upper stages of high-performance

launch vehicles. They can also be used for liquid propellant boosters, which is called a Common Core configuration if the booster stages are identical with the rocket's main stage (e.g. Delta IV Heavy, Falcon Heavy). Furthermore, they can be designed for reusability if stages of a launch vehicle or a spacecraft are to be recovered and reused.

	Solid Propellant Motors	**Liquid Propellant Engines**
Advantages	High thrust levels possible	High specific impulse
	Good storability	Can be stopped/throttled
	Ready to operate quickly	Can be designed for reusability
Disadvantages	Low specific impulse	Complex design/expensive
	Cannot be stopped/throttled	Cryogenic propellant handling
	Cannot be tested prior to use	Large temperature gradients

Table 2.3: Advantages and disadvantages of solid and liquid propulsion systems [15]

Propulsion System in the Optimization Program
The TSTO launch vehicle configuration with a reusable first stage that is optimized in this thesis neither includes solid nor liquid propellant boosters attached to the main stage. Therefore, solely liquid propellant engines are utilized for both upper and main stage of the rocket. There are different ways to categorize liquid propellant rocket engines, for example by their thrust level, their application, their propellants or by their feed system type [15]. For this work, only high-performance engines of the main propulsion system of the launch vehicle producing high levels of thrust are considered, requiring a pump-fed liquid bipropellant (oxidizer and fuel) system. The engines' functionality, possible propellant combinations and the calculation of engine parameters in the optimization program is described in the following sections.

2.2.1 Liquid Propellant Rocket Engines

For a bipropellant rocket engine, oxidizer and fuel are stored in separate tanks as a liquid and are injected into the combustion chamber where they mix under high pressure and the combustion reaction takes place. The hot reaction product gases are accelerated in the converging part of the nozzle, reaching Mach 1 in the nozzle throat (smallest diameter of the nozzle). After that, they are expanded to high exit velocities in the diverging section of the nozzle, producing thrust in the opposite direction. The pressure difference p_e-p_a at the nozzle exit also influences the produced thrust (see Eq. 2.2). A schematic of a thrust chamber assembly, consisting of injector, combustion chamber and nozzle, is shown in Fig. 2.8, visualizing the previously described process. Despite there being many more parameters characterizing a liquid propellant rocket engine and its operation, some that are important for the course of this thesis are subsequently defined and described.

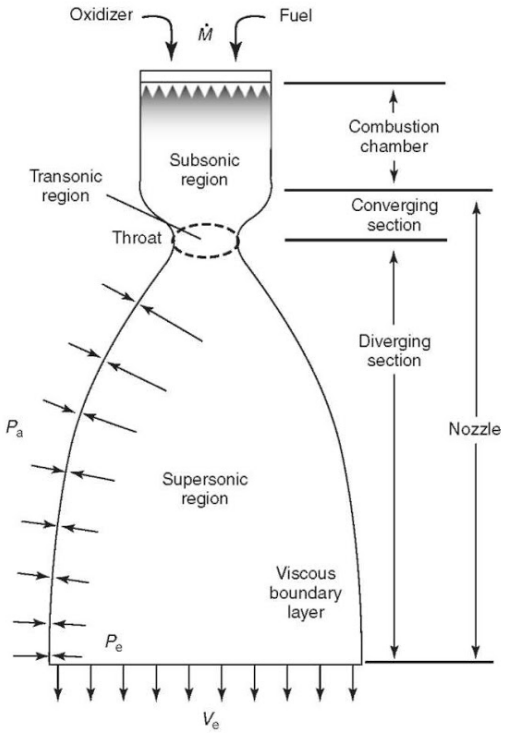

Figure 2.8: Schematic of a thrust chamber assembly

- Combustion chamber pressure p_c: For the same geometry, an increase in combustion chamber pressure p_c results in higher chamber temperatures and therefore higher exhaust velocities (see Eq. 2.3) as well as greater mass flow, thus increasing produced thrust. Keeping performance parameters constant, increasing combustion chamber pressure leads to smaller thrust chambers [15].

- Mixture ratio ROF: The mixture ratio is the ratio of oxidizer mass flow and fuel mass flow. It affects the temperature in the combustion chamber as well as the average molar mass of the exhaust gases, hence having an effect on exhaust gas velocity, produced thrust and I_{sp}. Stoichiometric ROF often does not make for highest performance [15].

$$ROF = \frac{\dot{m}_{ox}}{\dot{m}_{fu}} \tag{2.13}$$

- Nozzle throat area A_t: The nozzle throat is the cross-section of the nozzle with the smallest diameter d_t. Its area A_t influences the total mass flow through the nozzle and with that the achievable thrust, as the velocity in this cross-section is always Mach 1 for all supersonic flows in the diverging nozzle section [15].

- Nozzle area expansion ratio ε: Being an important parameter for nozzle design, the area expansion ratio is the ratio of the nozzle exit area A_e and the nozzle throat area A_t [15]. A greater area ratio leads to further expansion of the exhaust gases in the nozzle, increasing their velocity and decreasing the nozzle exit pressure p_e. The area ratio for which p_e is equal to the ambient pressure $p_e = p_a$ is called the optimum expansion ratio [15], eliminating the pressure term of the thrust equation (see Eq. 2.2). The ε of a nozzle needs to be carefully chosen according to its application, as it influences the nozzle flow stability, the I_{sp} of the engine and the engine length, as well as its mass.

$$\varepsilon = \frac{A_e}{A_t} \tag{2.14}$$

The type of tanks and the propellant feed system also characterize the engine. Storing propellants in high-pressure tanks allows feeding them merely by means of the pressure gradient. This is called a pressure-fed engine, the simplest form of liquid propellant rocket engine, as it only requires piping to connect the tanks with the thrust chamber and valves to control mass flow. To withstand the high pressure, the tanks need to be very sturdy and thrust is limited, rendering this system useless for large stage propulsion systems. On the other hand, using low-pressure tanks demands for a feed system that also pressurizes the propellants. This requires turbine powered pumps. The different propellant flow paths, methods of operating the turbopumps as well as handling of the turbine exhaust gases are called engine cycles and categorize the pump-fed liquid propellant rocket engines [15].

2.2.2 Engine Cycles

The three most common engine cycles are the gas generator cycle, the staged combustion cycle and the expander cycle. A schematic of their functional principle is shown in Fig. 2.9 and briefly described below.

Gas Generator Cycle
In the gas generator cycle a usually fuel rich portion of the propellants that amounts to 1-4% of the total propellant mass flow is fed to the gas generator and burned to create the hot gas required to power the turbine. The ROF of the gas generator is chosen so that the gas temperature stays in the range of 900-1350 K and the turbine blades do not require cooling. The remainder of the propellants are injected into the combustion chamber, the oxidizer directly and the fuel after it has been fed through cooling channels in the nozzle to minimize its inside wall temperature (regenerative cooling). This cycle is called an open cycle because the exhaust gases leaving the turbine are not injected into the combustion chamber. They can be either discharged overboard via one or two separate small low-area-ratio nozzles or aspirated into the main flow through openings in the diverging nozzle section further downstream from the nozzle throat to provide film cooling to the nozzle walls.

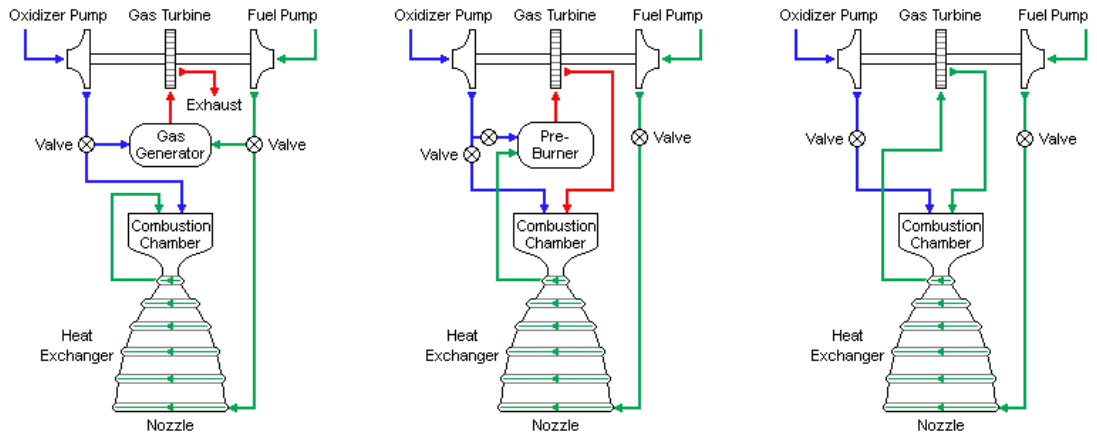

Figure 2.9: Engine cycles. From left to right: gas generator, staged combustion, expander [4]

Both methods provide a small amount of additional thrust. Because of relatively low system pressures, the gas generator cycle is a relatively simple cycle resulting in less expensive engines and low engine masses [15]. As part of the propellants is not available for combustion and expansion in the nozzle, the I_{sp} is lower than in closed cycles. Increasing the combustion chamber pressure results in an increased power demand of the turbines and therefore the need to burn a greater portion of the propellants in the gas generator, reducing the achievable I_{sp}. This makes the staged combustion cycle, a closed cycle, superior for higher combustion chamber pressures [3]. The relationship between the achievable specific impulse and combustion chamber pressure for a gas generator and a staged combustion cycle is shown in Fig. 2.10 (LOX/LH2 engine, $ROF = 6$, $F = 1000kN$, constant geometry, ε is increased with p_c). It can be observed that the maximum achievable I_{sp} of the gas generator cycle corresponds to a combustion chamber pressure of around 120 bar for this configuration. Europe has a long history of building gas generator engines (e.g. HM7B, Vulcain 1, Vulcain 2) and therefore a lot of experience with this cycle.

Staged Combustion Cycle

The staged combustion cycle is a closed engine cycle. The entire fuel mass flow is fed through the cooling channels in the nozzle before being burned with part of the oxidizer in a high-pressure pre-burner powering the turbopumps. The ROF in the pre-burner of the staged combustion cycle is also chosen so that the maximum entry temperature of the turbines is not exceeded. The turbine exhaust gases and the remainder of the oxidizer are then injected into the combustion chamber [15]. Different configurations of this cycle are possible, including one or multiple pre-burners and fuel-rich or oxidizer-rich combustion in the pre-burner depending on the propellant type [3]. This cycle leads to high combustion chamber pressures and even higher pre-burner pressures as all the hot gas from the pre-burner(s) is later

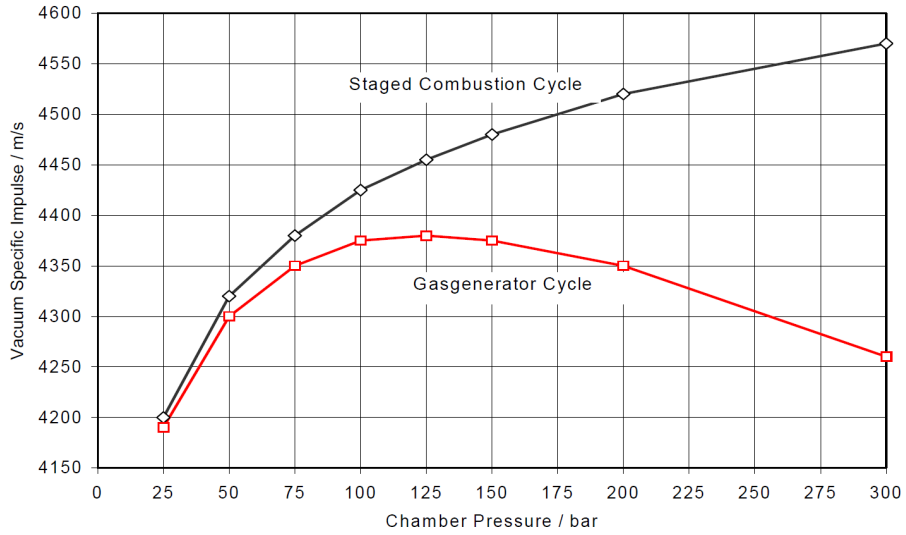

Figure 2.10: I_{sp} as a function of p_c for gas generator and staged combustion cycle ($I_{sp}\ [m/s]\ =\ I_{sp}\ [s] \cdot g\ [m/s^2]$) [3]

injected into the combustion chamber. Highest pump-exit pressures are necessary to operate this cycle. This results in smaller thrust chambers but heavier and more complex turbopumps and piping. High-thrust engines using the staged combustion cycle deliver the highest I_{sp} but are also heavier, much more complex and costly than gas generator engines [15].

Expander Cycle

In the expander cycle the entire fuel mass flow is also generally used as a coolant for the engine nozzle. Picking up energy while cooling down the nozzle walls, the fuel changes to the gaseous phase and expands in the turbine before being injected into the combustion chamber with the oxidizer. Being a closed engine cycle, the expander cycle has the advantages of high I_{sp}, simple design and low engine mass [15]. However, only relatively small combustion chamber pressures and thus thrust levels can be achieved as higher chamber pressures would require higher power for the turbopumps requiring the fuel to pick up more energy in the cooling channels. Longer combustion chambers with longer cooling channels would be necessary, increasing the engine mass and hence impairing the engine's thrust-to-weight ratio. Therefore, the maximum combustion chamber pressure of an expander cycle engine lies at around 6 MPa (60 bar) [3].

Comparison and Selection of Engine Cycles

The following comparison of the engine cycles aids in the understanding of their range of use as well as in the selection process in the context of this thesis. A summarization of the characteristics of each engine cycle and its application is given in Table 2.4. It can be observed that the expander cycle cannot deliver high thrust levels, hence regarding stage propulsion it is only capable of powering smaller upper stages. As the upper stage of a TSTO launch vehicle with a reusable first stage

tends to be larger than for expendable launch vehicles, the expander cycle cannot provide sufficient thrust and is not considered for use in the optimization process in this thesis.

Engine Cycle	**Application**	**Characteristics**
Expander	Upper stages	Chamber pressure: low ($<$ 60bar) Thrust: low-medium (80 - 200kN) Specific impulse I_{sp}: high Simple / low cost
Gas Generator	Main stages & Upper stages	Chamber pressure: medium ($<$ 130bar) Thrust: large range (30kN - 7MN) Simple / low cost
Staged Combustion	Main stages & Large upper stages	Chamber pressure: high ($<$ 300bar) Thrust: large range (80kN - 8MN) Specific impulse I_{sp}: high Complex / high cost

Table 2.4: Application and characteristics of various engine cycles [3]

In order to decide between the gas generator and the staged combustion cycle, several factors need to be taken into account. As both cycles are capable of producing a large thrust range and are eligible for both main and (large) upper stage propulsion, the decision is a trade-off between performance, reliability, reusability, costs and existing know-how. Having a clear performance-wise advantage, the staged combustion cycle is highly complex and consists of more moving parts than its counterpart. This leads to the assumption that in general gas generator engines are more reliable as with less moving parts less errors can occur. The staged combustion cycle's complexity is also reflected in its costs and reusability. The RS-25 engine, the Space Shuttle Main Engine (SSME), for example had a unit cost of more than 50 M$. It was designed to be reused for 55 missions but the real number of accomplished missions of the individual engines varied greatly with only one engine being used 22 times and others needing replacement after just one flight (see Fig. 2.11) [3]. Although there is no such data available yet for the reusable Merlin 1D gas generator engine that powers SpaceX's Falcon 9 rocket, it is decided to use gas generator engines for the launch vehicles that are optimized in this thesis. This is justified due to Europe's vast experience with this cycle, the reference vehicle (Falcon 9, see Ch. 4) also using gas generator engines, as well as the prospect of much lower costs. For the calculations in the optimization program, a gas generator temperature of 900 K, a maximum turbine pressure ratio of 20, and a turbine as well as oxidizer and fuel pump efficiency of 50% are applied.

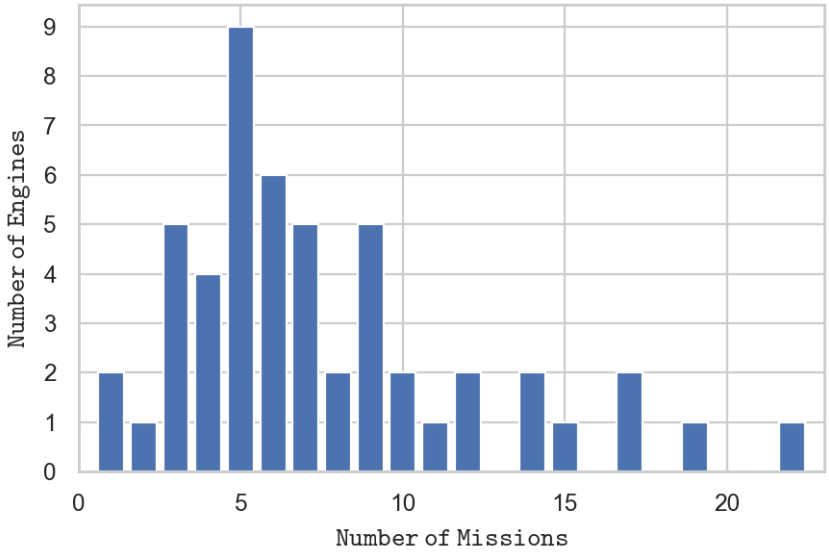

Figure 2.11: Number of accomplished missions of the Space Shuttle Main Engines [3]

2.2.3 Liquid Propellant Combinations

In contrast to a monopropellant system that uses thermal or catalytic decomposition of one propellant to create hot gas, a bipropellant system relies on the chemical reaction of an oxidizer and a fuel component. This reaction can be triggered by merely mixing the two propellants in the combustion chamber (*hypergolic propellants*) or by an ignition system that provides the required activation energy. Propellants can be further categorized by their state of matter at ambient conditions on earth's surface. If they are liquid, they belong to the *storable propellants* and if they need to be cooled to extremely low temperatures to maintain a liquid state, they are called *cryogenic propellants*. As the general properties of liquid propellant rocket engines were already explained in Ch. 2.2.1, in this section, some possible propellant combinations are presented and their characteristics compared regarding performance, impact on launch vehicle configuration and engine reusability. First, an overview of the propellant combinations and their properties is given in Table 2.5, followed by an elaboration of their effect on application. For each of the four liquid propellant combinations LOX/LH2, LOX/RP-1, LOX/LCH4 and NTO/MMH, the stoichiometric mixture ratio and the ROF that maximizes the specific impulse are given. For both ROFs, combustion temperatures and vacuum specific impulses for a combustion chamber pressure of 100 bar and the nozzle area ratios $\varepsilon = 45$ and $\varepsilon = 200$ are presented. Additionally, the densities at storage conditions, the boiling temperatures as well as other specific propellant characteristics are given.

Propellant combination Oxidizer / Fuel	$LOX/LH2$	LOX/RP-1	$LOX/LCH4$	NTO/MMH
ROF[1] Stoich./I_{sp} Opt.	7.94/4.9	3.41/2.8	3.99/3.5	2.5/2.4
Combustion temperature[2] $[K]$	3642/3280	3741/3750	3609/3607	3421/3430
Vacuum specific impulse[3] $[s]$	437/457	353/361	366/371	342/344
Vacuum specific impulse[4] $[s]$	467/477	380/384	393/395	363/363
Density[5] $[kg/m^3]$	1140/71	1140/807	1140/424	1447/879
Boiling temperature[6] $[K]$	90.0/20.4	90.0/460-540	90.0/111.6	294.3/360.6
Other characteristics	Excellent coolant/ Hydrogen embrittlement	Coking/ Soot	Heat transfer prediction	Hypergolic/ Toxic

Table 2.5: Propellant combination properties

Performance

It can be easily observed that the combination LOX/LH2 delivers the highest specific impulse of all presented propellants. The other combinations lie somewhat closer together regarding their performance, with LOX/LCH4 having the second highest I_{sp} values, followed by LOX/RP-1 and NTO/MMH. Typically, the latter has an I_{sp} of around 10-20 s less than LOX/RP-1 whose I_{sp} lies around 10-13 s under the LOX/LCH4 combination's specific impulse depending on the engine configuration. In Fig. 2.12 an overview of the vacuum specific impulses of various propellant combinations for different mixture ratios is depicted. Comparing ROF and I_{sp} values from Table 2.5 with Fig. 2.12 shows that performance is increased with a lower than stoichiometric ROF for all propellant combinations. This means an ROF corresponding to a fuel-rich combustion is favorable regarding a performance driven engine design, as this results in a larger portion of low-molecular-mass reaction products and thus higher exhaust velocities for many bipropellants (see Eq. 2.3) [15]. The ROFs for engines using LOX/RP-1 or LOX/LCH4 are commonly chosen close to their performance optimum [3].

[1] [3]
[2] For stoichiometric / I_{sp} optimum ROF at 100 bar [5]
[3] For stoichiometric / I_{sp} optimum ROF at 100 bar, ε=45 [5]
[4] For stoichiometric / I_{sp} optimum ROF at 100 bar, ε=200 [5]
[5] Under storage conditions [15]

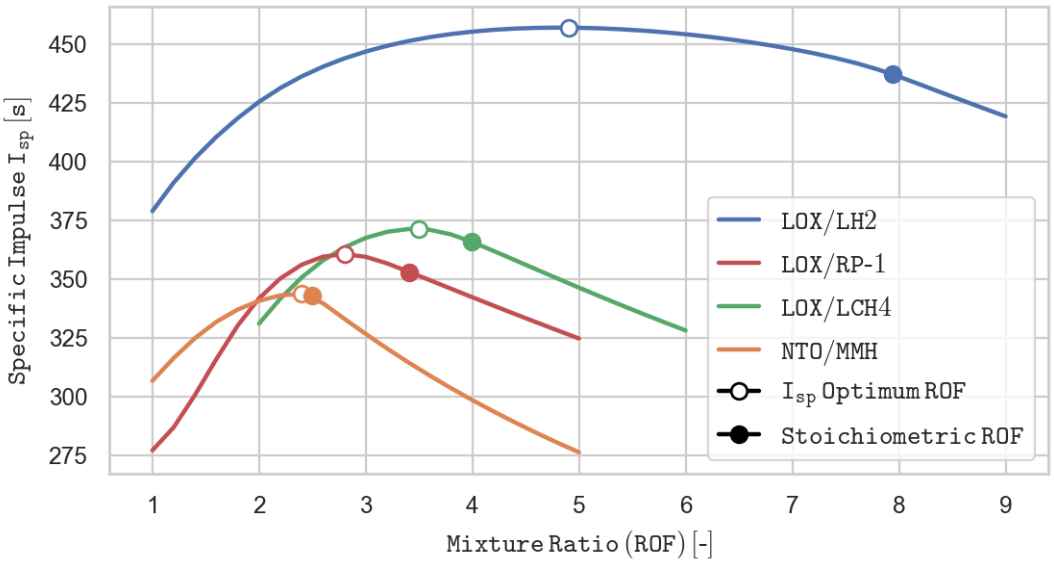

Figure 2.12: Vacuum specific impulse as a function of the mixture ratio (p_c=100bar, ε=45) [5]

Impact on Launch Vehicle Configuration

The propellant density has a visible influence on the launch vehicle configuration. Liquid hydrogen has a density of only 71 kg/m^3, which leads to large tank volumes and therefore large launch vehicles, increasing aerodynamic drag. Although LOX/LH2 has the best I_{sp} of the regarded propellants and therefore requires less propellant mass for the same mission, a launch vehicle using this propellant combination can still be larger and thus have a greater structure mass than its counterparts using other propellants, whilst having a considerably smaller overall mass. As the density of liquid oxygen is around 16 times greater than liquid hydrogen's density, the ROF for the LOX/LH2 combination is commonly not set to the fuel-rich performance optimum. In order to decrease overall rocket size and therefore structure mass, the ROF is chosen between stoichiometric and performance optimum. Another way to choose the mixture ratio for a propulsion system is aiming to use propellant tanks of the same size for both oxidizer and fuel, simplifying production of the tanks. This is usually done for rockets using the NTO/MMH combination, which results in an ROF that is even more fuel-rich than the optimum mixture ratio [3]. Due to their density difference, propellant tanks of similar size are also achieved by using the performance optimum ROF for LOX/LCH4.

Propellants can be categorized into storable or cryogenic propellants according to their boiling temperature. If their boiling temperature lies below -150°C (123 K), the propellant is cryogenic (liquefied gas at low temperature), if it lies above ambient conditions on earth, it is storable. Cryogenic propellant tanks require insulation to minimize vaporization losses and condensation on the tanks' outside as well as

[6] [15]

venting to prevent pressure increase [15]. Because of its extremely low boiling temperature of 20.4 K, this is especially important for liquid hydrogen. At temperatures this low many metals become brittle, making the choice of suitable tank and piping materials difficult [15]. Oxygen and methane also belong to the cryogenic propellants but have higher boiling temperatures, which entails simpler insulation.

Reusability
When reusability becomes a criterion for the selection of a propulsion system, the number of flights and reignitions, serviceability as well as the total cumulative firing time become key requirements of the rocket engine [15]. The impact of the propellant choice on these key requirements needs careful consideration.

Since the main stage engines of a TSTO launch vehicle with reusable first stage have to be fired multiple times, a reliable ignition system is required. Hypergolic propellants elude this necessity as they ignite when they are mixed, giving the NTO/MMH combination an advantage. On the other hand, NTO and MMH are both highly toxic and known carcinogens, resulting in more safety provisions and high-cost on ground operation [15], which especially impedes the handling and refurbishment of a reusable stage. As serviceability and low-cost operation are crucial for future reusable launch vehicles, the NTO/MMH propellant combination is not considered for the launch vehicle optimization carried out in this thesis and is therefore not further discussed.

Other important aspects impacting the reusability of an engine are fatigue failure and cumulative thermal stress cycles, which are strongly affected by the temperatures in the engine, regenerative cooling efficiency and material compatibility [15]. In general, higher combustion temperatures demand a more sophisticated combustion chamber as well as cooling system design. Looking at Table 2.5, it can be observed that the combustion temperature of LOX/LH2 is, apart from combustion chamber pressure, strongly dependent on its mixture ratio. For an often-used mixture ratio range of 6-7 the combustion temperature lies between 3525 and 3625 K [5]. The other propellant combinations do not show such distinct combustion temperature differences regarding changes in ROF in its applicable range. Comparing at stoichiometric ROF, the LOX/RP-1 propellant combination has the highest combustion temperature, with LOX/LH2 producing the second highest temperature closely followed by LOX/LCH4. As no material can withstand these temperatures, one propellant, typically the fuel, is used for regenerative cooling. The capacity of the cooling system is therefore dependent on the characteristics of the fuel. Here, LH2, RP-1 and LCH4 display very different properties. Hydrogen is deemed an excellent regenerative coolant [15], and in comparison with kerosene, methane is showing superior cooling properties, higher coking limits and less soot deposition, with the latter two being especially important in the context of reusability [25]. Although methane's physical properties in the cooling channels are difficult to predict since it is operated in the trans-critical regime [26], CFD-data trained artificial neural networks have already proven to be able to quickly deliver predictions with sufficient accuracy [27]. For hydrogen-rich atmospheres under high pressure, material

compatibility needs to be assessed, as hydrogen embrittlement can occur [3].

Propellants in the Optimization Program
In the optimization routine developed in the course of this thesis, the propellant characteristics that influence reusability, such as combustion temperature, cooling properties, coking and sooting, are not taken into account. However, the propellant and ROF choice impact the engines' specific impulse, the propellant mass, tank size, insulation requirements and ultimately the gross lift-off weight (GLOW) of the launch vehicle. This shows that the interdependencies between the subsystems necessitate optimization on launch vehicle system level. In this thesis, the propellant combinations LOX/LH2, LOX/RP-1 and LOX/LCH4 are examined with regard to their impact on the launch vehicle configuration.

2.2.4 Engine Parameter Calculation

In order to determine the characteristic properties for an engine, NASA's CEA (Chemical Equilibrium with Applications) program was integrated into the optimization routine. It can be used to obtain chemical equilibrium compositions of complex mixtures and it is able to deliver theoretical rocket performance parameters [28]. Existing engines' performance data was compared with calculated values to improve the results. As the specific impulse of the first stage engines changes during ascent, a simple trajectory simulator was implemented to calculate a mean I_{sp}, which is expected during the optimization routine to determine the required propellant mass (see Ch. 2.3.2).

CEA Program
The used propellants (fuel and oxidizer), the mixture ratio, the combustion chamber pressure and the nozzle area ratio are the necessary input parameters to receive the values for the hot gas density and sonic velocity at the nozzle throat as well as the sonic velocity, Mach number and pressure at the nozzle exit and the vacuum specific impulse for this engine configuration. These output parameters combined with the preset nozzle throat diameter are used to subsequently calculate mass flow, vacuum thrust, sea-level thrust and sea-level I_{sp}. For gas generator engines the mass flow that accounts for the hot gas powering the turbines is calculated according to [12], with the overall ROF of the engine and its I_{sp} changing accordingly. As this process is repeated often and the call of the CEA program takes a relatively long time, the output data for the propellant combinations LOX/LH2, LOX/RP-1 and LOX/LCH4 was precompiled into csv files which are crawled by the optimizer to find the current engine configuration and its properties.

For the execution of the CEA program the infinite-area combustion variant was chosen, because this configuration allows choosing between the assumptions of a shifting equilibrium composition or a frozen composition during expansion [28]. With the frozen equilibrium method, no chemical reactions or phase changes take place in the nozzle, hence the product composition at the nozzle exit is identical

to that in the combustion chamber. Performance is usually underestimated by 1 to 4%. On the other hand, the shifting equilibrium implies instantaneous chemical equilibria, reactions and phase changes between gaseous and condensed phases of all molecular species in the exhaust gas, resulting in a different product composition in the combustion chamber and the nozzle exit. This method typically overestimates performance by 1 to 4% [15]. In order to obtain more accurate performance data, Bray introduced the sudden-freezing criterion, which assumes shifting equilibrium nozzle flow until a freezing point, after which the subsequent expansion takes place with frozen equilibrium composition as the reaction rates of the recombination reactions decrease with decreasing density during adiabatic expansion [29]. It is indicated by [30] that Bray's freezing-point can be presumed to lie closely downstream of the nozzle throat for a combustion chamber pressure of around 50 bar, moving towards the nozzle exit with increasing combustion chamber pressure, resulting in a complete shifting equilibrium for combustion chamber pressures greater than 100 bar.

However, a successful application of the freezing point criterion can only be achieved after extensive evaluation of the kinetics of the recombination mechanisms for the particular propellants [31]. As this is beyond the scope of this thesis, performance parameters of a number of real engines were recalculated using the CEA program with shifting equilibrium and frozen equilibrium and compared to their actual values.

Improving Performance Data Accuracy
The deviations of the calculated I_{sp} from the I_{sp} of currently operational and historical engines in % are plotted over the combustion chamber pressure in Fig. 2.13 a). Detailed data can be found in Appendix B. It can be clearly observed that for lower pressures (< 80 bar) the calculation with frozen equilibrium delivers better results, whereas for higher combustion chamber pressures the shifting equilibrium method delivers more accurate results. Applying a linear regression line and using it as a correction formula in the engine parameter calculation of the optimization program promises sufficiently accurate results, as the phenomenon of overestimating performance of engines with lower combustion chamber pressure in shifting equilibrium calculations was successfully mitigated for the engines at hand (see Fig. 2.13 b)). As higher-pressure engines are assumed to be more important for the investigated optimization problems, the shifting equilibrium method with correction formula has been chosen to henceforth calculate engine parameters in the optimization program. It proved to be more accurate for calculations in this combustion chamber pressure regime and performance parameters will be less affected by the correction formula.

Trajectory Simulation
In order to determine the propellant mass of the first stage during the optimization, the optimizer expects a mean I_{sp} that reflects the variation of the first stage engines' specific impulse over the duration of the ascent. As its value depends on the engine thrust which in turn varies with the ambient pressure, a stepwise calculation of the engine parameters from launch until main engine cutoff (MECO) is required. As

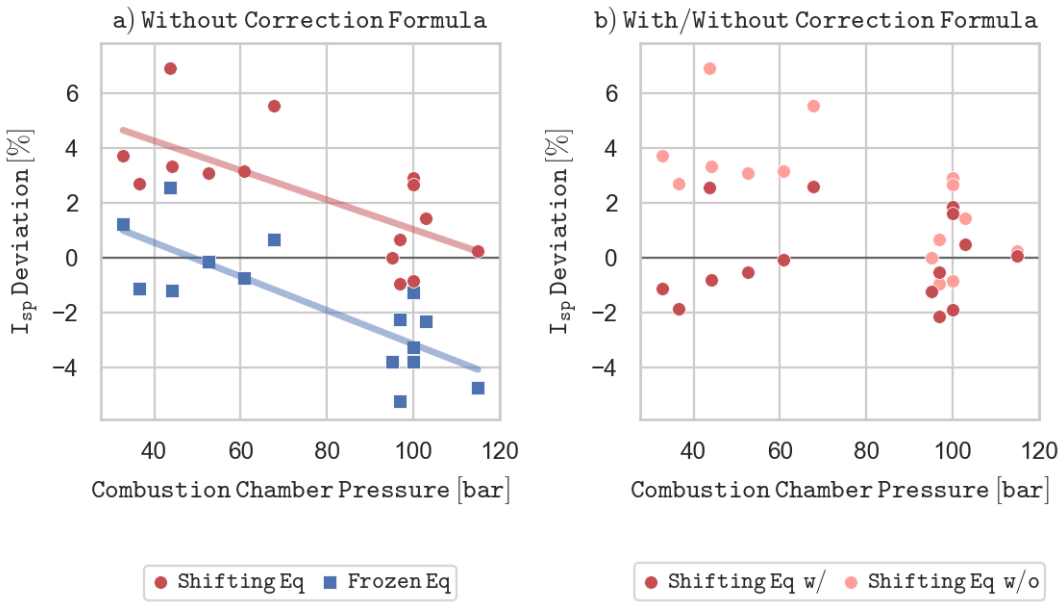

Figure 2.13: I_{sp} deviation of CEA engine data from data of real engines for shifting and frozen equilibrium with regression line (a)) as well as comparison of I_{sp} deviation with and without correction formula for shifting equilibrium (b))

a launch trajectory optimization is not part of this thesis, a simple 2D-trajectory simulation with an atmospheric model was implemented into the iterative rocket mass calculation process. The gravity turn is assumed to begin at an altitude of 250 m and to end at a final pitch-value of 25°. With a typical burn duration of Falcon 9's first stage, a constant pitch rate of 0.45 °/s was deduced [32]. This way, the current values for acceleration, velocity, altitude, ambient pressure, thrust, I_{sp} and propellant mass can be estimated for each time step and the mean I_{sp} can be derived. A time step of 1 s was deemed to be sufficiently small for this application. Since gravity losses are subject to the pitch angle [7], they are considered by this trajectory simulation, however atmospheric drag is neglected here for the sake of simplicity and its relatively small magnitude. Absolute accuracy is not the pretense of this method, but it reflects different launch vehicle configurations and therefore improves the results of the optimization program. For the first iteration the mean I_{sp} is calculated only from sea-level and vacuum specific impulse of the engines, as propellant mass and other launch vehicle masses are still unknown. An example for the difference between this value and the one derived from the stepwise trajectory simulation is plotted in Fig. 2.14. The blue graph represents the current I_{sp} for each point in time, the orange one the mean I_{sp} if only the latest I_{sp} and the sea-level I_{sp} are considered and the green one shows the mean I_{sp} if the current I_{sp}'s of all time steps until this point are taken into account. It can be observed that for this launch vehicle configuration the method that is represented by the orange graph overestimates the mean specific impulse until a flight time of approximately 95 s is reached. In this case, at engine cutoff the difference in mean I_{sp} between the two

methods is 6 s which amounts to roughly 2%.

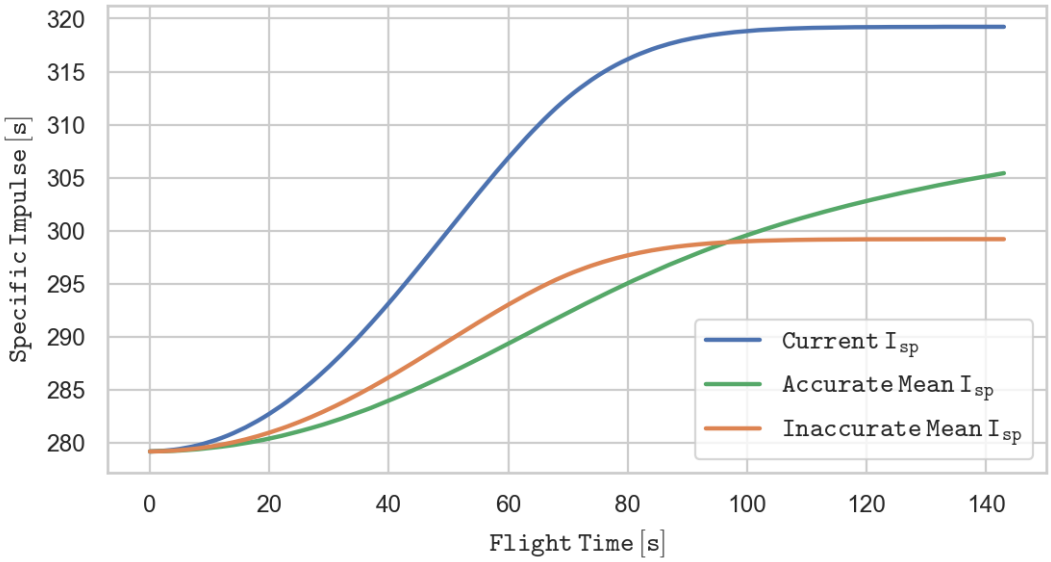

Figure 2.14: Current specific impulse and arithmetic mean specific impulses considering all past time steps (green) as well as only the latest and the first time step (orange) for the duration of the first stage engine burn

2.3 Rocket Staging

Looking at the Tsiolkovsky equation (Eq. 2.6), it becomes obvious that the performance of a rocket (delta-v) is limited by two factors, the specific impulse (I_{sp}) of its engines as well as the ratio of its initial mass before launch (m_0) and its final mass after burnout (m_f). As engine performance is restricted by propellant type and engine cycle, the mass ratio needs to be maximized in order to achieve maximum rocket performance. With m_0 being the sum of the rocket's structure mass m_s, its propellant mass m_p and the payload mass m_{pl}, the mass ratio can be written as:

$$\frac{m_0}{m_f} = \frac{m_s + m_p + m_{pl}}{m_s + m_{pl}} \tag{2.15}$$

Maximizing the mass ratio implies minimizing the rocket's final mass m_f, which can only be reasonably done by minimizing the structure mass m_s of the rocket for a given payload mass m_{pl}. A measure of the efficiency of a rocket design is the structural coefficient ε. It is equal to the structure mass divided by the structure mass plus propellant mass:

$$\varepsilon = \frac{m_s}{m_s + m_p} \tag{2.16}$$

Being independent of the payload mass, the structural coefficient is suitable for the comparison of different rockets and it is utilized for stage optimization (see Ch. 2.3.2). As delivering a payload into GTO via a single stage to orbit (SSTO) launch vehicle is not feasible with today's technology [15], the use of a multistage launch vehicle is required. The concept of rocket staging makes use of the fact that while propellant is burnt, some of the structure mass encasing it becomes useless. Allocating the propellant mass onto separate stages allows dropping off this dead mass when all propellant of a given stage is expended and its tanks are empty. This way, it is possible to accelerate the final stage with the payload to a higher terminal velocity than with a single stage configuration [15]. In the following sections, an overview of different staging configurations is given, and the process of stage optimization is explained.

2.3.1 Staging Configurations

The two most commonly used types of staging are serial staging and parallel staging. A depiction of both configurations is shown in Fig. 2.15. Serial staging effectively means stacking several rockets on top of each other. When the tanks of the bottom stage are empty, it is jettisoned and the following stage is ignited. The advantages of serial staging are that the engines can be adapted to the environment in which they are operated, thus optimizing performance of the propulsion systems, as well

as reducing the rocket's structure mass by jettisoning empty stages, resulting in an increased payload capacity [6].

On the other hand, parallel staging means mounting several stages and activating them in parallel. Compared to serial staging, parallel staging offers the advantage of using all engines during the entire propulsion time, meaning no engines of following stages have to be carried as dead weight. Furthermore, gravitational losses during the first part of ascent can be reduced as higher acceleration levels are feasible. Attaching a variable number of boosters allows building a launch vehicle family that is adaptable to a large range of payload masses. However, parallel staging leads to higher structural loads and aerodynamic drag losses as well as a less efficient propulsion system, because burn times are longer and the engines cannot be optimized for the entire ascent [6].

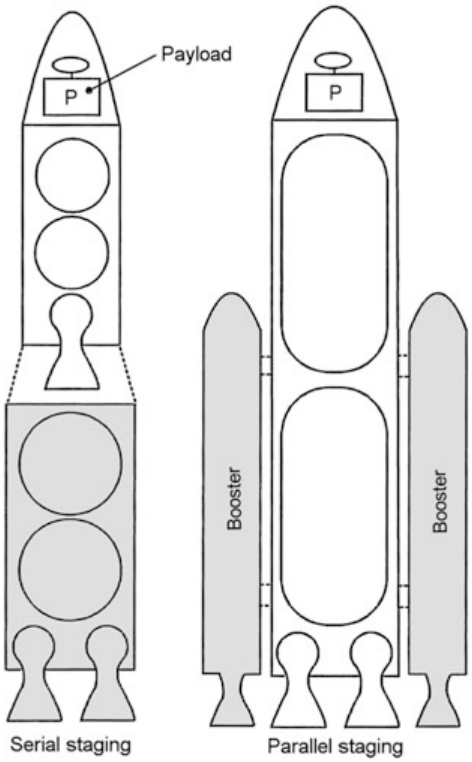

Figure 2.15: Serial vs. parallel staging [6]

In many currently used launch vehicles serial and parallel staging are combined in order to reap the benefits of both configurations. Yet, in the context of reusability, the usage of boosters is only beneficial if the boosters themselves are reusable as well, a configuration that is used by SpaceX's Falcon Heavy rocket to deliver super-heavy payloads into orbit. As SpaceX's Falcon 9 rocket is used as reference for the reusable launch vehicle optimization in this thesis, the focus lies on a serial staging configuration with two stages. Accordingly, the Tsiolkovsky equation can be written as:

$$\Delta v = \Delta v_1 + \Delta v_2 = I_{sp,1} \cdot g_0 \cdot ln\left(\frac{m_{0,1}}{m_{f,1}}\right) + I_{sp,2} \cdot g_0 \cdot ln\left(\frac{m_{0,2}}{m_{f,2}}\right) \tag{2.17}$$

where index 1 stands for first stage and index 2 for second (or upper) stage. $m_{0,1}$ is the total mass of the rocket before launch (GLOW), $m_{f,1}$ its mass after the propellant of the first stage $m_{p,1}$ is expended, $m_{0,2}$ the vehicle mass before ignition of the second stage after the first stage structure mass $m_{s,1}$ has been jettisoned and $m_{f,2}$ the final rocket mass after burnout of the upper stage. While the true payload mass m_{pl} is the payload in the calculation of $m_{0,2}$, the whole upper stage mass $m_{0,2}$ is the payload of the first stage (see Fig. 2.16). In conclusion, the total delta-v budget Δv is split up and allocated to the two stages. In order to obtain the optimum delta-v distribution, a stage optimization process is required.

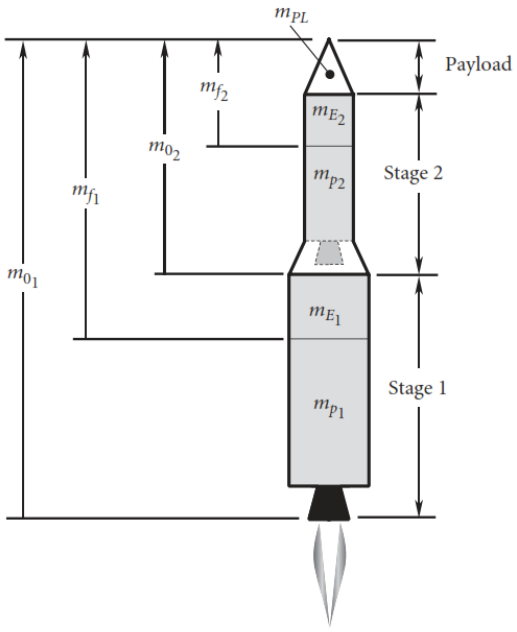

Figure 2.16: Serial staging configuration ($m_E = m_s$) [7]

2.3.2 Stage Optimization

Although staging needs to be optimized with regard to mission profile and payload, the following general rules can be given for sensible staging application [3]:

- Upper stages should be smaller than lower stages.
- Upper stages should have a higher specific impulse I_{sp} than lower stages.
- Stages with higher specific impulse I_{sp} should contribute a larger Δv than other stages.

As the weight of a multistage rocket is a cost driver and highly dependent on the delta-v allocation, the goal of the optimization is to find the launch vehicle configuration with the lowest gross lift-off weight (GLOW) for a given payload and mission delta-v budget. The different approaches for an expendable and a reusable stage optimization are described below.

Expendable Launcher Optimization
In order to obtain the optimal delta-v and therefore propellant mass allocation to the stages of an expendable multistage rocket, the Lagrange multiplier method is required. If $I_{sp,i}$ and ε_i of each stage are given, the minimum mass of an n-stage vehicle that is capable of a specified Δv while carrying a predefined m_{pl}, can be calculated. For the solution, the numerical Newton-Raphson method is applied.

As this technique is not used in this thesis, it is not further discussed at this point. Detailed explanations for its application in rocket staging optimization can be found in the literature [7, 6].

Reusable Launcher Optimization

A reusable first stage that lands downrange by means of retropropulsion cannot expend all of its propellant during ascent. After MECO and stage separation, Falcon 9's first stage uses its ACS thrusters to flip around, pointing its engines in direction of the velocity vector. On its way back to earth, it follows a ballistic trajectory until an altitude of approximately 70 km where three of the engines are re-ignited for around 20 s [32]. This so-called reentry burn slows the stage down before it enters the denser parts of the atmosphere, thus avoiding the need of heat shields. In order to land the stage, the center engine performs the landing burn, this time re-igniting for up to 32 s [32]. An optional third engine burn (boostback burn) directly after stage separation enables the stage to return to the launch site instead of landing downrange (see Fig. 2.17). As this consumes a lot of propellant, the boostback burn is not considered for high-performance GTO missions and is hence disregarded hereafter. The propellant amount that needs to be reserved for reentry and landing burn depends on the delta-v allocated to the first stage. Therefore, the optimization technique that has been briefly presented in the previous section is not applicable and a different approach is necessary. As its impact on launch vehicle performance is a subject of this thesis, values for the delta-v allocation are preset to allow the comparison of different configurations. However, if the allocation choice is included as a variable parameter in the optimization routine, the configuration leading to best performance can be found by the genetic algorithm. The procedure of propellant mass calculation for each stage, including the propellant needed for the landing of the first stage, and the required formulas are presented below. Consisting of three steps, the process expects values of payload mass, fairing mass, specific impulses of the engines, preset initial values of the structural coefficients for both stages and the total delta-v of the mission Δv as well as its allocation to the first stage ($\Delta v_{1,ascent}$) and the upper stage (Δv_2).

$$\Delta v = \Delta v_{1,ascent} + \Delta v_2 \tag{2.18}$$

1. **Upper Stage**

   For a given payload mass m_{pl}, fairing mass $m_{fairing}$, allocated delta-v Δv_2, vacuum specific impulse $I_{sp\_vac,2}$ and initial structural coefficient ε_2 of the upper stage, its propellant mass $m_{p,2}$ can be calculated as follows. Solving Eq. 2.16 for the structure mass and introducing it into the mass ratio (Eq. 2.15) of the upper stage delivers:

$$\left(\frac{m_0}{m_f}\right)_2 = \frac{m_{p,2} \cdot \frac{\varepsilon_2}{1-\varepsilon_2} + m_{p,2} + m_{pl}}{m_{p,2} \cdot \frac{\varepsilon_2}{1-\varepsilon_2} + m_{pl}} = \frac{m_{pl} + m_{p,2} \cdot \frac{1}{1-\varepsilon_2}}{m_{pl} + m_{p,2} \cdot \frac{\varepsilon_2}{1-\varepsilon_2}} \tag{2.19}$$

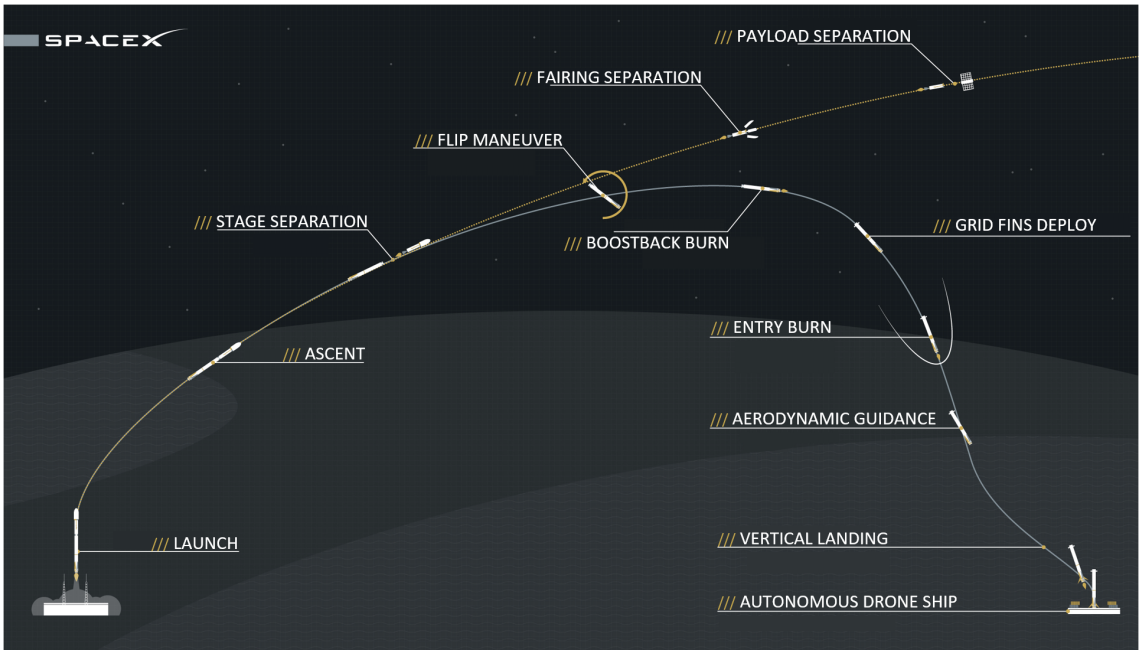

Figure 2.17: Falcon 9 trajectory [8]

Due to practicality reasons in the optimization program, m_{pl} includes the masses of fairing, payload adapter and avionics next to the actual payload mass (see Ch. 2.4), hence it can be regarded as the mass of the entire payload bay. To simulate fairing separation, which for Falcon 9 takes place shortly after stage separation (see Fig. 2.17), its mass is deducted from m_{pl} for the calculation of $m_{p,2}$. Inserting the previously transformed mass ratio into the Tsiolkovsky equation (Eq. 2.6), yields an expression that can be solved for the required propellant mass of the upper stage:

$$m_{p,2} = (m_{pl} - m_{fairing}) \cdot \frac{1 - e^{\frac{\Delta v_2}{I_{sp\_vac,2} \cdot g_0}}}{\frac{1}{\varepsilon_2 - 1} \cdot \left(1 - \varepsilon_2 \cdot e^{\frac{\Delta v_2}{I_{sp\_vac,2} \cdot g_0}}\right)} \tag{2.20}$$

As the structure mass of the upper stage $m_{s,2}$ is still unknown, an initial value for ε_2 must be preset (see Ch. 3.3.1). Hence, the calculated value of $m_{p,2}$ also represents an initial value. In the optimization routine, the masses of all other subsystems of the upper stage are determined and subsequently a new ε_2 is derived. Afterwards, the old and new structural coefficients are compared and the process is repeated in an iteration loop until convergence is achieved. Consequently, the overall mass of the upper stage $m_{0,2}$ before ignition of its engine is the sum of its structure mass, its propellant mass and the payload (bay) mass:

$$m_{0,2} = m_{s,2} + m_{p,2} + m_{pl} \tag{2.21}$$

2. **First Stage Landing**

In order to obtain the total propellant mass of the first stage $m_{p,1}$ as well as its division into the propellant mass needed for ascent $m_{p,1,ascent}$ and the propellant mass required to land the reusable first stage $m_{p,1,landing}$, a value for the structural coefficient of the first stage after stage separation $\varepsilon_{1,landing}$ has to be calculated first (see Eq. 2.22). Because there exists no payload on this stage anymore, this structural coefficient is equal to the inverse of the mass ratio for the landing procedure, hence it can be determined via the Tsiolkovsky equation (Eq. 2.6). Necessary input parameters are the sea level specific impulse of the first stage engines $I_{sp\_sl,1}$ and the delta-v of the landing maneuver $\Delta v_{1,landing}$, consisting of reentry and landing burn.

$$\varepsilon_{1,landing} = \frac{m_{s,1}}{m_{s,1} + m_{p,1,landing}} = \left(\frac{m_0}{m_f}\right)^{-1}_{landing} = -e^{\frac{\Delta v_{1,landing}}{I_{sp\_sl,1} \cdot g_0}} \tag{2.22}$$

Although the reentry burn is taking place in the upper atmosphere, the sea level specific impulse is chosen for the whole maneuver so as to receive conservative values for $m_{p,1,landing}$. As the delta-v for the landing procedure $\Delta v_{1,landing}$ is unknown and difficult to calculate due to the large influence of atmospheric drag during engine-first descent, the reference vehicle, Falcon 9, was thoroughly analyzed. According to its technical data (see Ch. 4) and the duration of reentry and landing burn as well as under the conservative assumption of a constant 100% engine throttle, it can be deduced that around 25 t of propellant are used up during these maneuvers. With its engine performance data and structural mass, this equals to a $\Delta v_{1,landing}$ of roughly 1900 m/s. To counteract potential inaccuracies in the calculation and assumptions, $\Delta v_{1,landing}$ required for this delta-v allocation is set to 2000 m/s in the optimization program. As the entire delta-v of the ascent of the first stage $\Delta v_{1,ascent}$ has to be compensated by the engines ($\Delta v_{1,landing}$) and aerodynamic drag (Δv_{drag}) during descent, Δv_{drag} is presumed to be 1500 m/s for the Falcon 9 configuration ($\Delta v_{1,ascent} = 3500$ m/s, see Ch. 4). For delta-v configurations that differ from the reference vehicle, $\Delta v_{1,landing}$ is adapted accordingly, considering the contribution of aerodynamic drag to be constant, though for small first stages 800 m/s is set as minimum for $\Delta v_{1,landing}$, which is equivalent to Falcon 9's landing burn. For launch vehicle configurations with $\Delta v_{1,ascent} \geq 3500$ m/s the calculation of $\Delta v_{1,landing}$ is considered to be accurate as excess velocity is compensated during reentry burn before denser parts of the atmosphere are entered, however in other cases potential inaccuracies due to deviations in Δv_{drag} might occur. Although atmospheric drag depends on the cross-sectional area of the first stage, for the sake of simplicity it was treated as being equal for all stage radius configurations in the framework of this thesis.

3. **First Stage Ascent**

For the given values of allocated delta-v $\Delta v_{1,ascent}$, mean specific impulse $I_{sp,1}$ and initial structural coefficient ε_1 of the first stage, as well as the already calculated values of $m_{0,2}$ and the structural coefficient after stage separation $\varepsilon_{1,landing}$, the first stage's total propellant mass $m_{p,1}$, the propellant mass needed for ascent $m_{p,1,ascent}$ and the propellant mass required for landing of the first stage $m_{p,1,landing}$ can be calculated. Inserting ε_1, $\varepsilon_{1,landing}$ and $m_{0,2}$ as the first stage's payload mass into the mass ratio of the launch vehicle ascent until MECO delivers:

$$\left(\frac{m_0}{m_f}\right)_{ascent} = \frac{m_{s,1} + m_{p,1,landing} + m_{p,1,ascent} + m_{0,2}}{m_{s,1} + m_{p,1,landing} + m_{0,2}} = \frac{m_{0,2} + \frac{m_{s,1}}{\varepsilon_1}}{m_{0,2} + \frac{m_{s,1}}{\varepsilon_{1,landing}}} \tag{2.23}$$

Introducing this expression together with $\Delta v_{1,ascent}$ and $I_{sp,1}$ into the Tsiolkovsky equation and subsequently solving it for $m_{s,1}$, yields an initial value for the first stage's structure mass:

$$m_{s,1} = m_{0,2} \cdot \frac{1 - e^{\frac{\Delta v_{1,ascent}}{I_{sp,1} \cdot g_0}}}{\frac{1}{\varepsilon_{1,landing}} \cdot e^{\frac{\Delta v_{1,ascent}}{I_{sp,1} \cdot g_0}} - \frac{1}{\varepsilon_1}} \tag{2.24}$$

Consequently, the values of the propellant masses can be determined using the known correlations:

$$m_{p,1} = m_{s,1} \cdot \frac{1 - \varepsilon_1}{\varepsilon_1} \tag{2.25}$$

$$m_{p,1,landing} = m_{s,1} \cdot \frac{1 - \varepsilon_{1,landing}}{\varepsilon_{1,landing}} \tag{2.26}$$

$$m_{p,1,ascent} = m_{p,1} - m_{p,1,landing} \tag{2.27}$$

Similar to the calculation of the upper stage mass, the final mass of the first stage is determined in an iteration loop. In each iteration, the reusable first stage is virtually built (see Ch. 3.3.2) and the actual structural coefficient as well as an updated mean specific impulse using the trajectory simulation are derived and compared to their previous values until convergence is achieved.

2.4 Mass Estimations

Whereas the propellant mass calculation and distribution has been presented in the last section, this chapter deals with mass calculations and estimations for all other parts of the launch vehicle. Their accuracy has a significant impact on how realistic the gross lift-off weight (GLOW) of the rocket can be predicted by the optimization program. The respective iterative mass calculations of the propellant and the various structural components represent the backbone of the evaluation of possible launch vehicle configurations (see Ch. 3.3.2). Fig. 2.18 depicts the composition of a launch vehicle in the optimizer. The rocket consists of its stages, in this case first stage and upper stage, and the payload bay, which encompasses payload, payload adapter, avionics and fairing. Having no impact on calculation outcome, the latter are assigned to the payload bay instead of the upper stage structure so as to be able to handle stage subsystem calculations similarly for all stages. Each stage consists of its structure, including the propellant tanks, intertank/interstage, thrust frame and the means to separate itself from the upper stage/payload as well as its engine(s), thrust vector control system and propellants. As the optimization program is based on an older version for expendable launch vehicles, some calculation methods were adopted, some altered and others newly added, such as the landing hardware for the reusable first stage. Subsequently, the updated and new mass estimations are presented in more detail, whereas the inherited ones are briefly summarized. In order to consider uncertainties in the mass estimations, margins were applied in the mass model. The margins were set to 10% for the upper stage and 15% for the first stage dry mass, comprising all stage structures, engines and TVC system. Similar to [19], a higher margin was applied to the first stage to reflect larger uncertainties with regard to the landing gear structures.

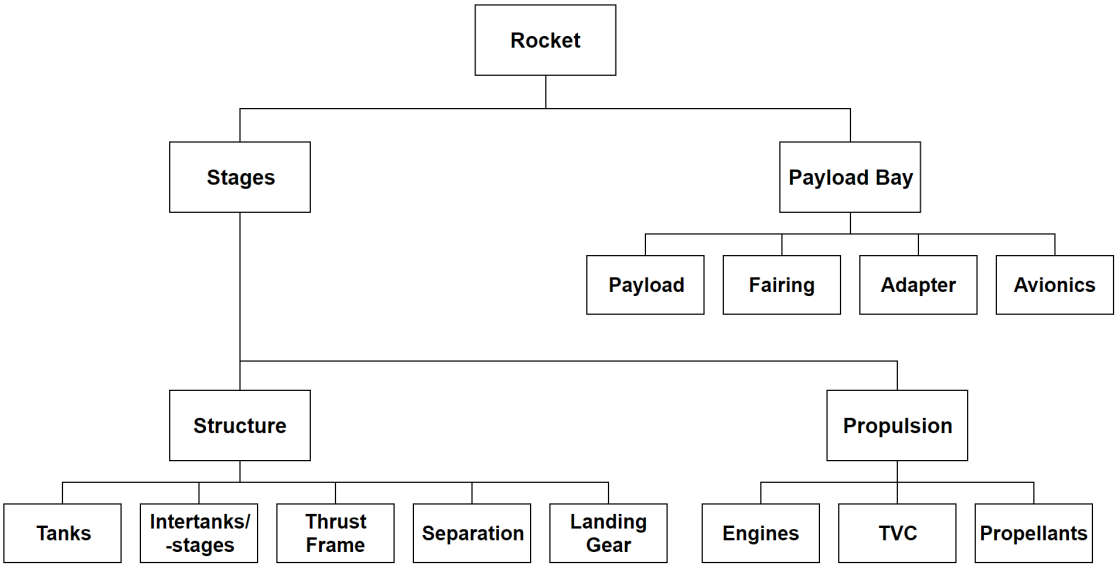

Figure 2.18: Schematic of the launch vehicle composition

2.4.1 Propulsion System

Engines

There exist various methods, differing in accuracy, to estimate the mass of a rocket engine. A high precision engine mass calculation expects detailed input parameters that are partially difficult to predict in advance, such as turbine torque of the turbopumps [33, 34]. Therefore, it is feasible to implement a mass estimation using empirical engine data into the optimization program. As some methods only consider vacuum thrust and potentially nozzle expansion area ratio as the basis of the mass calculation [35, 36], a sufficient distinction between the propellants that are compared in this thesis is not achieved. In contrast, Castellini developed detailed engine mass estimation models using regression analyses for 51 real engines with different engine cycles and propellant types [9]. Although combustion chamber pressure and nozzle expansion area ratio are not regarded in the calculation, this method is used to calculate engine masses in the optimization program, because it indicates the influence of propellant choice on engine mass. In Fig. 2.19-2.20 and Table 2.6 the graphical representation of the regression analysis and the resulting formulas for gas generator engines using the propellant combinations LOX/LH2 (cryogenic-cryogenic) and LOX/RP-1 (cryogenic-storable) are presented. A thrust range is given to limit the validity of the formulas. As there does not exist a history of LOX/LCH4 engines, their mass must be calculated using either of the two models. Although oxygen and methane are both cryogenic propellants, it was decided to use the cryogenic-storable mass calculation model, because methane's density is a lot closer to kerosene's density than to the one of hydrogen (see Table 2.5). This enables the use of a single shaft turbopump for both propellants, hence reducing engine mass, whereas LOX/LH2 engines require two separate turbopumps [3].

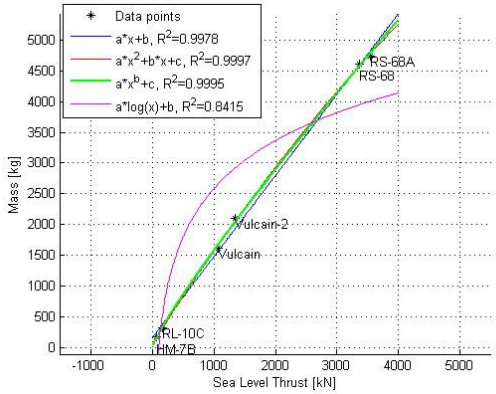

Figure 2.19: Cryogenic-cryogenic gas generator engine mass estimation [9]

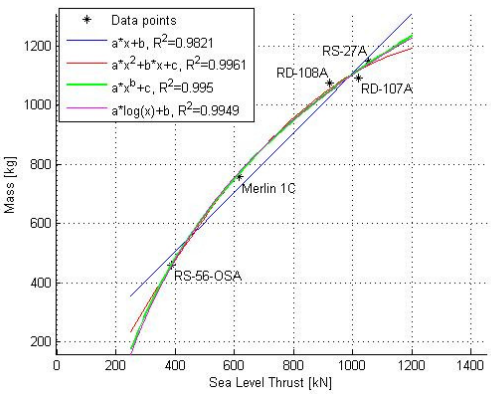

Figure 2.20: Cryogenic-storable gas generator engine mass estimation [9]

Propellant Type	Thrust Range $[kN]$	Mass Estimation with m_{engine} $[kg]$, F_{vac} $[N]$
Cryogenic-Cryogenic	[0; 8000]	m_{engine}=$7.54354 \cdot 10^{-3} \cdot (F_{vac})^{8.85635 \cdot 10^{-1}} + 2.02881 \cdot 10^{1}$
Cryogenic-Storable	[200; 2000]	m_{engine}=$3.75407 \cdot 10^{3} \cdot (F_{vac})^{7.05627 \cdot 10^{-2}} - 8.84790 \cdot 10^{3}$

Table 2.6: Rocket engine mass estimations [9]

Thrust Vector Control System
As the mass of the thrust vector control (TVC) system is typically not included in mass figures listed by engine manufacturers, it needs to be calculated separately. According to Castellini [9], a linear regression yields the TVC mass [kg] as a function of vacuum thrust $[N]$:

$$m_{TVC} = 0.1078 \cdot \frac{F_{vac}}{10^3} + 43.702 \tag{2.28}$$

2.4.2 Structure

Propellant Tanks
The propellant tanks are the largest structural components of the launch vehicle. It is their purpose to contain the propellants and often also to form the outer structure of the rocket. As only liquid bipropellant propulsion systems are considered in the framework of this thesis, each stage comprises two propellant tanks. Depending on propellant volume and stage radius, either spherical tanks (see Fig. 2.15 on the left) or cylindrical tanks with spherical lids (see Fig. 2.15 on the right) in tandem arrangement are utilized. In the optimization program, their mass is calculated according to the formulas in Table 2.7.

First, the required tank volume V_{tank} is determined by the propellant mass m_p and its density ϱ_p. A factor of $f_{ull} = 1.05$ is applied to regard 5% volume ullage in the tanks to allow for thermal expansion of the gases [15]. Next, the tank surface S_{tank} is derived using the tank volume and the tank radius r, which is the same as the stage radius. The wall thickness t of the tanks is calculated via Barlow's formula, which expects the tank pressure p_{tank}, the tank radius and the maximum allowable stress σ. A safety margin of $s_m = 1.5$ is applied and the minimum wall thickness is set to $t_{min} = 2\ mm$. In addition to the mass of the tank wall, the total tank mass m_{tank} includes the mass of the stringer and ring frame reinforcement as well as insulation. In the optimizer, the tank reinforcement is assumed to consist of an H-profile for both stringers and ring frames with a total edge length of 0.2 m and a profile thickness of 4 mm. This results in a profile area of $A_{profile} = 8 \cdot 10^{-4}\ m^2$. A distance of 1 m between ring frames and 0.5 m between stringers leads to a number

of $n_{profile} = 3$ profiles per square meter, each with a length of 1 m. Although no strength analysis has been done for this reinforcement calculation, the results reflect tank masses realistically and the tendency of Barlow's formula to prefer long and slim cylindrical tanks over shorter and wider ones is counteracted by the weight penalty per square meter. Furthermore, the thermal insulation that is required for tanks containing cryogenic propellants is considered by the factor f_{ins}, which represents the mass of the insulation per square meter. For hydrogen f_{ins} is equal to 2.88 kg/m^2, for oxygen and methane f_{ins} is equal to 1.123 kg/m^2 and for kerosene f_{ins} is 0, as it is not a cryogenic propellant [35]. Just as with Ariane 5 and Falcon 9 [24, 16], most rocket propellant tanks are made of high-performance aluminium-lithium alloys to minimize structure mass, however no detailed information is published about their composition and properties. Therefore, alloy 2090-T83 [37] is chosen as material for tanks and reinforcement structures in the optimizer, as it is suitable for aerospace applications. It features a density of 2590 kg/m^3 and a yield strength of 483 MPA, which is set as maximum allowable stress in the wall thickness calculation.

Parameter	Cylindrical Tank + Spherical Lids	Spherical Tank
Tank Mass	$m_{tank} = \rho \cdot S_{tank} \cdot \left(t + A_{profile} \cdot 1m \cdot \frac{n_{prof}}{m^2}\right) + f_{ins} \cdot S_{tank}$	
Wall Thickness	$t = s_m \cdot \frac{p_{tank} \cdot r}{\sigma}$	$t = s_m \cdot \frac{p_{tank} \cdot r}{2\sigma}$
Tank Surface	$S_{tank} = 2\pi rl + 4\pi r^2$	$S_{tank} = 4\pi r^2$
Cylindrical Length	$l = \frac{1}{\pi \cdot r^2} \cdot (V_{tank} - V_{lids})$	–
Volume	$V_{tank} = \frac{m_p}{\rho_p} \cdot f_{ull}$; $V_{lids} = \frac{4}{3}\pi r^3$	$V_{tank} = \frac{m_p}{\rho_p} \cdot f_{ull} = \frac{4}{3}\pi r^3$

Table 2.7: Propellant tank mass calculation formulas

Pressurization Gas + Tank

In order to maintain a constant pressure in the tanks while propellant is fed to the engines, they must be pressurized with a gas, for example helium. According to [9], the pressurization gas mass m_{gas} can be estimated as follows:

$$m_{gas} = 1.1 \cdot \frac{p_{tank} \cdot V_{tank}}{R_{gas} \cdot T_{gas}} \cdot \frac{\gamma_{gas}}{1 - \frac{p_{tank}}{p_{gas}}} \tag{2.29}$$

where $R_{gas} = 2077\ J/(kg \cdot K)$, $\gamma_{gas} = 1.667$, $p_{gas} = 286\ bar$ and $T_{gas} = 293\ K$ [12]. Via the ideal gas law and the relations in Table 2.7, the pressurization gas tank mass can be calculated similarly to the propellant tank mass.

Intertank Structure
The intertank structure represents the mechanical joint between two propellant tanks as well as the structural extension at the end of each tank. It transfers mechanical forces and forms the aerodynamic outer shell of the rocket. As it is of cylindrical shape, its surface S_{it} can be calculated with the stage radius and its mass estimation m_{it} is given by [38]:

$$S_{it} = 8\pi r^2 \tag{2.30}$$

$$m_{it} = 4.95 \cdot {S_{it}}^{1.15} \tag{2.31}$$

Interstage Structure
Having a similar purpose as the intertank, the interstage structure connects the first stage with the upper stage and the upper stage with the payload bay. If the radius differs between stages, the interstage features a conical shape and its surface S_{is} is calculated as follows [38]:

$$S_{is} = \pi(r_{upper} + r_{lower}) \cdot \sqrt{(l_{engine} + 0.4 \cdot r_{upper})^2 + (r_{upper} - r_{lower})^2} \tag{2.32}$$

where r_{upper} and r_{lower} are respectively the radii of the upper and lower stage and l_{engine} is the length of the upper stage engine. The interstage structure mass is then calculated the same way as m_{it}.

Thrust Frame
The thrust frame is the mechanical structure that connects the engines to the stage and transfers the generated thrust force to the launch vehicle. Its mass m_{tf} is determined with the maximum thrust F_{max} $[N]$ generated by the engines [38].

$$m_{tf} = 2.04 \cdot 10^{-5} \cdot {F_{max}}^{1.15} \tag{2.33}$$

Separation
Explosive charges are often used in order to sever two stages at stage separation. They are situated in the interstage structure and their mass m_{sep} can be estimated subject to the upper stage mass m_{upper} [38].

$$m_{sep} = 8.7 \cdot 10^{-4} \cdot m_{upper} \tag{2.34}$$

Landing Hardware
In contrast to an expendable rocket, a launch vehicle with reusable first stage requires additional equipment in order to be able to execute the landing successfully, from which the landing legs are the most prominent. Using the example of Falcon 9, the landing legs are made of carbon fiber with aluminium honeycomb to ensure structural stability at minimum weight [39]. According to SpaceX, the four landing

legs together weigh less than 2100 kg whilst having a span of around 18 m in deployed state [40]. Furthermore, at its upper end the first stage is equipped with four foldable titanium grid fins with a size of roughly $1.2 \cdot 1.5$ m, which manipulate the stage's lift and thus enable steering in super- and subsonic flight inside the atmosphere [41]. At last, a set of cold-gas thrusters gives extra steering control authority besides the gimballed main engines and is used to flip the first stage around after stage separation (see Fig. 2.17) [42]. For Falcon 9, the additional landing hardware is estimated to increase the structure mass by approximately 11% in comparison with an expendable version [43]. Nevertheless, to counteract potential inaccuracies a conservative factor of $f_{reusable} = 1.15$ was applied to the total first stage structure mass in the optimization program to account for 15% additional landing gear mass of the reusable first stage. Grid fins and landing legs of a landing Falcon 9 first stage are depicted in Appendix A.

$$m_{s,1,reusable} = f_{reusable} \cdot m_{s,1,expendable} \tag{2.35}$$

2.4.3 Payload Bay Subsystems

Payload Adapter
The payload adapter represents the interface between the launch vehicle's uppermost stage and the payload. Its mass m_{pla} can be estimated utilizing the payload mass m_{pl} [9]:

$$m_{pla} = 0.0477536 \cdot {m_{pl}}^{1.01317} \tag{2.36}$$

Avionics
According to Castellini [9], the mass of the avionics subsystem m_{avi}, comprising the electronic devices for communication, guidance, navigation and control as well as the power supply, can be assessed as follows:

$$m_{avi} = m_{electronic} + m_{power} \tag{2.37}$$

with the mass of the electronic devices $m_{electronic}$:

$$m_{electronic} = K_{RL} \cdot (246.76 + 1.3183 \cdot S_{rocket}) \cdot (1 - TRF_{electronic}) \tag{2.38}$$

and the power supply mass m_{power}:

$$m_{power} = K_{RL} \cdot 0.405 \cdot m_{electronic} \cdot (1 - TRF_{power}) \tag{2.39}$$

where $K_{RL} = 0.7$ is a redundancy factor, S_{rocket} the total surface of the rocket, $TRF_{electronic} = 0.75$ and $TRF_{power} = 0.18$ technology reduction factors.

Fairing

The fairing protects the payload from aerodynamic and thermal loads during ascent as well as the environmental conditions on the launch pad. It is shaped so as to maximize aerodynamic performance of the launch vehicle whilst safely containing the payload. The fairing is jettisoned shortly after stage separation in order to increase launch vehicle performance and maximize payload capacity. In the optimizer, its surface $S_{fairing}$ is calculated based on the geometric characteristics of Vega's fairing and its mass $m_{fairing}$ is subsequently determined using Eq. 2.31 [38]. An extensive derivation of $S_{fairing}$ is not conducted at this point but can be found in the literature.

2.5 Genetic Algorithms

In the previous chapters, the tools to determine the performance characteristics of a given launch vehicle configuration were examined. Subsequently, this chapter deals with the applied method of finding the optimum launch vehicle configuration. Genetic algorithms (GAs), being a class of evolutionary algorithms, are numerical optimization algorithms that are inspired by natural selection and natural genetics [10]. Biological evolution, first formulated by Charles Darwin, builds the basis of this optimization method, which mimics the adaptive change of species by means of natural selection, reproduction and the occurrence of mutations in light of the current environment [44]. One quality of genetic algorithms is that they are a robust method for estimating a series of unknown parameters within a model of a physical system and that they can be applied to many different practical optimization problems. Typically, they consist of the following components, which are described in more detail in the next section [10]:

- A population, representing a number of guesses of the solution to the problem
- A method for evaluating the quality of the individual solutions within the population
- A way of mixing fragments of better solutions to develop new, potentially better solutions
- A mutation operator to avoid loss of diversity and thus local extrema within the solutions

The entire area of solutions to the problem at hand, consisting of all possible parameter combinations, is called the search space from which the goal is to find the optimum solution representing the optimum parameter combination. With a growing number of parameters and values they can take on, this search space becomes very complex. Fig. 2.21 shows an exemplary search space for a problem with only two variables, as visualization becomes difficult for higher dimensional optimization problems. Each point represents a potential solution, with the extrema indicating better (or worse) solutions. Because optimization can be a maximization or minimization problem either the global maximum or global minimum represent the best solution. Looking at the complex topography featuring many local extrema (see Fig. 2.21), the advantage of GAs in comparison with traditional algorithms becomes apparent. As some search algorithms that sequentially adjust one single solution can get trapped in local optima and thus their solution depends on the starting point of the search, highly complex optimization problems resulting in highly complex search spaces require a different approach. Here, random searches combined with the manipulation of a whole population of solutions via emulating natural selection

and natural genetics, genetic algorithms, have proven to be among the most successful [10]. An explanation of the general procedure of a GA is given in the following section.

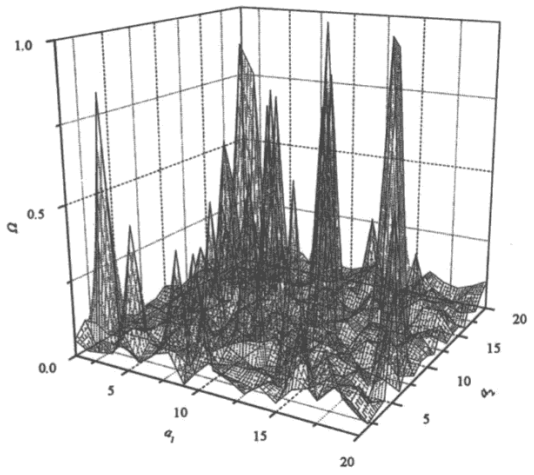

Figure 2.21: Exemplary search space [10]

2.5.1 Procedure

In the first step of the genetic algorithm, an initial population of possible solutions, each representing one individual, is generated and subsequently evaluated. The goal of the evaluation is to assign a fitness value to each individual, which is required to distinguish between good and bad solutions. Starting the generational cycle, a number of individuals are then selected to be the parents of the next generation, whereby individuals with a higher fitness value have a higher chance to be selected. In the following variation offspring is created by stochastically altering parents' attributes (crossover) and subjecting them to random changes (mutation). Afterwards, the offspring is evaluated and replaces the old population. This cycle is repeated until the termination condition is fulfilled. Fig. 2.22 schematically shows the fundamental procedure of the genetic algorithm as well as a corresponding pseudocode. The final population contains individuals with better fitness values than the ones in the initial population, hence the solutions to the problem are improved. The individual with the best fitness value represents the optimized solution. As the performance of the GA is strongly influenced by the choice of methods for selection, crossover and mutation as well as other parameters, such as population size and number of generations, the optimized solution might be the global or only a local optimum. Next, each step of the previously depicted process is described in more detail in the context of its application in this thesis.

```
population = init();
evaluate(population);
while termination condition not true do
    parents = select(population);
    offspring = vary(parents);
    evaluate(offspring);
    population = replace(offspring);
end
```

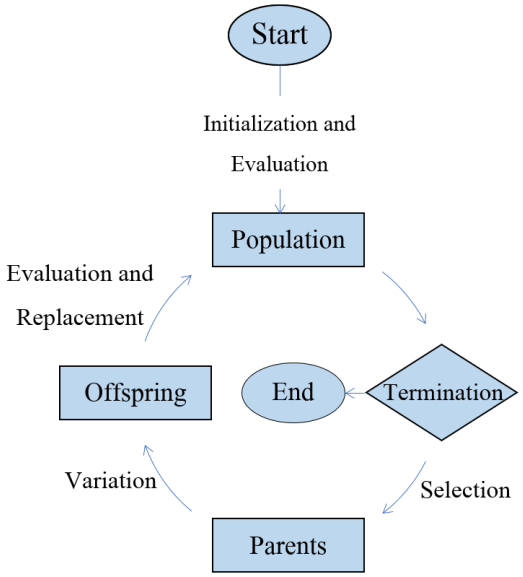

Figure 2.22: Pseudocode and evolutionary cycle

2.5.2 Population Initialization

In order to initialize the population, the way of representation of an individual solution in the computation space needs to be decided first, as it builds the basis for the genetic operators that simulate biological evolution. In genetics one distinguishes between the genotype, being the entirety of the genes of an organism, and the phenotype, which is the aggregate of all its characteristics. Regarding the GA, the genotype can be considered as a chromosome that comprises all genes, with the genes being the variables that identify the individual. In the context of this thesis, the genes consist of all parameters of a launch vehicle that are necessary to apply the tools presented in the previous chapters (see Ch. 3). After implementation of this framework in the algorithm, a preset number of individuals with all their genes are created randomly across the entire search space. Together, these individuals represent the initial population.

2.5.3 Evaluation

For the next step, the initial population (and later the offspring) are evaluated and each individual is assigned a fitness value based on a predefined fitness function. The fitness value is the key measure in the process of the genetic algorithm because it enables the distinction between better and worse solutions according to the objective of the optimization. As the fitness value is usually derived from the characteristics of an individual, the genotype of each individual needs to be transformed to the phenotype. Depending on the optimization problem, this transformation and the

determination of the fitness value are the most complicated and computation time consuming part of the algorithm, hence they have a significant influence on the performance of the GA. Regarding this thesis, during the evaluation the already explained methods are used to derive a launch vehicle with all its characteristics from the parameters that represent its genes. After that, the rocket's gross lift-off weight (GLOW) is determined and assigned as the fitness value. As the objective is to optimize launch vehicle configurations with respect to their weight, the optimization at hand is a minimization problem. To compare different optimization objectives with respect to their outcome, other fitness values were implemented and tested in the course of this work (see Ch. 6.4).

2.5.4 Selection

In a manner similar to that of natural selection, selection in the GA applies pressure upon the population [10]. Hence, the survival-of-the-fittest mechanism is imposed on the candidate solutions [45]. The method of selecting parents for the next generation influences the behaviour of the algorithm. Exploration of the search space and exploitation of already discovered good solutions need to be carefully balanced to avoid a completely random search of solutions on the one hand and a loss of diversity and thus the possibility of entrapment in a local optimum on the other hand. The method applied in the optimization program is the *tournament selection*, where a preset number (turnsize) of individuals are randomly selected from the population and of which the individual with the best fitness value is chosen to be a parent (see Fig. 2.23).

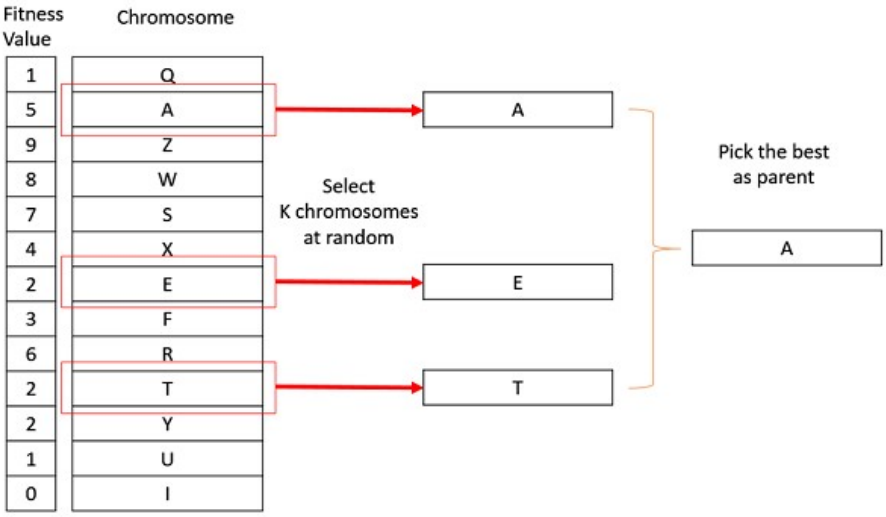

Figure 2.23: Tournament selection schematic [11]

This process is repeated as often as there are individuals in the population so as to form an offspring population of the same size that is subsequently altered by crossover and mutation. With tournament selection, individuals with a better fitness value are favored to further exist and pass on information to the offspring, however individuals with worse fitness values are not completely removed from the gene pool to ensure diversity in the solutions. The turnsize is the parameter that affects the selection ratio of better to worse solutions. A greater turnsize leads to higher exploitation, whereas a smaller turnsize leads to a greater exploration.

2.5.5 Variation

The variation of the population is achieved by crossover and mutation of the previously selected parents. Four probability values that characterize the process and influence the algorithm performance need to be predefined. Their impact on the algorithm's functionality is examined in Ch. 5.

Crossover
Being the part of the GA that simulates procreation in the real world, crossover combines two parental solutions to create two new and potentially better solutions. In the optimization program *uniform crossover* was chosen as crossover method. A predefined probability decides if two parental solutions are to form offspring and if so, another probability value is used to decide for each separate gene if it is swapped with the corresponding gene of the other parent (see Fig. 2.24). In the end, two new individuals, differing from the parents but combining their traits in a novel way, emerge as offspring [45].

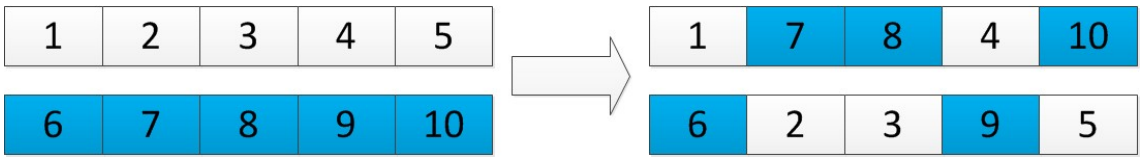

Figure 2.24: Uniform crossover schematic [12]

Mutation
After crossover is executed, mutation is performed on single individuals. In the GA, mutation is expressed by randomly changing genes, in this case the values of rocket parameters (see Fig. 2.25). Again, two probability values need to be preset, one being used to determine if an individual will be subjected to mutation at all and the other being the probability with which each gene of the chosen individuals is randomly altered. This genetic operator represents a heuristic approach and, correctly implemented, convergence on local extrema can be avoided. Probability of mutation should always be lower than probability for crossover in order to keep the randomness of the search at an acceptable level. Simply put, mutation is used to perform a walk in the vicinity of an individual solution [45].

Figure 2.25: Mutation schematic [12]

2.5.6 Termination

The new offspring population, consisting of individuals altered by crossover and mutation as well as unaltered parents, is evaluated and replaces the old population. The generational counter is increased by one and the process starts over. This cycle continues as long as the termination condition, which could be some form of convergence criterion or a maximum number of generations, is not fulfilled [10]. The latter is used as termination condition in the optimization program developed in the course of this thesis.

Chapter 3

Implementation

While the previous chapter concerned itself with the necessary theoretical knowledge, this chapter sheds light upon implementation of the aforementioned into the optimization program. Its general setup, the structure of the optimizer, as well as the workflow with the required input parameters and settings are explained in this section. A special focus is laid on the evaluation process of the genetic algorithm.

3.1 Software

Because the optimization program is based on a former version covering expendable launch vehicles, the current version has been developed using the same programming language, *Python*, however a migration from *Python 2.7* to *Python 3.7* with all related changes in the existing code architecture was necessary. As already mentioned in Ch. 2.4, parts of the original structure and code being valid for both expendable and reusable launch vehicles were adopted. Python being a programming language that facilitates object-oriented programming, the class structure of the original version made the expansion and advancement of the optimizer feasible. Fig. 2.18 shows the breakdown of a rocket how it is represented in the optimizer and the hierarchy of its subsystems, which are each implemented as an own object class. This enables further work on extension of the software in the future. In order to implement the genetic algorithm in the optimization routine, the *Distributed Evolutionary Algorithms in Python* (DEAP) computation framework was applied. Its explicit algorithms and transparent data structure allow for easy customization and adaption to the problem at hand [46].

3.2 Genetic Algorithm Setup

As explained in section 2.5, the parameters of the launch vehicle represent the genes of an individual solution that are subsequently used to determine its characteristics and eventually its fitness value. The following rocket parameters were implemented into the framework of the GA:

- Number of stages
- List of delta-v allocation
- List of stage radii
- List of engine cycles
- List of propellants
- List of mixture ratios
- List of combustion chamber pressures
- List of nozzle throat diameters
- List of nozzle area expansion ratios

Apart from the number of stages, all other parameters are lists containing the parameter values for each stage. Because the optimization program is designed for many different use cases, some of the parameters do not apply to the work in this thesis and hence were simplified or preset. Next to the parameters concerning solid rocket boosters which are not regarded and therefore not listed above, the number of stages was preset to two and possible engine cycles were limited to the gas generator cycle for all calculations carried out in the course of this thesis. Depending on whether launch vehicle performance was compared for different propellants and delta-v allocations, these parameters were preset or left open for the optimizer. In case of a two-stage rocket, the delta-v allocation is defined by the mission requirements and one fixed value for either first or upper stage. As all other parameters represent numerical values, sensible boundary values were implemented for population initialization and mutation in order to improve the performance of the optimizer (see Appendix C).

The algorithm *eaSimple* of DEAP is used as the framework for the GA developed in this thesis. Whereas the built-in tournament function is applied as the selection method, the generation of individuals, population initialization, crossover and mutation methods were built and implemented according to Ch. 2.5, 3.2 and 3.3.2. In order to maximize the optimizer performance, an additional evaluation step was incorporated into the population initialization to ensure that the first population consists exclusively of individuals that satisfy all requirements. This results in a high-quality data basis for the subsequent algorithm.

3.3 Workflow

The following sections give an overview of the input parameters that need to be defined by the user before running the optimization routine. Furthermore, the workflow of the evaluation part of the algorithm is explained in more detail.

3.3.1 Input Parameters

The input parameters include mission requirements, launch vehicle configuration, settings for the genetic algorithm as well as initial values and constraints for the optimizer.

Mission
Being the problem for which the optimizer searches the optimum solution, the mission needs to be defined first. It comprises the payload mass and its measurements as well as the required delta-v. The delta-v budget can either be set directly or it is calculated via a specified target orbit (perigee, apogee and inclination) as well as the launch site characteristics (latitude and altitude). If desired, the estimated delta-v losses can be adapted.

Launch vehicle configuration
As already stated, the optimization program was developed for diverse use cases. Therefore, some settings regarding the launch vehicle configuration must be chosen in advance. These consist of reusability of the first stage, utilization of solid rocket boosters, attachment of two additional first stages as liquid propellant boosters (Common Core configuration) and the usage of the same combustion chamber in all stages. The latter is applied in SpaceX's Falcon 9 rocket, which is why this configuration is used for the calculations in this thesis unless otherwise specified. This setting entails that propellant, mixture ratio, combustion chamber pressure and nozzle throat diameter are the same for all stages. According to the subject of this thesis, only launch vehicle configurations with a reusable first stage were considered, booster configurations were disregarded. Using the same engine (with different nozzles) on both stages entails several advantages. Development costs are reduced (one instead of two engine types), production costs decrease with higher production numbers (multiple first stage engines required), involuntary engine shutdown during ascent may not lead to mission loss (engine-out capability) and a higher number of engines on a reusable first stage result in better controllability during landing (a single Falcon 9 first stage engine is still too powerful to hover the empty rocket). On the other hand, the necessity of a larger quantity of engines implies in general an increased number of parts as long as complexity cannot be reduced, as well as an increased GLOW in comparison with rockets having fewer engines [47].

Genetic Algorithm
Parameters regarding the GA are called hyperparameters and consist of the population size, the number of generations until termination, the turnsize of the selection process and the four probability values for crossover and mutation (see Ch. 2.5.5): mating probability, mutation probability, probability that two corresponding genes are crossed and the probability that one gene mutates. Hyperparameters need to be chosen carefully as they strongly impact the behaviour of the algorithm and thus the performance of the optimizer. Therefore, a hyperparameter tuning was conducted to determine the settings for all following calculations (see Ch. 5).

Initial Values and Constraints
The first iteration of the propellant mass calculation during evaluation of the individuals expects initial values for the structural coefficient of each stage (see Ch. 2.3.2). Here, $\varepsilon_1 = 0.06$ and $\varepsilon_2 = 0.05$ were chosen for the first and upper stage, respectively. Furthermore, several constraints were implemented in the optimization program with respect to launch vehicle configuration and performance. To name but a few, the number of engines was limited to 15 in the first stage and one in the upper stage, minimum acceleration at engine ignition was set to 1.3 g for the first stage and 0.95 g in the upper stage unless specified otherwise and the maximum length to diameter ratio of the rocket was restricted to 20 (see Appendix C). In general, launch vehicles throttle down during certain phases of the ascent, for example to minimize the aerodynamic pressure or to limit acceleration towards the end of each stage engine burn. As this is difficult to model in the first stage trajectory simulation and because the upper stage is not included in the simulation, this is not reflected in the optimization program. Nevertheless, a throttle range of 60-100% similar to Falcon 9 [16] is assumed to reflect these procedures sufficiently. In order to improve algorithm capacity, a time constraint was incorporated into the population initialization to terminate the algorithm if not a single individual that satisfies all requirements is found in one day or to continue the optimization routine with a smaller population size if not as many individuals satisfying all requirements as preset by the population size are found in the given time window of two days.

3.3.2 Evaluation Procedure

The evaluation procedure transforms the genotype of an individual into its phenotype. The rocket parameters representing the genes are used to virtually build the launch vehicle, which gives information about its characteristics. The goal of the evaluation is the assignment of the fitness value. Within the scope of this thesis, the rocket's gross lift-off weight (GLOW) was chosen as the fitness value, however other fitness values were also examined later on (see Ch. 6.4). In the case that an individual does not satisfy all requirements or constraints, it is assigned the enormously high fitness value of 10^{19} to indicate its inadequacy. The following sections depict the evaluation procedure in more detail.

Build Engines
In accordance with Ch. 2.2.4 and Eq. 2.2, the propellants, mixture ratios, combustion chamber pressures, nozzle throat diameters and nozzle area expansion ratios are used to derive the engine characteristics, such as thrust, specific impulse, mass flow and nozzle diameter for all stages, which are subsequently adapted for gas generator engines. Furthermore, the engines' sizes and masses are estimated. At first, a predefined minimum number of engines is added to each stage.

Build Payload Bay
Then, the payload bay mass and measurements are determined. At this point it consists of the payload, the payload adapter and the fairing. As the avionics mass is subject to the not yet known rocket size, it is added later in the iteration loop.

Build Upper Stage
In the next step, the upper stage is virtually assembled. With its allocated delta-v, initial structural coefficient, engine vacuum specific impulse and the payload bay mass, the required propellant mass of the upper stage is calculated (see Ch. 2.3.2). To simulate fairing separation, its mass is deducted from the payload bay mass. After that, the masses and measurements of all other subsystems of the upper stage are determined (see Ch. 2.4). Now, the actual structural coefficient can be derived and it is used as input for the propellant mass calculation in the first iteration step. The whole process is repeated in an iteration loop until the difference between structural coefficients of two consecutive iterations amounts to less than 0.0001. If convergence is not achieved after 50 iterations, this individual is deemed inadequate and it is assigned the fitness value 10^{19}.

Build Launch Vehicle
After convergence of the upper stage iteration loop, the process is extended to the entire launch vehicle. First, the upper stage characteristics are calculated in the same way as before, only this time with the already converged structural coefficient as initial value. Then, the upper stage mass, the initial structural coefficient of the first stage, its engine vacuum I_{sp} as well as sea-level I_{sp}, the delta-v allocated to the first stage and its correlation with the delta-v necessary for the retropropulsive landing, are used to calculate the total propellant mass of the first stage and the amount reserved for the landing (see Ch. 2.3.2). Again, all other subsystem masses and measurements are estimated in accordance with Ch. 2.4. The iteration loop over the entire launch vehicle uses the structural coefficients of both stages with the same accuracy as before as well as the mean I_{sp} determined by the trajectory simulation (see Ch. 2.2.4) with an accuracy of 0.1 s as convergence indicators. Similarly, if convergence is not achieved after 50 iterations, the individual is assigned the fitness value 10^{19}. As the avionics mass is part of the payload bay and its estimation is subject to the size of the entire rocket, it is necessary to include the upper stage in this second iteration loop.

Acceleration Check
Only now after completion of the second iteration loop, all launch vehicle characteristics are obtained and the rocket's ability to take off and fly can be assessed. At this point, the acceleration at engine ignition is calculated for all stages and compared to the predefined minimum acceleration values. If they are not achieved and the preset maximum number of engines is not yet reached, the number of engines of the corresponding stage is increased by one and the previously described processes are repeated. In case the number of engines cannot be further increased and the acceleration requirements are still not met, the individual is assigned the fitness value 10^{19}.

Constraints Check
After checking some geometrical constraints regarding the engine and stage diameters as well as the rocket's length to diameter ratio, the individual is assigned its fitness value.

Chapter 4

Validation

In order to validate the model of the TSTO launch vehicle with reusable first stage that was developed in the course of this thesis, the Falcon 9 FT Block 5 rocket was used as reference vehicle, as it is currently the only operational launch vehicle with this configuration. Falcon 9 is developed, manufactured and operated by the Space Exploration Technologies Corporation (SpaceX) and is considered a medium-lift launch vehicle. Its first stage is powered by nine Merlin engines and the upper stage by one Merlin engine featuring a larger nozzle with greater expansion ratio. The engines burn a LOX/RP-1 propellant mixture and apply the gas generator cycle as feed system.

As SpaceX is a private company, not much official information is available and technical data is published very scarcely. Furthermore, the rapid evolution of the Falcon 9 rocket resulted in many modifications and thus various versions of the vehicle, making a distinction difficult. Therefore, the data used hereafter is based on unofficial estimations and cannot be expected to be 100% precise, however the values are assumed to depict Falcon 9 sufficiently accurate. Because SpaceX does not quantify its payload capacity for reusable Falcon 9 configurations [16] and it is not known if published values of its GLOW include the payload, payload adapter and fairing mass, a different approach than comparing the raw data was chosen.

Using available Falcon 9 parameters as input, the optimization program was executed for a 5000 kg payload GTO mission and a 15600 kg payload LEO mission, which are numbers that already have been demonstrated by Falcon 9 in reusable configuration. Assuming that they are not included in published data and the exact figures being unknown, the payload bay object masses calculated by the optimizer were added to the real Falcon 9 data and the resulting launch vehicle performance values were compared to the ones of the individuals which were output by the optimizer. This way, not only absolute values but also performance characteristics could be compared under equal assumptions.

The chosen mission input parameters, fixed rocket parameter values, boundaries for unknown parameter values and constraints for the launch vehicle configuration are summarized in Table 4.1. Rocket parameters and constraints were set to achieve results similar to Falcon 9. The delta-v allocation was estimated for a Falcon 9 GTO mission and the first stage delta-v was kept constant for the LEO mission, with the upper stage delta-v being adapted. The payload measurements were set according to the maximum payload size with constant diameter that Falcon 9's fairing is able to accommodate [16]. The missions' delta-v budgets were calculated in Ch. 2.1.4. The applied hyperparameters are outlined in Ch. 5.

	GTO	**LEO**
Mission		
Delta-v [m/s]	12000	9500
Payload Mass [kg]	5000	15600
Payload Height [m]	6.7	
Payload Diamter [m]	4.6	
Fixed Parameters		
Number of Stages	2	
Delta-v Allocation (First/Upper) [m/s]	3500/8500	3500/6000
Stage Radii (First/Upper) [m]	1.8/1.8	
Propellant	LOX/RP-1	
Engine Cycle	Gas Generator	
Comb. Chamber Pressure (First/Upper) [bar]	97/97	
Nozzle Area Expansion Ratio (First/Upper) [-]	16/165	
Parameter Boundaries		
Mixture Ratio [-]	1.5-3.5	
Nozzle Throat Diameter [m]	0.2-0.3	
Constraints		
Minimum Acceleration (First/Upper) [g]	1.3/0.8	
Maximum L/D Ratio [-]	25	
Minimum Number of Engines (First/Upper)	9/1	
Maximum Number of Engines (First/Upper)	9/1	

Table 4.1: Falcon 9 configuration [16, 17, 18]

For both mission configurations, the results of the optimizer are compared to Falcon 9 data in Table 4.2. At the top, the payload bay data with the masses that were calculated by the optimizer and which were also used for performance calculation of Falcon 9 can be found. Subsequently, an overview of mass and geometry characteristics of upper and first stage is given, followed by a comparison of the real and

calculated propulsion system data for both stages. At the end, the launch vehicles' gross lift-off weights (GLOW) and overall lengths are listed and the performance capabilities of each launch vehicle configuration is presented. For the exemplary performance calculation, the fairing was assumed to be jettisoned simultaneously with stage separation, the first stage mean I_{sp} was increased by 2% in accordance with Ch. 2.2.4 and 25 t of propellants were estimated for Falcon 9's reentry and landing burn.

Mass comparison
Overall, the launch vehicles which were calculated by the optimizer show a very good correlation with Falcon 9. With respect to the GLOW, a deviation of 3.6 and 0.6% was achieved for the GTO and LEO mission, respectively. Comparing the structure mass, it can be observed that the upper stage structure mass of the optimized individuals is up to 9.3% higher than Falcon 9's upper stage structure mass, while the first stage structure mass shows a maximum deviation of merely 0.8%. All stages of the optimized launch vehicles except the upper stage of the LEO mission comprise greater propellant masses than their counterpart of Falcon 9. Deviations of 4.2 and 3.0% are achieved for the first stage propellant mass and 1.9% for the upper stage propellant mass of the GTO mission. The difference of -9.1% between the upper stage propellant mass of the optimizer's LEO mission and Falcon 9's upper stage propellant mass is addressed in the performance comparison in more detail. The resulting structural coefficients show that the upper stage structure mass is calculated rather conservatively in the optimization program, whereas the calculated first stages feature a slightly better structural coefficient than Falcon 9. The latter is mostly due to additional propellant mass, as the tank mass increases only slightly with increasing propellant mass. Regarding the propellant mass necessary for landing the reusable first stage, the 5.6 to 6.4% increase in comparison to the estimated landing propellant mass of Falcon 9 on the one hand and only 0.4 to 0.8% greater first stage structure mass on the other hand represent the conservative assumptions made in Ch. 2.3.2.

Size comparison
Although the fairing is shorter, both calculated launch vehicles are longer than Falcon 9 whilst having a similar diameter. This is mainly caused by a greater propellant mass and therefore longer tanks as well as the tank configuration. As described in Ch. 2.4, in the optimization program the fuel and oxidizer tanks are considered to be separate, each with spherical lids at the top and bottom. However, Falcon 9 features a common bulkhead tank configuration with ellipsoidal tank ends, which reduces stage length. Furthermore, the method how engine nozzles are designed makes engine length estimations difficult. In the optimizer the engine nozzle length calculation is based on a conical nozzle length, which can be another reason for inaccurate length estimations. Although the interstage is attributed to the first stage in the optimization program, here its length is added to the upper stage as it houses the upper stage engine.

			Falcon 9		Optimizer	
			GTO	**LEO**	**GTO**	**LEO**
Mass and Geometry	**Pl. Bay**	Payload Mass [kg]	5000	15600	5000	15600
		Adapter + Avionics Mass [kg]	592	1166	592	1166
		Fairing Mass [kg]	1766		1766	1766
		Fairing Length [m]	13.2		10.7	10.7
	Upper Stage	Structure Mass [kg]	4500		4917	4715
		Propellant Mass [kg]	111500		113664	101731
		Structural Coefficient [-]	0.039		0.041	0.044
		Length [m]	16.0		20.5	19.3
		Diameter [m]	3.66		3.66	3.66
	First Stage	Structure Mass [kg]	27200		27429	27302
		Propellant Mass Total [kg]	418700		436550	431453
		Propellant Mass Landing [kg]	25000		26605	26389
		Structural Coefficient [-]	0.061		0.059	0.060
		Length [m]	40.9		48.3	47.9
		Diameter [m]	3.66		3.66	3.66
Propulsion System	**Upper Stage**	Number of Engines	1		1	1
		F_{vac} [kN]	981		1074	1066
		I_{sp_vac} [s]	348		351	350
		t_b [s]	397		364	328
	First Stage	Number of Engines	9		9	9
		F_{vac} [kN]	8227		8536	8519
		F_{sl} [kN]	7607		7770	7753
		I_{sp_vac} [s]	312		310	311
		I_{sp_sl} [s]	283		282	283
		t_b [s]	162		156	154
Total		GLOW [kg]	569258	580432	589918	583733
		Length [m]	70.1		80.6	78.9
Delta-v		Delta-v Upper Stage [m/s]	8497	6252	8503	5998
		Delta-v First Stage [m/s]	3502	3376	3516	3518
		Total Delta-v [m/s]	11999	9628	12019	9516

Table 4.2: Comparison of Falcon 9 with the results of the optimization program [16, 17, 18]

Propulsion system comparison
The calculated engines display higher thrust levels than Falcon 9's Merlin 1D engines. Whereas in the upper stage the vacuum thrust is up to 9.4% higher, the nine engines in the first stage produce 3.7% more thrust in vacuum and only 2.1% higher thrust at sea level. Nevertheless, a direct comparison regarding thrust cannot be made as no information about Merlin's nozzle throat diameter is available. With respect to specific impulse, a maximum deviation of 0.8% shows a very good conformity between calculated and real engine data. Although not presented in Table 4.2, it has to be noted that for the GTO mission, the optimizer chose an ROF of 2.9 whereas for the LEO mission an ROF of 2.8 was the optimum choice. This is because for the mixture ratio of 2.9 the upper stage I_{sp} is 1 s higher and the first stage I_{sp} is 1 s lower. Albeit very small, this difference leads to the different optimum ROF choices, as for the GTO mission the upper stage must deliver a higher delta-v and hence has a greater impact on launch vehicle configuration. Comparing the burn duration t_b, the first and upper stages of the calculated launch vehicles have shorter engine burn times than Falcon 9. This is mostly caused by higher thrust levels and thus higher mass flow as well as Falcon 9's engines being throttled during parts of the flight, which is not represented in the optimization program. A propulsion system weight comparison is not performed at this point because official numbers published by SpaceX differ greatly in comparison with historical and current engine mass data, giving rise to the question which engine parts are included in the calculation.

Performance comparison
Regarding launch vehicle performance, a very good conformity between the GTO configurations of the calculated launch vehicle and Falcon 9 is achieved. The difference in delta-v ranges between 0.4% and 0.07% for the first and upper stage, respectively. This does not surprise, as the delta-v allocation was determined according to Falcon 9's GTO configuration. Because for some reusable GTO missions Falcon 9 is estimated to have transported slightly heavier payloads than 5000 kg [18], it can be presumed that Falcon 9's upper stage structure mass already includes the payload adapter and avionics masses or that a GTO can be achieved with a marginally lower delta-v budget than 12 km/s. However, for the course of this thesis this value is kept for the sake of conservative assumptions. In Ch. 6.3.1 the influence of the total delta-v budget on launch vehicle performance is examined. Although for the LEO mission the GLOWs of the calculated launch vehicle and Falcon 9 are very similar, the same delta-v values were not obtained by applying the same first stage delta-v allocation as for the GTO mission. The lower upper stage and total delta-v as well as the lower upper stage propellant mass of the calculated launch vehicle indicate that Falcon 9 could be capable of transporting even heavier payloads into a low earth orbit. Aiming to achieve better conformity between calculated launch vehicle and Falcon 9 for the LEO mission, the calculation of the LEO mission was repeated with the total delta-v and its allocation derived from Falcon 9 in Table 4.2. Furthermore, the payload bay of the LEO mission was added to the before calculated GTO launch vehicle in order to test if it is capable of delivering sufficient delta-v and thus completing the considered LEO mission. For both, an overview

of the resulting mass and performance values is given in Table 4.3. To be able to directly compare the results with Falcon 9, its values of the LEO configuration are also listed. The obtained results show that the new calculated launch vehicle fits Falcon 9's LEO configuration perfectly and that the calculated GTO launch vehicle is also capable of successfully completing the investigated LEO mission. All in all, the optimization program delivers very accurate results and the optimized launch vehicles show realistic characteristics.

	Falcon 9	**Optimizer**	
	LEO	**GTO (LEO payload)**	**LEO new**
Mass			
Payload Bay			
Payload Mass [kg]	15600	15600	15600
Adapter + Avionics Mass [kg]	1166	1166	1166
Fairing Mass [kg]	1766	1766	1766
Upper Stage			
Structure Mass [kg]	4500	4917	4893
Propellant Mass [kg]	111500	113664	111959
First Stage			
Structure Mass [kg]	27200	27429	27147
Propellant Mass Total [kg]	418700	436550	423481
Propellant Mass Landing [kg]	25000	26605	24134
Total			
GLOW [kg]	580432	601092	586012
Performance			
Delta-v Upper Stage [m/s]	6252	6306	6248
Delta-v First Stage [m/s]	3376	3393	3399
Total Delta-v [m/s]	9628	9699	9647

Table 4.3: Updated comparison of Falcon 9 LEO configuration with the results of the optimization program [18]

Chapter 5

Hyperparameter Tuning

As described in Ch. 3.3.1, the parameters that control the settings of the genetic algorithm are called hyperparameters and comprise the population size, number of generations, turnsize, mating probability, mutation probability, crossover probability of two corresponding genes and the probability that one gene mutates. Whereas the influence of the first three on representation of the search space, diversity of the solutions and quality of the results is easily conceivable (see Ch. 2.5), the interaction of the parameters regarding variation of the population as well as their impact on the algorithm are not as clear. Therefore, a hyperparameter tuning was conducted to obtain the optimum set of parameters for the following calculations. Four different combination sets of the four variation probabilities were chosen in order to examine their influence on the performance of the optimizer. Each combination and corresponding case denomination are presented in Table 5.1.

Probability of	Gene Crossover = 0.3 Gene Mutation = 0.1	Gene Crossover = 0.7 Gene Mutation = 0.5
Mating = 0.3 Mutation = 0.1	Case 1	Case 3
Mating = 0.7 Mutation = 0.5	Case 2	Case 4

Table 5.1: Overview of the tested hyperparameter combinations

For each case, the optimization program was executed with the four population sizes 100, 1000, 5000 and 10000. The number of generations was set to 50 and a turnsize of 3 was chosen. For each calculation, the minimum GLOW of each generation is plotted over the duration of the algorithm in Fig. 5.1, with the beginning of the graphs marking the time required to initialize the first population. In order to obtain a satisfactory basis for the following algorithm, the optimization program was designed in such a way that the initial population can only contain individuals

that satisfy all requirements. This leads to the initialization process taking more than half of the entire computation time, which is why the choice of population size has a great influence on the efficiency of the optimizer. The evolution of the best fitness value over the generational cycles gives information on the effectiveness of the represented probability parameters.

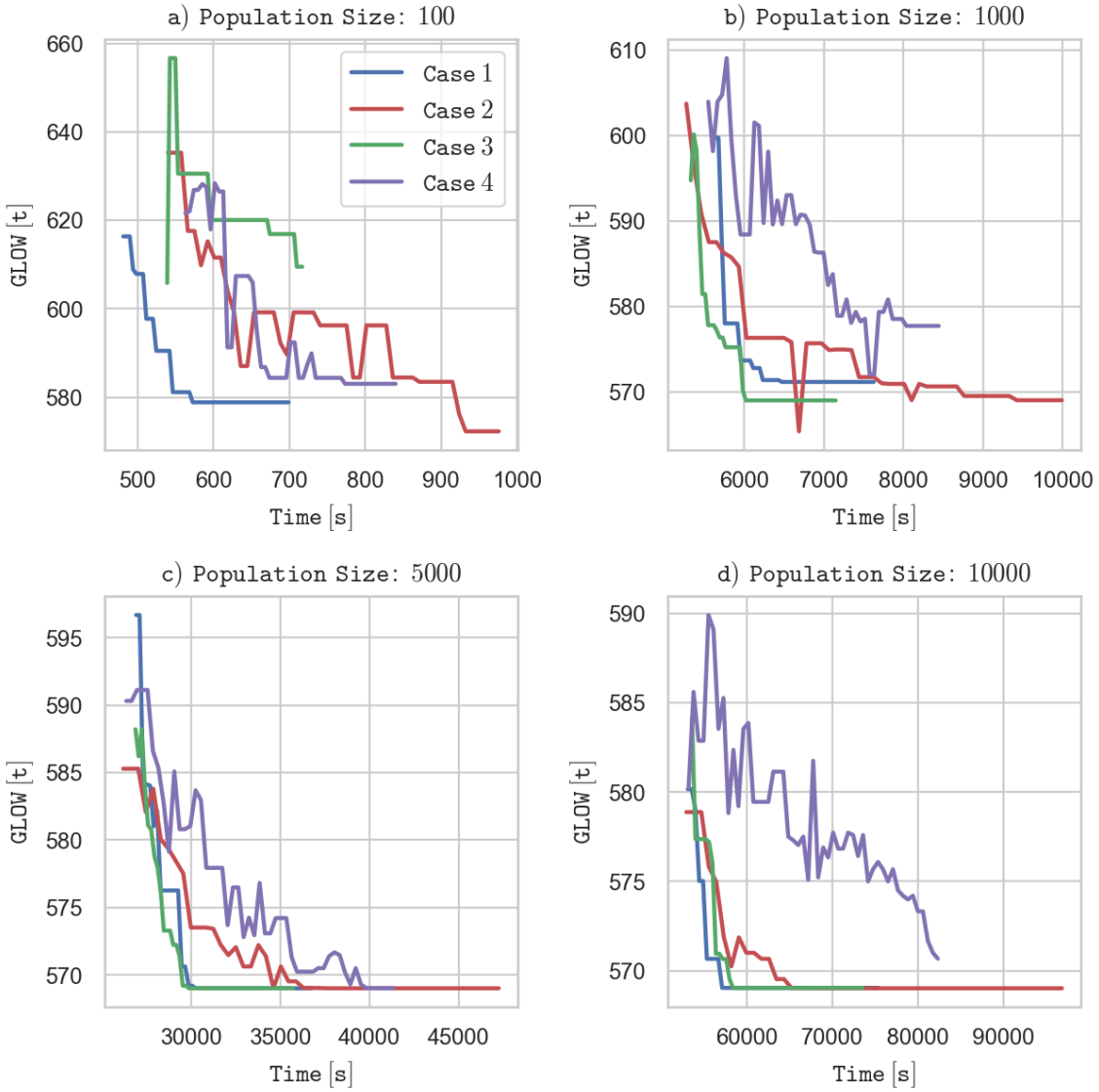

Figure 5.1: Minimum GLOW evolution over 50 generations for various hyperparameter combinations and population sizes

The input parameters regarding mission and rocket are not important at this point as only the trends and not the absolute values of the results are analyzed. It can be observed that the calculations with case 2 and case 4 parameters take significantly longer than with case 1 and case 3. This is, because the probability that parents are chosen to mate or mutate is higher and thus a larger number of new individuals is created that needs to be evaluated. Moreover, case 2 and case 4

graphs show a serrated contour. Due to a larger percentage of parents being altered by variation, loss of the best individual of a particular generation can occur, which is indicated by the curve rising. This results in the algorithm taking longer to achieve convergence on an optimum. Because of greater gene crossover and gene mutation probabilities, this effect is more pronounced in case 4 than in case 2, for which the effect lessens with increasing population size. Nevertheless, case 2 and 4 were deemed inefficient and thus unsuitable for usage in the optimizer.

Comparing case 1 and case 3, it becomes clear that the optimum parameter choice depends on the population size. For a small population size (see Fig. 5.1 a)), case 3 yielded the worst results due to a loss of solution quality during the first generational cycle and case 1 yielded the best results with a rapid improvement of the fitness value over the generations. Although convergence occurred on an individual with a higher fitness value than with greater population sizes, this setting is suitable for rapid testing of configurations or changes to the optimization program. For medium population sizes (see Fig. 5.1 b) and c)), case 3 had a slight performance and time advantage, whereas for the largest population size (see Fig. 5.1 d)) case 1 converged slightly faster. Because initialization and algorithm take twice as long for a population size of 10000 in comparison with a population of 5000 individuals while delivering the same results, the former was not used for the calculations in this thesis. Looking at Fig. 5.1 b) and c), it can be seen that for both population sizes, 1000 and 5000, case 3 converged on the same fitness value. It has to be noted that the individual with the best fitness value was found with case 2 configuration and a population size of 1000. However, it vanished within one generational cycle and was not found again.

The results in Fig. 5.1 impressively demonstrate the strengths of genetic algorithms and also reveal their weakness. In contrast to random search algorithms, which can be compared to the population initialization as individuals are randomly generated, the GA finds and improves the solutions substantially faster. Nearly for all cases and population sizes, individuals with significantly better fitness values were found by the GA after just a few generations and in a fraction of the time that was required for generating the first population. For a population size of 100 and case 1 configuration, within less than 600 s a better individual was found than the four initial populations of 10000 individuals contained after a creation time of more than 50000 s. On the other hand, the disadvantage of GAs is that it is not guaranteed that the best solution will be found. This is exposed by case 2 in Fig. 5.1 b) finding an individual with better fitness value than was found by any other configuration. Even with population sizes ten times larger, the optimizer converged on an individual with inferior fitness value.

In order to ensure a high solution quality and a stable process flow whilst keeping computation duration at a reasonable level, the case 3 parameter combination and a population size of 5000 individuals was chosen for all following calculations in this thesis. Although convergence typically occurs much earlier, the number of generations was kept at 50. While the lower mating and mutation probability of

the selected parents leads to a robust basis of individuals for each generation, the higher gene crossover and gene mutation probabilities result in a higher diversity and better representation of the search space. In combination with the relatively large population size and number of generations, this increases the probability of finding the best solution.

Chapter 6

Results and Discussion

Whereas the previous chapters dealt with the settings and validation of the optimization program, this chapter is focused on its application and the discussion of the results. First, optimized launch vehicle configurations for various mission objectives are compared with regard to propellant combination and delta-v allocation. Then, input parameters of other current launch vehicle research studies are applied and the results compared. Subsequently, sensitivity analyses are conducted to investigate the influence of specific impulse, delta-v budget and structural coefficient on launch vehicle performance. The implementation of alternative optimization objectives forms the end of this chapter. As it is of special interest, the impact of the propellant combination on the characteristics of the optimized launch vehicles is thoroughly examined. All configurations are TSTO launch vehicles with reusable first stage using gas generator engines. Unless otherwise specified, the boundaries and constraints of Appendix C were applied and the payload measurements were chosen according to Ch. 4.

6.1 Comparison of Optimized Launch Vehicle Configurations

In this section, the influence of propellant combination and delta-v allocation on the performance of a medium-lift launch vehicle similar to Falcon 9 is analyzed. For a 5000 kg payload GTO mission (12000 m/s delta-v) and a 15600 kg payload LEO mission (9500 m/s delta-v), the optimization program was executed separately for the three propellant combinations LOX/LH2, LOX/RP-1 and LOX/LCH4. As the oxidizer component is the same, only the fuel component is referred to hereafter to distinguish between the propellant combinations. Seven different delta-v allocations were investigated by fixing the first stage delta-v.

6.1.1 GTO Mission

With a GTO delta-v requirement of 12000 m/s, the following delta-v allocations were set for each of the three propellant combinations (see Table 6.1). The optimized launch vehicles of each configuration are subsequently discussed. For better overview, the results are plotted over the delta-v allocation. Detailed data can be found in Appendix D.1.

Delta-v Upper Stage [m/s]	7000	7500	8000	8500	9000	9500	10000
Delta-v First Stage [m/s]	5000	4500	4000	3500	3000	2500	2000

Table 6.1: GTO delta-v allocations

Regarding the GLOW of the launch vehicles, it can be observed that the optimized LH2 launch vehicles are significantly lighter than the RP-1 and LCH4 launch vehicles for a given delta-v allocation (see Fig. 6.1), which is the result of the high specific impulse of the LH2 combination. While showing a similar trend, the LCH4 launch vehicles are around 10% lighter than the corresponding RP-1 launch vehicles, with the difference becoming greater for bigger first stages. This is also due to the slightly better specific impulse of the LCH4 propellant combination in comparison with RP-1. For all propellant combinations, the minimum GLOW was achieved for a delta-v allocation of 3000 m/s for the first stage and 9000 m/s for the upper stage (LH2: 332 t; LCH4: 485 t; RP-1: 534 t, see Appendix D.1). Altering the allocation in any way leads to an increase of the GLOW. For the extreme delta-v allocation of 2000/10000 the optimizer did not find any solution for the RP-1 and the LCH4 propellant combination in the given time frame. This is because of the restrictions of the engine mass calculation in the optimization program, which has a range of validity of only up to 2 MN per engine for these two propellants. As the upper stage mass increases with increasing allocated delta-v, one engine producing less than 2 MN of thrust is too weak to achieve the predefined minimum acceleration for an upper stage of 10000 m/s. For launch vehicles with first stages producing more than 4000 m/s the GLOW increases drastically, becoming more than twice as large with the 5000/7000 delta-v allocation. Hence, the delta-v allocation plays an important role in launch vehicle design and needs to be considered carefully.

In Fig. 6.2, the length of the optimized launch vehicles, the total structure mass, its allocation onto the first stage and the upper stage as well as the structural coefficients of both stages are presented for each configuration.

Although the LH2 launch vehicles feature the lowest GLOWs, they are 10-30% longer than the LCH4 launch vehicle of the corresponding delta-v allocation, which in turn is up to 8% bigger than the RP-1 rocket (see Fig. 6.2 b), Appendix D.1). For the delta-v allocations 5000/7000 and 2500/9500 both hydrocarbon propellant combinations show very similar lengths. The difference in size is mostly due to the

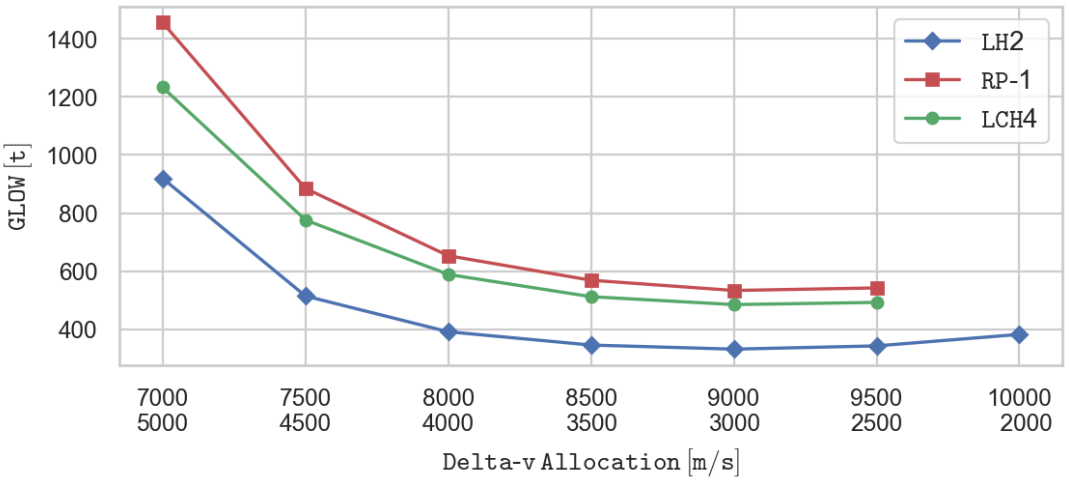

Figure 6.1: GLOW comparison of the optimized GTO mission launch vehicles

differing propellant densities of the fuel components (see Table 2.5). Although LH2 and LCH4 rockets feature higher ROFs and require less propellant because of their specific impulse, RP-1 is more than eleven times as dense as LH2 and close to two times as dense as LCH4, which leads to smaller rocket sizes.

The total structure mass and first stage structure mass of the launch vehicles show a trend similar to the GLOW, however more pronounced and with a different order (see Fig. 6.2 a) and c)). According to the rocket length, the LH2 launch vehicles have the highest structure mass, whereas RP-1 and LCH4 have nearly equivalent total and first stage structure masses. For large upper stages RP-1 has a small structure weight advantage and for large first stages, LCH4 has slightly lighter structures, because for this configuration the difference in GLOW becomes greater, which means that RP-1 rockets require more powerful and thus heavier propulsion systems. The fact that the LH2 first stage structure mass increases with decreasing first stage delta-v for the delta-v allocations 2500/9500 and 2000/10000 is addressed later on.

Regarding the upper stage, the logical trend of larger structure masses for larger upper stages can be observed (see Fig. 6.2 d)). However, a minimum is achieved for LCH4 and RP-1 launch vehicles for the delta-v allocation 4000/8000 and for LH2 launch vehicles for the 4500/7500 delta-v allocation, with the upper stage structure mass increasing for a decreased upper stage delta-v past that point. The propulsion system is responsible for this phenomenon, which is similar to the higher LH2 structure mass of smaller first stages. This is also addressed in the following discussion of the propulsion systems. For very large upper stages the structure mass is increased dramatically, by up to 70% for RP-1 and LCH4 and by up to 140% for the LH2 launch vehicle in comparison with the minimum value. For all configurations, LH2 launch vehicles have the highest upper stage structure mass, followed by LCH4 launch vehicles while RP-1 launch vehicles have the lightest upper stage structures.

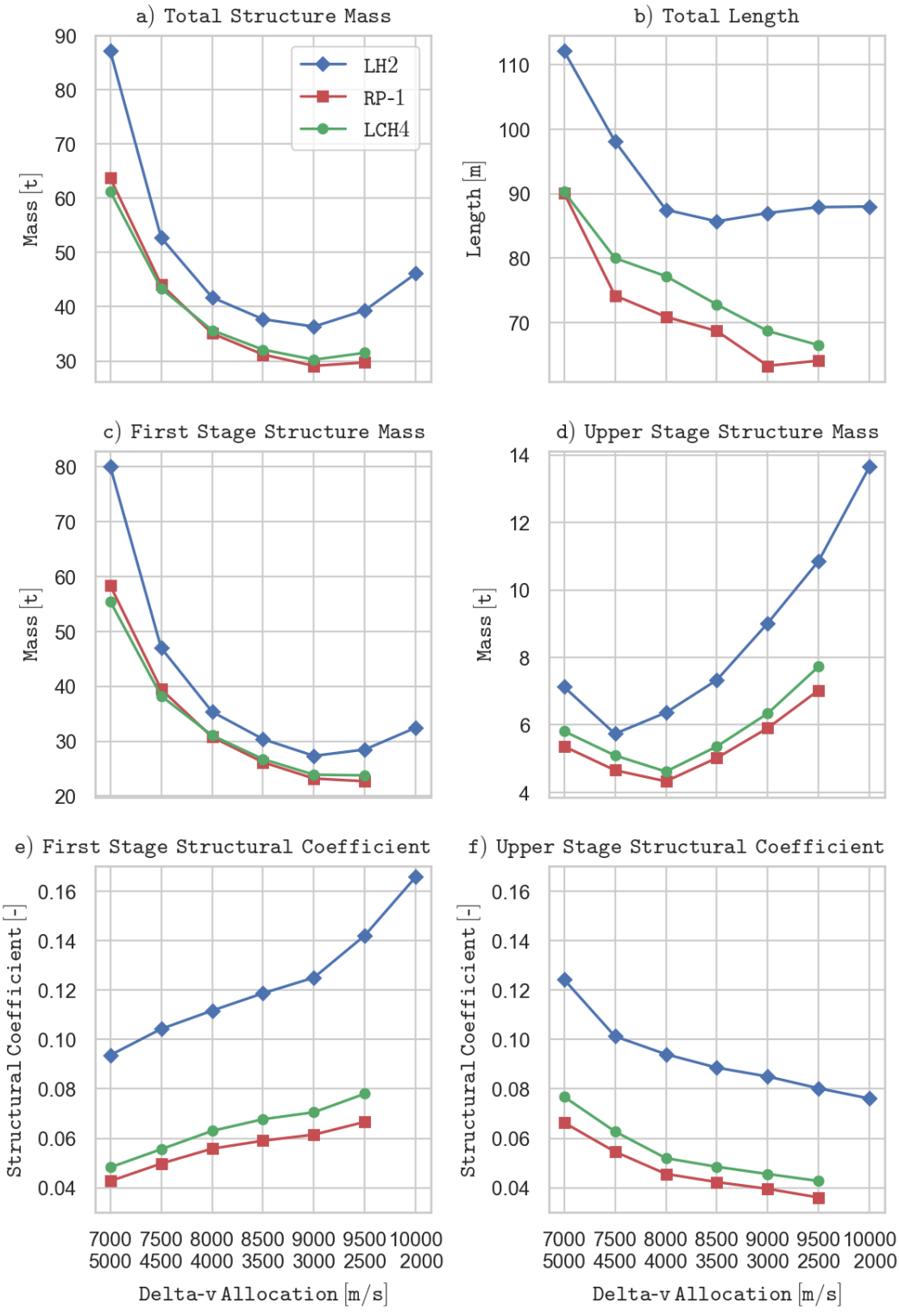

Figure 6.2: Structure comparison of the optimized launch vehicles

With respect to the structural coefficients (see Fig. 6.2 e) and f)), a clear dependence on the delta-v of the respective stage can be seen. Increasing the delta-v and hence the required propellant mass of a stage leads to a smaller structural coefficient which is beneficial for performance. Starting with the minimum first stage structural coefficient, the rate of increase declines until the minimum GLOW configuration with the 3000/9000 delta-v allocation. Decreasing the first stage delta-v further results in a greater increase of the structural coefficient. This is because for first stages with less than 3000 m/s the structure mass increases (LH2) or stays nearly constant (RP-1, LCH4) while the propellant mass decreases. Similarly, the upper stage structural coefficient is minimal for the largest upper stage configuration and increases approximately linearly until the 4000/8000 (RP-1, LCH4) and the 4500/7500 delta-v allocation (LH2), respectively. This coincides with the minimum upper stage structural mass of the respective propellant combination. Further decreasing the upper stage delta-v leads to a sharper increase in the structural coefficient, as the propellant mass decreases while the structure mass increases. For both stages, the LH2 launch vehicles feature the largest structural coefficients with a great margin towards the LCH4 launch vehicles, which in turn have a slightly higher structural coefficient than the RP-1 rockets.

In Fig. 6.3, an overview over the propulsion systems of the optimized launch vehicles is given. The total thrust of first and upper stage, the number of first stage engines as well as combustion chamber pressure, mixture ratio, nozzle area expansion ratio and the specific impulses of the engines are presented and subsequently discussed.

The curves of the total first stage sea level thrust look similar to the curves of the GLOW, as the first stage engines need to accelerate the entire launch vehicle with the predefined minimum acceleration at engine ignition (see Fig. 6.3 a)). Therefore, LCH4 and RP-1 launch vehicles require propulsion systems that deliver higher thrust levels than LH2 launch vehicles. It has to be noted that the first stage thrust increases more strongly than the GLOW for the 2500/9500 and 2000/10000 delta-v allocations, indicating a more powerful propulsion system than necessary. Fig. 6.3 b) shows the total upper stage vacuum thrust, which is equal to the thrust of one upper stage engine, because only one engine is used to power the upper stage. Here, a similar trend can be observed as with the upper stage structure mass. The engine thrust increases for launch vehicles with larger upper stages, however the thrust is minimal for the 4000/8000 (LCH4, RP-1) and for the 4500/7500 delta-v allocation (LH2), respectively. For smaller upper stages, the engine thrust is increased, again indicating the use of an oversized propulsion system.

As the same combustion chamber must be used for first and upper stage engines, the thrust of one first stage engine is similar to the thrust of the upper stage engine, albeit slightly lower. This method implies that multiple engines are required to power the first stage. The number depends on the GLOW of the launch vehicle and the weight of the upper stage, which has influence on the minimum size of one engine. For the delta-v allocations that result in the heaviest launch vehicles,

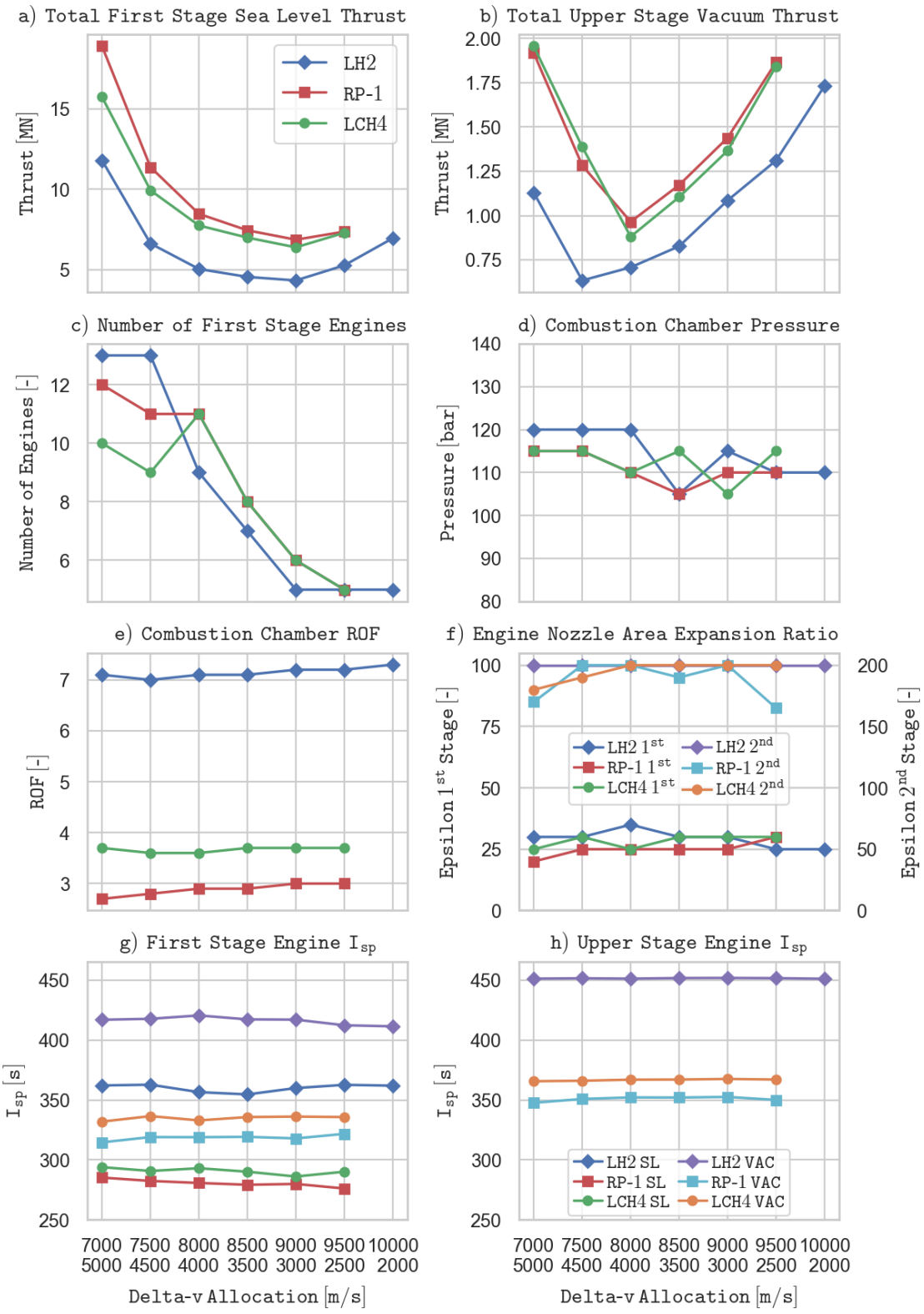

Figure 6.3: Propulsion system comparison of the optimized launch vehicles

10-13 engines are used for the first stage depending on the propellant combination (see Fig. 6.3 c)). This number decreases to 5 for lighter launch vehicles with a large upper stage delta-v, as this entails engines that are two times (LCH4, RP-1) or three times (LH2) as powerful as the configuration with minimum thrust engines (see Fig. 6.3 b)). For the delta-v allocations that lead to the smallest engines, a peak in the number of first stage engines can be observed for the LCH4 launch vehicle and the number of first stage engines for the LH2 and RP-1 launch vehicles stays the same as for the next heavier configuration with stronger engines.

The combustion chamber pressure (see Fig. 6.3 d)) and mixture ratio (see Fig. 6.3 e)) are the same for first and upper stage engines due to the requirement of the same combustion chamber and the resulting method of calculation in the optimization program. For all configurations and propellant combinations, the combustion chamber pressure ranges between 105 and 120 bar, which is close to or at the optimum of a gas generator engine (see Fig. 2.10). Regarding the mixture ratio, the optimizer chose ROFs that deliver the optimum specific impulse or slightly higher ROFs for LCH4 and RP-1 launch vehicles, whereas the ROF of the LH2 launch vehicles was chosen closer to the stoichiometric combustion, which requires more oxidizer than the composition for the optimum specific impulse thus leading to smaller tanks and a reduced rocket size (see Table 2.5). With ROF ranges of 2.7-3.0 and 7.0-7.3 for RP-1 and LH2 respectively, a slight increase in ROF is observable with increasing upper stage delta-v, whereas the ROF of the LCH4 launch vehicles varies between 3.6-3.7 (see Appendix D.1).

Differing between first and upper stage engines, the nozzle area expansion ratio influences the engines' specific impulse as well as flow stability in light of the ambient conditions. Looking at Fig. 6.3 f), it can be seen that with two exceptions the first stage engine expansion ratio lies between 25 and 30. Most upper stage engines have an expansion ratio of 200, which was the predefined upper boundary. The deviations for a large upper stage delta-v (RP-1) and large GLOWs (RP-1, LCH4) are the result of high-thrust engines with greater nozzle throat areas that would not fit in the upper stage diameter with a greater expansion ratio.

The specific impulse of the engines is subject to the propellant combination, the combustion chamber pressure, the ROF and the nozzle area expansion ratio. Although the sea level and vacuum I_{sp} of the first stage engines and the vacuum I_{sp} of the upper stage engines is mostly constant for all configurations of each propellant combination (see Fig. 6.3 g) and h)), some trends and coherences can be analyzed. As expected, the LH2 launch vehicles feature by far the highest specific impulses, followed by LCH4 launch vehicles, which have an around 2-5% higher I_{sp} than the RP-1 rockets, depending on the configuration (see Appendix D.1). Regarding the LCH4 first stage engines, the highest sea level specific impulses are achieved with the 5000/7000 and 4000/8000 delta-v allocations, which coincide with the lowest vacuum specific impulses. This is the result of the lower nozzle area expansion ratio of 25. Similarly, for the RP-1 launch vehicles the first stage engine expansion ratio of 20 results in the highest sea level and the lowest vacuum I_{sp} (5000/7000 delta-v

allocation) and the expansion ratio of 30 leads to the lowest sea level and highest vacuum I_{sp} (2500/9500 delta-v allocation). The expansion ratio of 35 of the LH2 launch vehicle with 4000/8000 delta-v allocation yields the highest first stage vacuum I_{sp} but also a lower sea level specific impulse. Examples of the influence of the combustion chamber pressure are the sea level specific impulses of the 3000/9000 LCH4 and the 3500/8500 LH2 launch vehicles. The relatively low combustion chamber pressure of 105 bar leads to the lowest sea level I_{sp} of all configurations of the respective propellant combination. This influence appears to be smaller in case of the vacuum specific impulse. Regarding the vacuum specific impulse of the upper stage engines, nearly constant values are achieved for most launch vehicles of each propellant combination. Only the configurations with smaller nozzle area expansion ratio exhibit a slightly lower I_{sp}. Comparing the RP-1 launch vehicles with the two largest upper stages shows the influence of the expansion ratio as ROF and combustion chamber pressure are the same. Reducing the expansion ratio from 200 to 165 entails a decrease in I_{sp} of 2.5 s, which amounts to only 0.7% (see Appendix D.1). A more detailed engine mass estimation model, which better reflects the weight of the nozzle, could be implemented in the future to examine the behaviour of the optimization program to choose the highest possible expansion ratio.

In order to understand the optimum propulsion system choice, the stages' acceleration at engine ignition is examined. Fig. 6.4 a) shows that for the delta-v allocations of 4000/8000, 3500/8500 and 3000/9000 the propulsion systems of both the first and the upper stage deliver minimum acceleration levels just above the requirements. For larger first stages, more powerful propulsion systems are required, which results in a larger number of and more powerful engines. This leads to oversized engines in the upper stage and hence acceleration levels well above the required minimum. On the other hand, very large upper stages also require a powerful engine, leading to higher acceleration levels of the first stage propulsion system. These trends were already indicated by Fig. 6.3 a) and b). The minimum acceleration of 1.85 g of the LH2 launch vehicle with 2000/10000 delta-v allocation implies that four instead of five engines would have delivered sufficient thrust levels, but a minimum of five engines was set for the first stage. While this requirement makes sense to prioritize a greater number of first stage engines over the optimum upper stage engine size, adding an extra engine that is thrust-wise not needed defeats the purpose. The oversized engines of very small upper and first stage configurations as well as the unnecessary additional first stage engine of the LH2 launch vehicle with 2000/10000 delta-v allocation are the reason behind the already discussed increase in stage structure mass for a decrease in delta-v of the respective stage (see Fig. 6.2 c) and d)). Furthermore, the excessively strong engines of small upper stages and the required high thrust engines of the largest upper stages lead to unsuitable acceleration levels towards the end of the upper stage engine burn, even with consideration of an engine throttle (see Ch. 3.3.1, Appendix D.1). The LH2 launch vehicles feature higher structure masses whilst requiring lower thrust propulsion systems, hence experiencing lower maximum acceleration levels. Additional constraints that lead to smaller upper stage engines and thus a higher number of first stage engines as well

as a lower upper stage minimum acceleration could resolve this issue in the future.

Fig. 6.4 b) depicts the propulsion system mass, including engines and TVC system, of upper and first stage for all configurations. The graphs show trends similar to the total stage thrust, however because of heavier engines, LH2 launch vehicles do not always have the lightest propulsion systems. Depending on the delta-v allocation, either LH2 or LCH4 launch vehicles feature smaller propulsion system masses, with RP-1 launch vehicles having propulsion system masses similar to LCH4 launch vehicles in all upper stages and in first stages for large upper stage delta-v's. The influence of the number of engines on the propulsion system mass can be observed by comparing LCH4 launch vehicles with the 5000/7000 and 4000/8000 delta-v allocations. The higher thrust level and smaller number of engines of the former leads to a thrust-to-weight ratio of 93, whereas the lower thrust level and higher number of engines of the latter results in a thrust-to-weight ratio of 69 for the entire first stage propulsion system. This is indicated by a small peak in first stage propulsion system mass for the 4000/8000 LCH4 launch vehicle in relation to the other configurations.

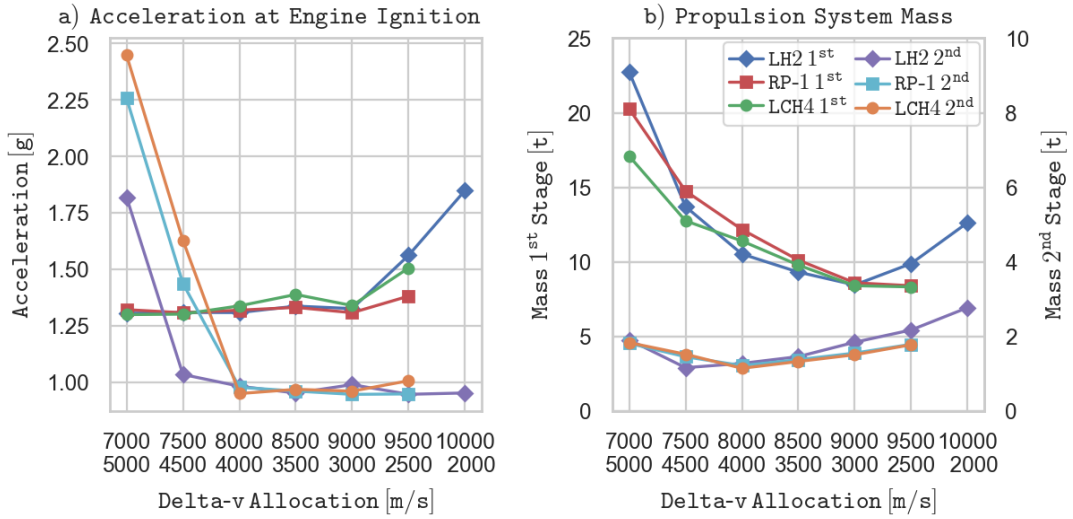

Figure 6.4: Minimum acceleration and propulsion system mass comparison of the optimized launch vehicles

6.1.2 LEO Mission

Whereas the characteristics of the optimized GTO launch vehicles were discussed in great detail in the last section, this section is focused on the comparison of GTO and LEO launch vehicles. With a LEO delta-v requirement of 9500 m/s, the following delta-v allocations were set for each of the three propellant combinations (see Table 6.2). Subsequently, the optimized launch vehicles of each configuration are compared to their counterpart of the GTO mission to determine the versatility

of the launch vehicles. For better overview, the results are plotted over the first stage delta-v, as the upper stage delta-v differs between the two missions. Detailed data can be found in Appendix D.1 and D.2.

Delta-v Upper Stage [m/s]	4500	5000	5500	6000	6500	7000	7500
Delta-v First Stage [m/s]	5000	4500	4000	3500	3000	2500	2000

Table 6.2: LEO delta-v allocations

Comparing the GLOWs of the optimized launch vehicles of both missions, it can be observed that for most delta-v allocations the curves of the GTO and the LEO mission are very similar, diverging only for configurations with small first stages (see Fig. 6.5). The LCH4 and RP-1 rockets of the GTO mission are heavier than of the LEO mission for all delta-v allocations except for the 4000 m/s first stage. Of the LH2 launch vehicles, LEO configurations with a first stage delta-v equal to or greater than 3500 m/s are heavier than the respective GTO mission rocket.

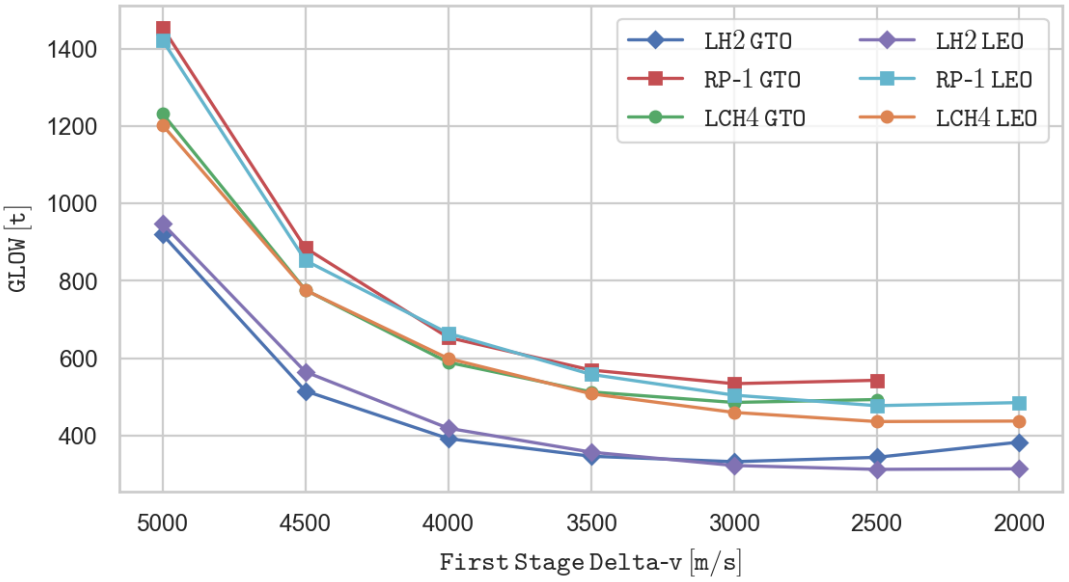

Figure 6.5: GLOW comparison of the GTO and LEO mission launch vehicles

In order to determine if the GTO launch vehicles are capable of accomplishing the LEO mission and vice versa, the delta-v performance of each vehicle was calculated for both payload bay mass configurations. Fig. 6.6 shows for each propellant combination the achievable delta-v of the GTO launch vehicle and the LEO launch vehicle with the GTO payload (see Fig. 6.6 a), c) and e)) as well as the achievable delta-v of the LEO launch vehicle and the GTO launch vehicle with the LEO

payload (see Fig. 6.6 b), d) and f)). It can be seen that for all delta-v allocations the LEO launch vehicles are not capable of delivering the same delta-v as the GTO launch vehicles for the same payload. On the other hand, all GTO launch vehicles are capable of accomplishing the LEO mission.

Regarding the LEO launch vehicles, the configurations with a first stage delta-v of 3500 m/s (LCH4, RP-1) and 4000 m/s (LH2) present the highest performance for the GTO mission. While the latter nearly achieves 12 km/s delta-v, the LCH4 and RP-1 rockets show a poorer performance. Contrarily, the LCH4 and RP-1 GTO launch vehicles outperform the LH2 rockets of the respective configurations for the LEO mission for most delta-v allocations (see Appendix D.1 and D.2). The GTO launch vehicles with a 4000 m/s delta-v first stage present the lowest LEO mission performance and are closest to the performance of the LEO launch vehicles. These trends indicate that the hydrocarbon propellants yield an advantage for LEO missions and hydrogen for GTO missions. This is examined later in Ch. 6.4.

As the first stage delta-v calculations for the data in Fig. 6.6 were made using the mean I_{sp} that was determined via the trajectory simulation, a small inaccuracy could be the result of altering the payload bay mass and therefore changing the acceleration values. However, for GTO vehicles with LEO payload minimum acceleration values did not fall under 0.85 g for the upper stage and 1.27 g for the first stage, which is deemed to be acceptable albeit lower than the minimum acceleration constraint in the optimization program.

Overall, the GTO launch vehicles with the 3000/9000 delta-v allocation have the smallest GLOW of all launch vehicles that are capable of completing both GTO and LEO mission. Nevertheless, in terms of reusability it could be economically advantageous to opt for a launch vehicle configuration with a higher first stage delta-v. Although this entails a heavier launcher, a greater portion of the rocket would be reusable. A correlation of the number of reuses of the launch vehicle's first stage and the optimum delta-v allocation is investigated in Ch. 6.4. While the LH2 propellant combination achieves the launch vehicles with the smallest gross lift-off weight, their disadvantages are a larger size and structure mass. Comparing the LCH4 and RP-1 launch vehicles shows that the former have a lower GLOW while the latter have a small size advantage. Both feature similar structure masses.

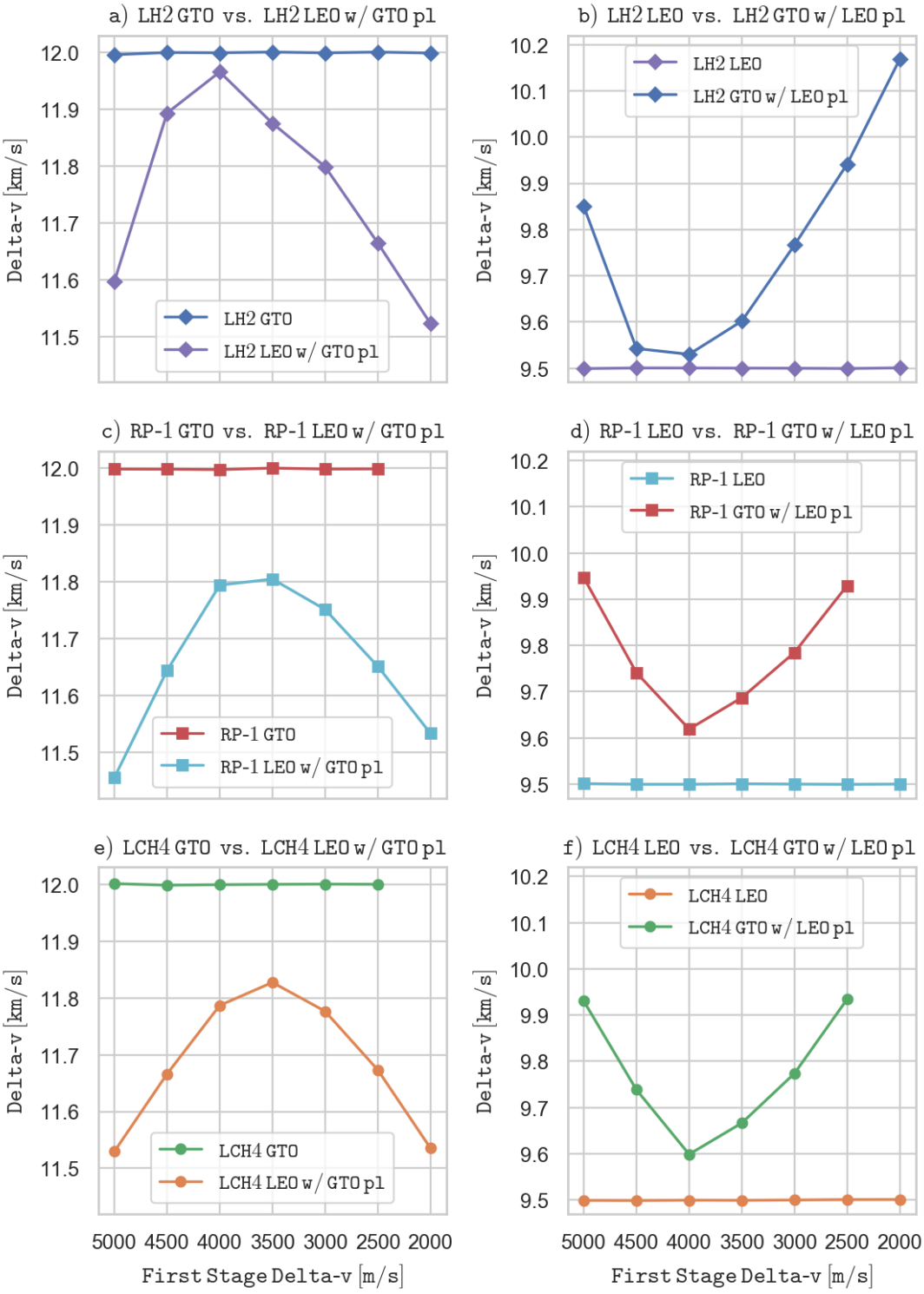

Figure 6.6: Delta-v capability comparison of GTO and LEO launch vehicles with GTO payload as well as LEO and GTO launch vehicles with LEO payload

6.2 Comparison with Current Launch Vehicle Research Studies

This chapter is focused on a comparison of the results of the optimization program that was developed in the course of this thesis with various current launch vehicle research studies. For this purpose, the studies XTRAS, AKIRA, ENTRAIN and RETALT were chosen, as they all investigate launch vehicle configurations with reusable first stages. Here, comparisons are only made with TSTO launch vehicles that land downrange by means of retropropulsion using gas generator engines with the LOX/LH2, LOX/RP-1 and LOX/LCH4 propellants or a combination of those. As the oxidizer is the same for all propellant combinations, only the fuel is referred to in order to distinguish between different combinations hereafter.

6.2.1 XTRAS / AKIRA (DLR)

The XTRAS and AKIRA studies were conducted at the DLR in Bremen, Germany, to compare different methods of landing reusable first stages regarding performance and other characteristics as well as to identify necessary key technologies [19, 20]. As both studies were conducted by the same authors and the same mission objective was applied, they are examined in the same section. The considered mission consists of delivering a 7500 kg payload into a GTO orbit. Furthermore, the same propellant combination and combustion chamber are used for both stages. In both studies, launch vehicles were calculated with a 6600 and 7000 m/s upper stage delta-v. Unfortunately, no direct information is given on the total delta-v budget or the assumed delta-v losses in the XTRAS study. Thus, the first stage delta-v is unknown. The relatively low upper stage delta-v's are the reason why the optimization program was also executed for 11500 m/s in addition to the standard 12000 m/s delta-v budget. Calculations were made for the three propellant combinations LOX/LH2, LOX/RP-1 and LOX/LCH4 with the same first stage delta-v allocations as in the previous section. Detailed data can be found in Appendix D.3 and D.4.

For both delta-v budgets, the GLOWs of the optimized launch vehicles are presented in Fig. 6.7. If a launch vehicle configuration is not represented, no individual was found by the optimization program in the given time frame. As already observed, the GLOW increases dramatically for low upper stage delta-v allocations. This raises the question of the reason behind the delta-v allocations chosen for final investigation in XTRAS and AKIRA.

XTRAS
In a first design loop, launch vehicle masses were calculated with historical structural indices. As no data exist for LCH4 launchers, the values were interpolated with the ones for LH2 and RP-1 launch vehicles according to their density. The first results with upper stage delta-v's ranging between 6.6 and 7.6 km/s indicated

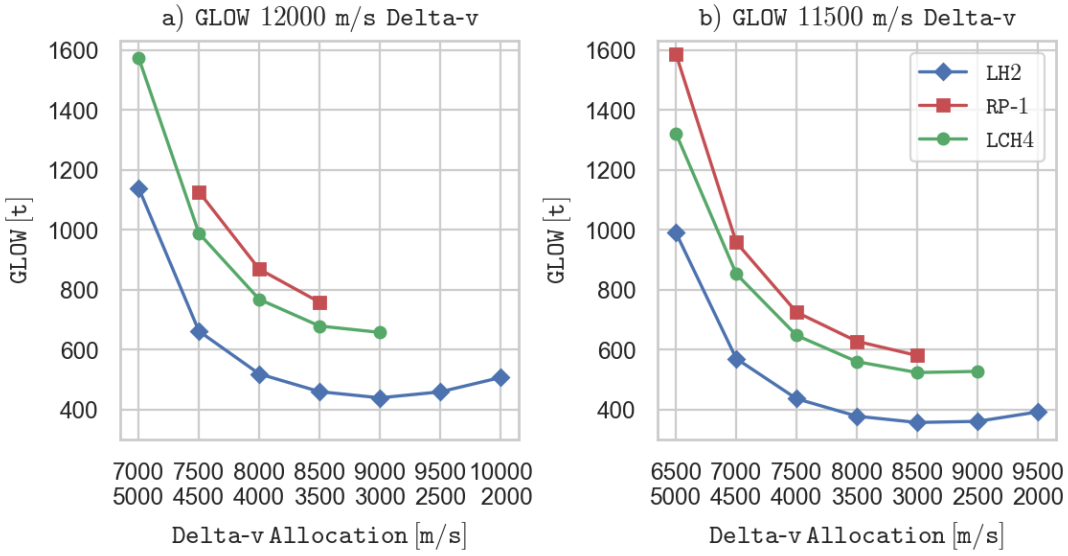

Figure 6.7: GLOW comparison for a 12000 m/s and a 11500 m/s delta-v budget

that the optimum lies between 6.6 and 7.0 km/s with 6.6 km/s yielding a weight advantage [19]. This is why those two upper stage delta-v's were chosen for further study. The final results are presented in Table 6.3 and show a reversed trend with the launch vehicles with 7.0 km/s upper stage delta-v being significantly lighter, however it was not taken into consideration that an even higher upper stage delta-v might further decrease the GLOW. RP-1 launch vehicles were not included at this point in the study.

Comparing the LH2 and LCH4 optimized launch vehicles with the results of the study, it can be seen that the trend of lighter launch vehicles for higher upper stage delta-v's is similar. However, for a delta-v budget of 12 km/s the lowest examined upper stage delta-v was 7 km/s as this delta-v allocation yields a significant increase in GLOW, higher than in the XTRAS study. In comparison with the results of the 11.5 km/s delta-v budget, the LH2 vehicles of the XTRAS study feature 15-40% lower GLOWs and the LCH4 vehicles 33-62% higher GLOWs than the launch vehicles output by the optimization program with 6.5 and 7.0 km/s upper stage delta-v (see Appendix D.4). Regarding the length, the same trend is observed for these configurations, with the XTRAS LH2 vehicles being around 20% smaller and LCH4 vehicles being 10-20% larger than their counterparts of the optimization program. One measure for the structural efficiency of a launch vehicle in the XTRAS, AKIRA and ENTRAIN studies is the structural index (SI), which is defined as the structure mass of a stage divided by its propellant mass. Values that were deduced from graphs are marked with an asterisk (*).

$$SI = \frac{m_s}{m_p} \tag{6.1}$$

Propellant Combination	**LOX/LH2**		**LOX/LCH4**	
Upper Stage Δv [km/s]	6.6	7.0	6.6	7.0
Length [m]	89.6	82.2	99.2	92.8
GLOW [t]	602	479	1761	1384
Upper Stage SI [%]	12	10.5	7.8*	6.4*
First Stage SI [%]	12.5	14	8.8*	8.9*
Landing Propellant Mass Fraction [%]	10	6.5	9.0	7.0
Upper Stage I_{sp} (ε=120) [s]	440.4		348	
First Stage Sea Level/Vacuum I_{sp} (ε=20) [s]	366/405.5		289/320	

Table 6.3: XTRAS study results [19]

As the upper stage SI in the studies includes the fairing mass [19], all payload bay masses except the payload itself were included in the calculation of the upper stage SI in the optimization program. Comparing the SIs, a 50-60% higher upper stage SI for both propellant combinations and a 20% (LH2) and 40% (LCH4) lower first stage SI can be seen in the optimized launch vehicles with 11.5 km/s delta-v budget and 6.5 as well as 7.0 km/s upper stage delta-v in contrast to the vehicles of the XTRAS study. The results of the optimizer indicate that the SIs are strongly dependent on the delta-v allocation. For the largest first or upper stage delta-v's the SI is reduced by around 50% in comparison with the smallest stage delta-v's.

The landing propellant mass fraction is used as a measure in the XTRAS study and represents the ratio of the propellant mass required to land the first stage to the first stage wet mass (structure mass + propellant mass). This is also highly dependent on the delta-v allocation because a higher upper stage delta-v implies a lower first stage delta-v, which reduces the velocity at stage separation. For the optimized launch vehicles that were already used for comparison, landing propellant mass fractions of 13.3 and 11.6% as well as 9.9 and 8.6% were obtained for the LH2 and LCH4 launch vehicles with 6.5 and 7.0 km/s upper stage delta-v, respectively (see Appendix D.4). This represents 33-78% (LH2) and 10-23% (LCH4) higher values than for the launch vehicles of the XTRAS study. As no assumptions for the calculation of the descent propellant mass are given, these major and uneven deviations cannot be analyzed at this point.

Regarding the engines in the XTRAS study, a combustion chamber pressure of 120 bar, a nozzle area expansion ratio of 20 for the first stage and 120 for the upper stage as well as an engine ROF of 6.0 for LH2 and 2.5 for LCH4 were fixed. The ROFs of the combustion chamber are not listed. For the calculations in the optimization program, no parameters were fixed and no additional boundaries were applied. The engines of the optimized launch vehicles feature combustion chamber pressures of 110-120 bar, expansion ratios of 20-30 in the first stage and 170-200 in the upper stage.

In order to compare the performance of the first stage engines, the LH2 launch vehicle with 3000/8500 and the LCH4 launch vehicle with 5000/7000 delta-v allocation are selected, because both feature a first stage engine expansion ratio of 20. Whereas the sea level and vacuum I_{sp} of the LH2 launch vehicle show a deviation of only 0.2% in comparison with the XTRAS study, the LCH4 vehicle of the study features a 2.8 and 2.4% lower sea level and vacuum I_{sp} than the vehicle of this thesis. As the upper stage engine expansion ratio of the optimized launch vehicles is higher than of the vehicles in the XTRAS study, higher specific impulses are expected and a direct comparison cannot be made, however the trend is similar with an around 2.7% higher upper stage engine vacuum I_{sp} of the optimized LH2 vehicles and a 4.9% higher vacuum I_{sp} of the LCH4 vehicles in comparison with the XTRAS study.

Overall, a direct comparison is aggravated by missing information regarding the total delta-v budget in the report of the XTRAS study. Most trends of the study could not be replicated with the optimization program, e.g. the massive discrepancy between the two propellant combinations regarding the GLOW, LH2 launch vehicles being smaller than the LCH4 rockets as well as the upper stage SI being lower than the first stage SI for this upper stage delta-v. On the basis of the results obtained in this thesis, the upper stage delta-v allocation choice in the XTRAS study seems questionable. Furthermore, the 35% decrease in landing propellant mass fraction between LH2 launch vehicles with 6.6 and 7.0 km/s upper stage delta-v raises the question of how the landing propellant mass is estimated. The nonexistent or lower differences in I_{sp} between the LH2 launch vehicles on the one hand and the significant deviations in I_{sp} between the LCH4 launch vehicles on the other hand, indicate rather conservative assumptions solely for the calculation of the LCH4 engines in the XTRAS study.

AKIRA

The AKIRA study is assumed to have been conducted in the same framework as XTRAS, which is why a different focus is laid on in the comparison with the optimized launch vehicles. The GLOW of the launch vehicles with LOX/LH2, LOX/RP-1 and LOX/LCH4 propellant combination and 7.0 km/s upper stage delta-v are presented in Table 6.4. As the study deals with the delta-v of the landing maneuver, values for the delta-v's that represent the velocity increase due to gravitation during descent as well as the velocities that are compensated by aerodynamic drag and the engines are also given. The total velocity reduction is the sum of the three components. All values were deduced from graphs and may therefore be not completely accurate.

For the following comparison, the optimized launch vehicles with a delta-v budget of 11.5 km/s and a 7.0 km/s upper stage delta-v are selected. The GLOWs of the AKIRA study are lower than the ones of the XTRAS study. In comparison with the optimized launch vehicles, the LH2 AKIRA launch vehicle features a 23% lower GLOW and the RP-1 and LCH4 launch vehicles a 19% and 34% higher GLOW, respectively (see Appendix D.4).

Propellant Combination	**LOX/LH2**	**LOX/RP-1**	**LOX/LCH4**
GLOW [t]	440	1140	1150
Δv Gravitation [m/s]	+875	+700	+700
Δv Drag [m/s]	-2500	-2125	-2125
Δv Engines [m/s]	-1250	-1425	-1500
Total Velocity Reduction [m/s]	-2875	-2850	-2925
Δv First Stage Ascent [m/s]	+4050	+3850	+3925
Δv Losses Ascent [m/s]	-1175	-1000	-1000

Table 6.4: AKIRA study results [20, 21]

Regarding the delta-v for the landing, the AKIRA launch vehicles deliver between 1250 and 1500 m/s delta-v with their engines and a total velocity reduction of 2850-2925 m/s is achieved considering drag and the velocity added by gravitation. This is assumed to be equal to the total first stage delta-v of the ascent reduced by the delta-v losses during ascent, which are presented by the same authors in [21] and are also depicted in Table 6.4. In [21] the landing delta-v of the engines is added to the first stage ascent delta-v for comparison, however this is highly misleading as the delta-v calculation for ascent incorporates the entire upper stage as payload whereas the delta-v calculation for the descent of the first stage comprises only the first stage structure mass as the final mass of the vehicle (see Eq. 2.6).

Values of around 4.0 km/s are given for the first stage ascent delta-v, differing slightly between the launch vehicles. This means that with a 7.0 km/s upper stage delta-v the total delta-v budget of the launch vehicles is roughly 11.0 km/s, which is only sufficient for a GTO mission with launch site in Kourou if the accumulated delta-v losses do not exceed relatively low 1000 m/s and no safety margins are considered. As the first stage delta-v's of the RP-1 and LCH4 launch vehicles are lower than 4.0 km/s and the delta-v losses for the LH2 launch vehicle are higher than 1000 m/s, the delta-v budget of the presented launch vehicles is deemed critically low for a GTO mission if these values are correct.

Comparing the delta-v which is compensated by aerodynamic drag during reentry, it can be observed that the LH2 launch vehicle features a 17% higher value than the RP-1 and LCH4 launch vehicles (see Table 6.4). This is justified with a lower ballistic coefficient of the LH2 launch vehicle stemming from the low bulk density of the LOX/LH2 propellant combination and the resulting higher ratio of launcher volume to mass [20]. As no definition of the ballistic coefficient (BC) is given, the following will be used for a trend analysis of the optimized launch vehicles [48]:

$$BC = \frac{M}{C_d \cdot A} \tag{6.2}$$

with M being the launch vehicle mass at the considered point in time, C_d the drag coefficient and A the cross-sectional area of the rocket. The drag coefficient is assumed to be similar for all regarded launch vehicles and is not analyzed. Regarding the M to A ratio of the reusable first stages after stage separation, the RP-1 and LCH4 launch vehicles feature a 0.7% and 5.4% higher value than the LH2 launch vehicle for the 4500/7000 delta-v allocation, respectively (see Appendix D.4). As the RP-1 and LH2 first stages have the same stage radius, the similar mass at MECO leads to this small difference. The LCH4 first stage has a 7.5% lower cross-sectional area and a 2.5% lower mass than the LH2 stage, resulting in the higher M to A ratio. The similar first stage mass for all propellant combinations at stage separation might surprise as the GLOWs of the LCH4 and RP-1 launch vehicles are 50% and 68% higher than the GLOW of the LH2 launch vehicle with this configuration (see Appendix D.4). However, the hydrocarbon first stages feature a 20% smaller first stage structure mass, which in combination with a 12% (LCH4) and 19% (RP-1) higher landing propellant mass leads to similar stage masses before the reentry burn for this delta-v allocation (see Fig. 6.8). It can be assumed that this composition results in lower masses of the hydrocarbon stages and therefore a lower ballistic coefficient during the descent, which increases drag.

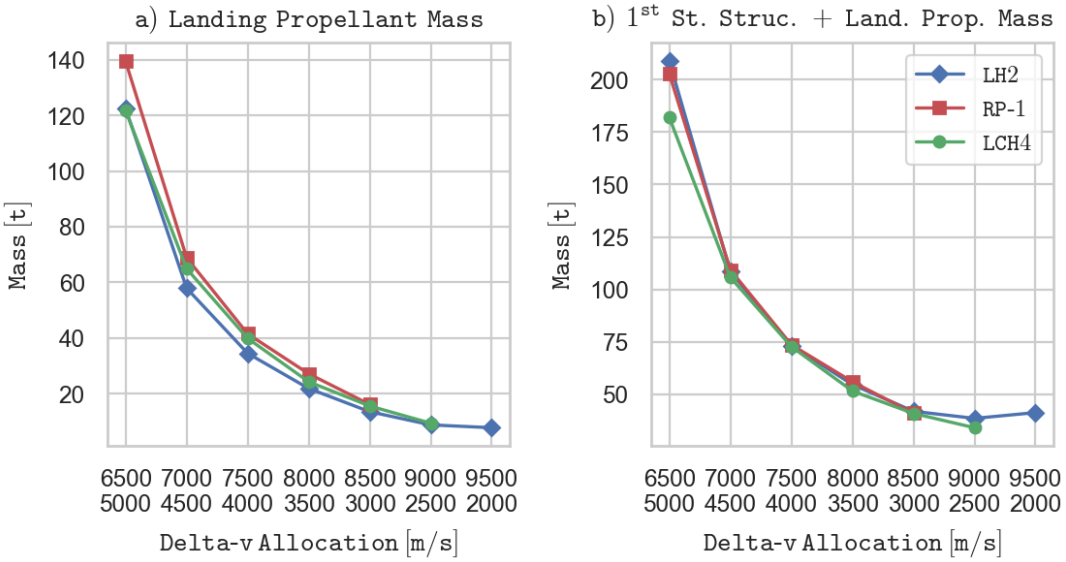

Figure 6.8: Landing propellant mass comparison and first stage structure + landing propellant mass comparison

In the optimization program the delta-v due to atmospheric drag is considered to be constant 1500 m/s for all propellant combinations and first stage ascent delta-v's. It was derived from the delta-v that the engines of the Falcon 9 rocket provide during descent and its ascent delta-v. This way, the descent delta-v of launch vehicles with different delta-v allocations are linked to the Falcon 9 delta-v allocation. Differences are compensated by varying the reentry burn, hence a constant stage velocity can

be assumed upon entering the denser parts of the atmosphere in which atmospheric drag becomes of importance. This also keeps the reentry loads at a constant level. For first stages with very small ascent delta-v, the minimum descent delta-v was set equal to Falcon 9's landing burn delta-v (see Ch. 2.3.2).

With respect to the examination of the ballistic coefficient, the assumption of the same drag delta-v for all propellant combinations in the optimization program is deemed valid. In comparison with the AKIRA study, the large difference in BC entailing an advantageous higher drag delta-v of the LH2 launch vehicle could not be replicated with the optimized launch vehicles. The estimated delta-v due to atmospheric drag in the optimization program is much lower than in the AKIRA study and is set against the total first stage ascent delta-v, which leads to the engines having to provide a higher delta-v for the landing. Less efficient engines and higher structural indices are assumed to be responsible for the hydrocarbon launch vehicles of the AKIRA study still being heavier than the corresponding optimized launch vehicles despite having lower delta-v performance. In the future, a more detailed consideration of the atmospheric drag in the optimization program could increase the accuracy of the results.

6.2.2 ENTRAIN (DLR)

The ENTRAIN study is a continuation of the previously presented studies. A TSTO launch vehicle with retropropulsive landing first stage was designed for a 5500 kg payload GTO mission. In the first stage the propellant combination LOX/LCH4 is used and in the upper stage LOX/LH2, with gas generator engines being applied in both stages. For comparison, the optimization program was executed with the same parameters that were chosen for the ENTRAIN launch vehicle (see Table 6.5). As no information is given on the delta-v budget and its allocation [22], the launch vehicle was optimized for a 12 km/s delta-v budget with 3700/8300 delta-v allocation. This does not achieve the lowest GLOW but is assumed to be a good tradeoff between low mass and maximizing the size of the reusable first stage.

Fixed Parameters	**First Stage/Upper Stage**
Stage Radius [m]	2.4/2.4
Combustion Chamber Pressure [bar]	120/120
Nozzle Area Expansion Ratio [-]	22/150
Constraints	**First Stage/Upper Stage**
Number of Engines [-]	9/1
Minimum Acceleration [g]	1.4/0.9

Table 6.5: ENTRAIN study launch vehicle characteristics [22]

The characteristics of the optimized launch vehicle are compared to the ENTRAIN launch vehicle in Table 6.6. It can be observed that the GLOW and length of the vehicles are very similar. The optimized launch vehicle is slightly smaller and the ENTRAIN launch vehicle is 10 t lighter. Regarding the upper stage, the ENTRAIN launch vehicle features a significantly lower structure mass. It is assumed that the fairing mass is included which is why the fairing, avionics and payload adapter mass are included in the upper stage structure mass of the optimized launch vehicle as well. This results in a structural index of 13.1% in comparison with 9.5% of the ENTRAIN vehicle. As the upper stage of the optimized launch vehicle is around 26 t heavier, its engine is also more powerful. With respect to the first stage, the optimized launch vehicle features an around 7 t lower structure mass and 7.7 t lower propellant mass, resulting in a structural index of 7.2% in contrast to 8.95% of the ENTRAIN vehicle. Both sea level and vacuum thrust of the first stage engines are similar, however the sea level and vacuum I_{sp} of the optimized launch vehicle are 2.7 and 2.1% higher than of the ENTRAIN launcher. The difference in I_{sp} between the LH2 engines of the upper stage is only 0.6%. A comparison regarding the total delta-v, its allocation and the descent delta-v cannot be made, as the landing propellant mass of the ENTRAIN vehicle is not known.

	ENTRAIN	**Optimizer**
Upper Stage		
Structure Mass [kg]	5700	10635
Propellant Mass [kg]	60200	81333
SI [%]	9.5	13.1
Vacuum Thrust [kN]	$1 \cdot 635$	$1 \cdot 832$
Vacuum I_{sp} [s]	444	446.7
First Stage		
Structure Mass [kg]	33800	26713
Propellant Mass [kg]	378000	370319
SI [%]	8.95	7.2
Vacuum Thrust [kN]	$9 \cdot 838$	$9 \cdot 834$
Vacuum I_{sp} [s]	322.5	329.4
Sea Level Thrust [kN]	$9 \cdot 748$	$9 \cdot 750$
Sea Level I_{sp}[s]	288	296
Complete Launch Vehicle		
Length [m]	67.25	66.02
GLOW [kg]	484500	494500

Table 6.6: Comparison of the ENTRAIN launch vehicle with the launch vehicle of the optimization program [22]

6.2.3 RETALT

RETALT is a joint project of various contributors to create a foundation of know-how for research and industry in the key technologies of retropropulsive landing [23]. The investigated TSTO launch vehicle with reusable first stage is capable of delivering a 14000 kg payload into GTO. In both stages, gas generator engines using the LOX/LH2 propellant combination are applied. In order to compare the results of RETALT with the optimization program, the input parameters were chosen according to the RETALT configuration (see Table 6.7). Parameters that are not listed were subject to the standard boundaries (see Appendix C). Although not stated in [23], the available information allowed an estimation of the delta-v capabilities of the RETALT launcher. Treating the 7.5 t of excess propellant in the first stage as inert mass [23], a total delta-v budget of 12.1 km/s and a delta-v allocation of 3800/8300 was determined. A payload radius of 2.9 m and height of 7 m were chosen to achieve a fairing of similar size and weight.

Fixed Parameters	**First Stage/Upper Stage**
Stage Radius [m]	3.0/3.0
Nozzle Area Expansion Ratio [-]	15/70
Constraints	**First Stage/Upper Stage**
Number of Engines [-]	9/1
Minimum Acceleration [g]	1.3/0.64

Table 6.7: RETALT study launch vehicle characteristics [23]

The characteristics of the resulting optimized launch vehicle are compared to the RETALT launcher in Table 6.8. Regarding the upper stage, a very good accordance is achieved. The structure mass of the optimized launch vehicle (here containing the avionics and payload adapter mass) is slightly higher and the propellant mass slightly smaller, which is also reflected by the 1.25% higher vacuum I_{sp}. The structural coefficient differs only by 0.2%, proving the assumptions made in the optimization program to be reasonable. As the total masses of the upper stages differ only by around 1.5 t, the higher upper stage engine thrust of the optimized launch vehicle results in a higher minimum acceleration of 0.74 g in contrast to 0.64 g of the RETALT upper stage. With respect to the first stage, the 21% higher structure mass and 4% higher propellant mass lead to a structural coefficient of 10.1% in contrast to 8.7% of the RETALT first stage. Deviations of 0.4 and 0.2% in vacuum and sea level I_{sp} of the first stage engines show a very good accordance of the engine performance characteristics. In combination with the difference in first stage structure mass, the 17% greater landing propellant mass of the optimized launch vehicle is assumed to be reasonable, however a performance analysis is subsequently conducted. Comparing the overall mass and size of the launch vehicles shows only a small difference of 3.8% with regard to the GLOW, whereas a length difference of 13.6% is obtained.

This is partially attributed to the tank design, as the RETALT launcher features a common bulkhead configuration and the optimized launch vehicle separate tanks with spherical ends in tandem configuration. Because of the relatively large stage radius, the latter results in an empty volume of 113 m^3 between the first and upper stage tanks.

A performance analysis was made to compare the delta-v capabilities of the two launch vehicles (see Table 6.8). As the delta-v budget and allocation of the optimized launch vehicle were chosen based on an estimation for the RETALT vehicle, the good accordance between the two does not surprise. For first stage ascent and descent delta-v calculation, a mean I_{sp} 1.6% higher than the middle of sea level and vacuum I_{sp} was used. This value was derived from the trajectory simulation of the optimized launch vehicle. As already stated, 7.5 t of the first stage propellant of the RETALT vehicle are not used for acceleration or deceleration and were therefore treated as inert mass in the delta-v calculation [23]. The fairing was assumed to be jettisoned simultaneously with stage separation and thus was not included in the upper stage delta-v calculation. In addition to the total delta-v budget and its allocation being congruent for the two launch vehicles, the similarity of the delta-v provided by the engines during descent proves the reasonability of the assumptions and calculations in the optimization program. If the RETALT vehicle were to use part of its propellant reserve during descent, a descent delta-v of 2300 m/s is also achievable.

	RETALT	Optimizer
Payload Bay		
Payload Mass [kg]	14000	14000
Fairing Mass [kg]	2500	2575
Fairing Length [m]	12	12
Upper Stage		
Length [m]	19.8	23.6
Structure Mass [kg]	16700	17280
Propellant Mass [kg]	187500	185272
Structural Coefficient [%]	8.3	8.5
Vacuum Thrust [kN]	$1 \cdot 1364$	$1 \cdot 1564$
Vacuum I_{sp} [s]	431.9	437.3
First Stage		
Length [m]	71.2	79.6
Structure Mass [kg]	59300	72021
Propellant Mass [kg]	621500	644506
Propellant Mass Landing [kg]	50000	58589
Structural Coefficient [%]	8.7	10.1
Vacuum Thrust [kN]	$9 \cdot 1273$	$9 \cdot 1442$
Vacuum I_{sp} [s]	401.6	403.2
Sea Level Thrust [kN]	$9 \cdot 1179$	$9 \cdot 1329$
Sea Level I_{sp} [s]	372.2	371.4
Complete Launch Vehicle		
Length [m]	103	117
GLOW [kg]	901500	935655
Performance		
Delta-v Upper Stage [m/s]	8309	8300
Delta-v First Stage [m/s]	3789	3799
Total Delta-v [m/s]	12098	12099
Descent Delta-v [m/s]	2155	2298

Table 6.8: Comparison of the RETALT launch vehicle with the launch vehicle of the optimization program [23]

6.3 Sensitivity Analyses

In order to examine the various influences on launch vehicle performance, three different sensitivity analyses were carried out. With respect to the Tsiolkovsky rocket equation, the impact of delta-v budget, specific impulse and structural coefficient on the launch vehicle GLOW is investigated hereafter for a 5000 kg payload GTO mission.

6.3.1 Delta-v Budget

To study how the total delta-v budget affects the launch vehicle characteristics, the optimization program was executed for the delta-v budgets of 12000 m/s and 11500 m/s. For all three propellant combinations, Fig. 6.9 depicts the GLOWs of the optimized launch vehicles plotted over the first stage delta-v, as the upper stage delta-v differs between two respective configurations.

The results show that for each delta-v allocation, the lower total delta-v yields a lower GLOW. With around 60 t (LH2), 100 t (RP-1) and 90 t (LCH4), the absolute difference is smallest for medium first stage delta-v's and it is maximum for large first stage delta-v's with 110 t (LH2), 200 t (RP-1) and 160 t (LCH4). For all three propellant combinations, the percental difference ranges between around 15-30%, increasing with a decreasing first stage delta-v and lower GLOW. It can be concluded that a reduction of delta-v losses by 500 m/s achieves a significant GLOW decrease.

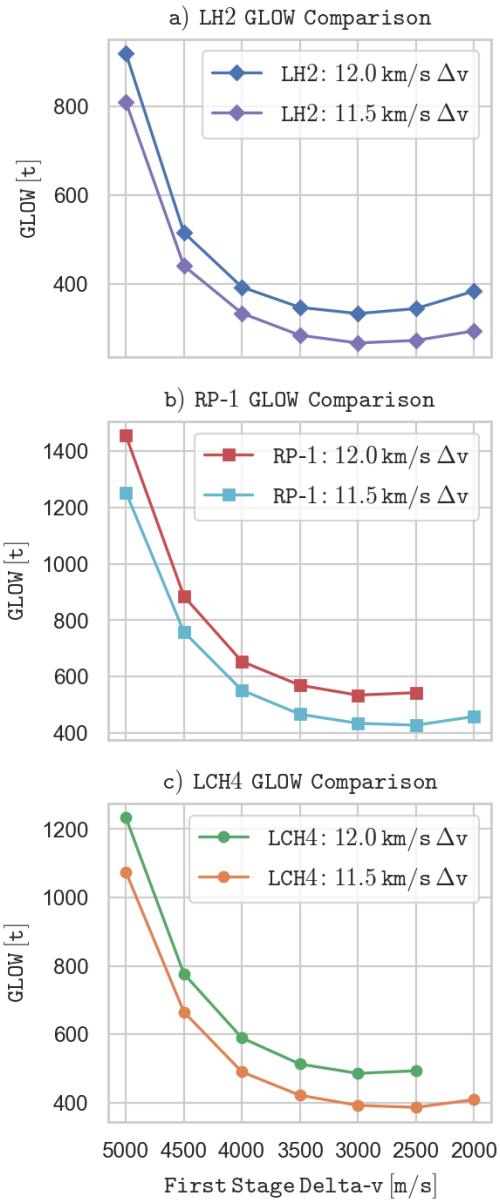

Figure 6.9: Delta-v budget sensitivity

6.3.2 Specific Impulse

In general, an improvement of the propulsion system performance has a direct influence on vehicle size, cost and reliability [15]. By means of an I_{sp} sensitivity analysis, the impact of a higher or lower I_{sp} on the launch vehicle characteristics can be investigated. Here, the difference in GLOW is examined by comparing the optimized launch vehicles with regular I_{sp} calculation to the ones with a by 2% increased as well as decreased I_{sp} (see Fig. 6.10).

With the 2% lower I_{sp}, the GLOW is increased by a minimum of 34 t (10%) for the LH2 and 68 t (12%) for the RP-1 launch vehicles with 3500/8500 delta-v allocation as well as 50 t (10%) for the LCH4 launch vehicle with 3000/9000 delta-v allocation. For all propellants, the maximum percentage-wise increase in GLOW of around 25% yields the 5000/7000 delta-v allocation with 230 t for LH2, 343 t for RP-1 and 312 t for LCH4.

Increasing the I_{sp} by 2% results in a minimum 10% lower GLOW for the 3000/9000 delta-v allocation, which amounts to 34 t for LH2, 50 t for RP-1 and 44 t for LCH4. The maximum decrease in GLOW of 15-17% is achieved for the 5000/7000 delta-v allocation, amounting to 155 t for LH2, 254 t for RP-1 and 190 t for LCH4.

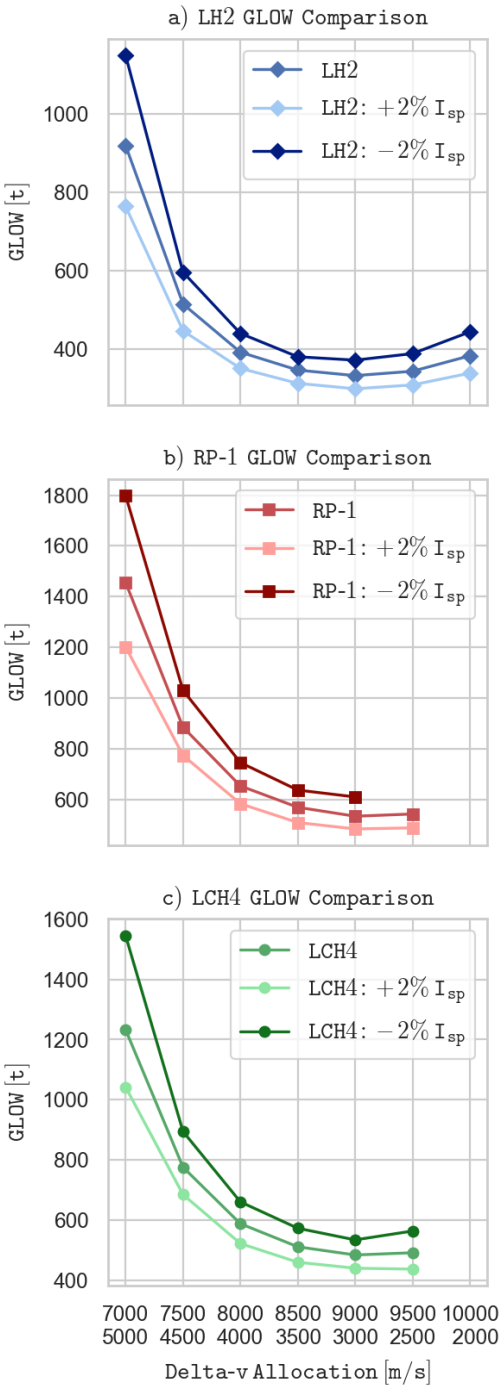

Figure 6.10: Specific impulse sensitivity

6.3.3 Structural Coefficient

As a measure of the efficiency of the rocket structure, the structural coefficient is an indicator for the performance of a launch vehicle. Manipulating the structure mass calculations in the optimization program, a sensitivity analysis regarding the structural coefficient was conducted for launch vehicles with the 3500/8500 delta-v allocation. The factors 0.90, 0.95, 1.05 and 1.10 were applied to decrease and increase the structure mass of both stages by 5% and 10% with respect to the regular configuration. The impact on GLOW, the percental GLOW deviation and the first stage structural coefficient deviation are presented in Fig. 6.11.

It can be observed that the GLOW increases linearly with increasing structure mass for all propellant combinations. Comparing the GLOW deviation shows that the LH2 launch vehicles are affected stronger by varying the structure mass than the RP-1 and LCH4 launch vehicles, whose GLOWs change approximately with the same rate as the structure mass alteration. The deviation of the structural coefficient depicts that for LH2 and LCH4 the structural coefficient rises slower while increasing the structure mass and decreases faster while decreasing the structure mass in comparison with the RP-1 launch vehicles.

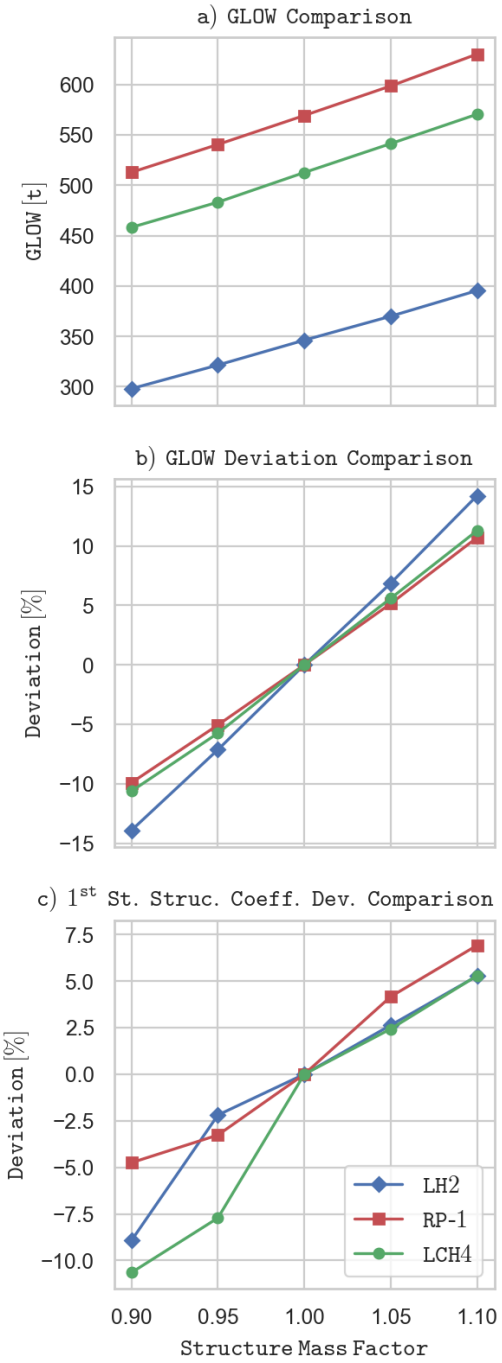

Figure 6.11: Structural coefficient sensitivity

6.4 Alternative Optimization Objectives

Until now, exclusively the gross lift-off weight (GLOW) of the launch vehicles was used as the fitness value representing the optimization objective in the optimization program. This way, the problem to solve was finding the overall lightest launch vehicle that fulfills all requirements. As the propellant mass constitutes the bulk of the GLOW while only being responsible for around 0.4% of the launch vehicle costs [49], it is reasonable to explore different optimization objectives. Because reducing costs is the main purpose of rocket reusability and cost functions not being implemented in the optimization program, the approach of minimizing the mass of the launch vehicle parts that make up the majority of the costs was chosen (see Fig. 2.6). Therefore, two different optimization objectives were implemented: minimization of the total structure mass of the launch vehicle, as well as minimization of the expendable structure mass comprising the upper stage structure mass and a fraction of the first stage structure mass.

6.4.1 Total Structure Mass

Applying the total structure mass as the fitness value and not fixing the delta-v allocation led to the optimizer finding the launch vehicle configuration with the lightest overall structure. In addition to fixing the propellant choice to one of the three propellant combinations, the optimization program was executed twice with freedom of choice between LH2 and RP-1 as well as LH2 and LCH4 as fuel for each stage. The restriction of the mandatory use of the same combustion chamber for all stages was removed to allow selection of different propellants. The results of the optimizer are depicted in Fig. 6.12.

For each run of the optimizer, the total structure mass and delta-v allocation of the optimized launch vehicle are presented. The structure mass is further broken down into the propulsion system mass, consisting of the engines and TVC system, and the residual structure mass of each stage. It can be observed that with freedom of choice between hydrogen and one of the hydrocarbon rocket fuels, a combination with the former in the upper stage and the latter in the first stage was output by the optimizer. This way, a smaller structure mass is achieved than with the same propellant combination for both stages. Comparing the two launch vehicles with different propellant combinations, the launch vehicle with RP-1/LH2 in first/upper stage with 3200/8800 delta-v allocation yields a slightly lower total structure mass while the LCH4/LH2 launch vehicle features a 3500/8500 delta-v allocation with a lower upper stage structure mass, which leads to a larger portion of the structure mass being reused. Regarding the single propellant combination launch vehicles, the LH2 launch vehicle has the highest structure mass with a delta-v allocation of 3000/9000, the RP-1 rocket the lowest structure mass with a 3200/8800 delta-v allocation and the LCH4 launch vehicle a slightly higher structure mass with a

3100/8900 delta-v allocation. Whereas for the upper stage the propulsion system makes up around 20% (LH2) to 27% (RP-1) of the structure mass, the first stage propulsion system constitutes 23% (LH2) to 28% (RP-1) of the total structure mass.

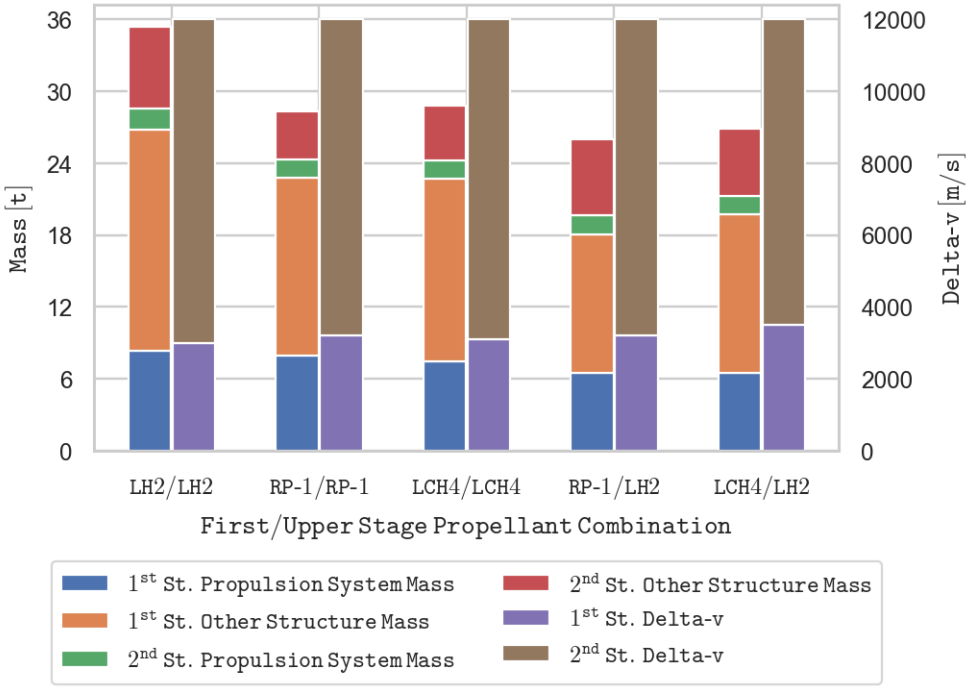

Figure 6.12: Total structure mass breakdown and delta-v allocation comparison

Fig. 6.13 depicts the length and GLOW as well as their allocation to first stage, upper stage and payload bay for each of the optimized launch vehicles. While the LH2, RP-1 and LCH4 launch vehicles show the already observed trends regarding size and length, the RP-1/LH2 and LCH4/LH2 launch vehicles present a significant decrease in GLOW and a slight increase in length in comparison with the launch vehicles using only RP-1 and LCH4.

Comparing the hybrid rockets using RP-1/LH2 and LCH4/LH2 with the LH2 launch vehicle, a decrease in length of 15 m and 12.5 m is achieved, whereas the GLOW is increased by 62 t and 57 t, respectively. In contrast to the RP-1 launch vehicle, the RP-1/LH2 rocket's length is increased by 5 m but its GLOW is decreased by 151 t. The LCH4/LH2 launch vehicle features a 93 t smaller GLOW and 2.5 m greater length than the LCH4 launch vehicle. Comparing the two hybrid rockets, LCH4/LH2 yields the overall lighter vehicle while RP-1/LH2 has a slight size advantage.

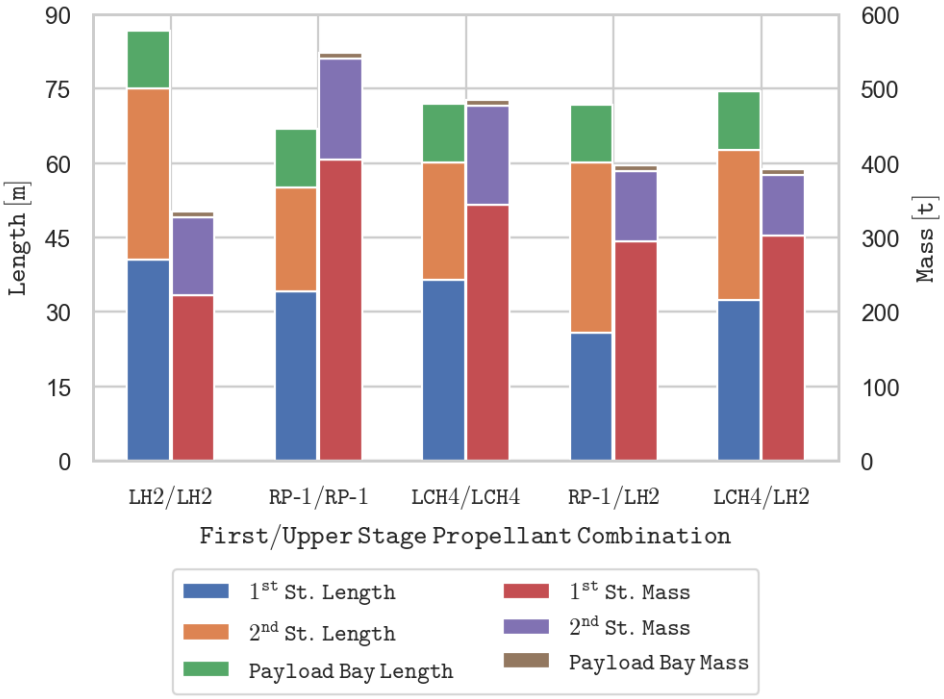

Figure 6.13: Length and GLOW breakdown comparison

6.4.2 Expendable Structure Mass

Although the previously used optimization objective does achieve the goal of reducing the total structure mass, which represents the major cost driver of rockets [50], it does not consider the effect of reusability. Therefore, the expendable structure mass was implemented as optimization objective. It consists of the upper stage structure mass and a fraction of the first stage structure mass depending on the number of reuses. For example, if the first stage is expected to be reused ten times, 10% of the first stage structure mass are assumed to be expendable. As cost functions for the evaluation of recovery and refurbishment costs are not part of this work, it is possible that the optimum configuration regarding costs may differ from the results of the optimization program. However, if these costs can be put in relation to the structure costs, the results can be easily adapted.

Four scenarios with 5, 10, 20 and 50 reuses of the first stage were investigated for the same five propellant combination configurations as in the previous section. For the hybrid rockets, the propellant combination had to be fixed for upper and first stage, as otherwise the optimizer had only selected the hydrocarbon fuel for both stages of the optimized vehicle using this optimization objective. For each propellant combination and reuse case, the expendable structure mass, the GLOW and the first stage delta-v of the optimized launch vehicles are depicted in Fig. 6.14.

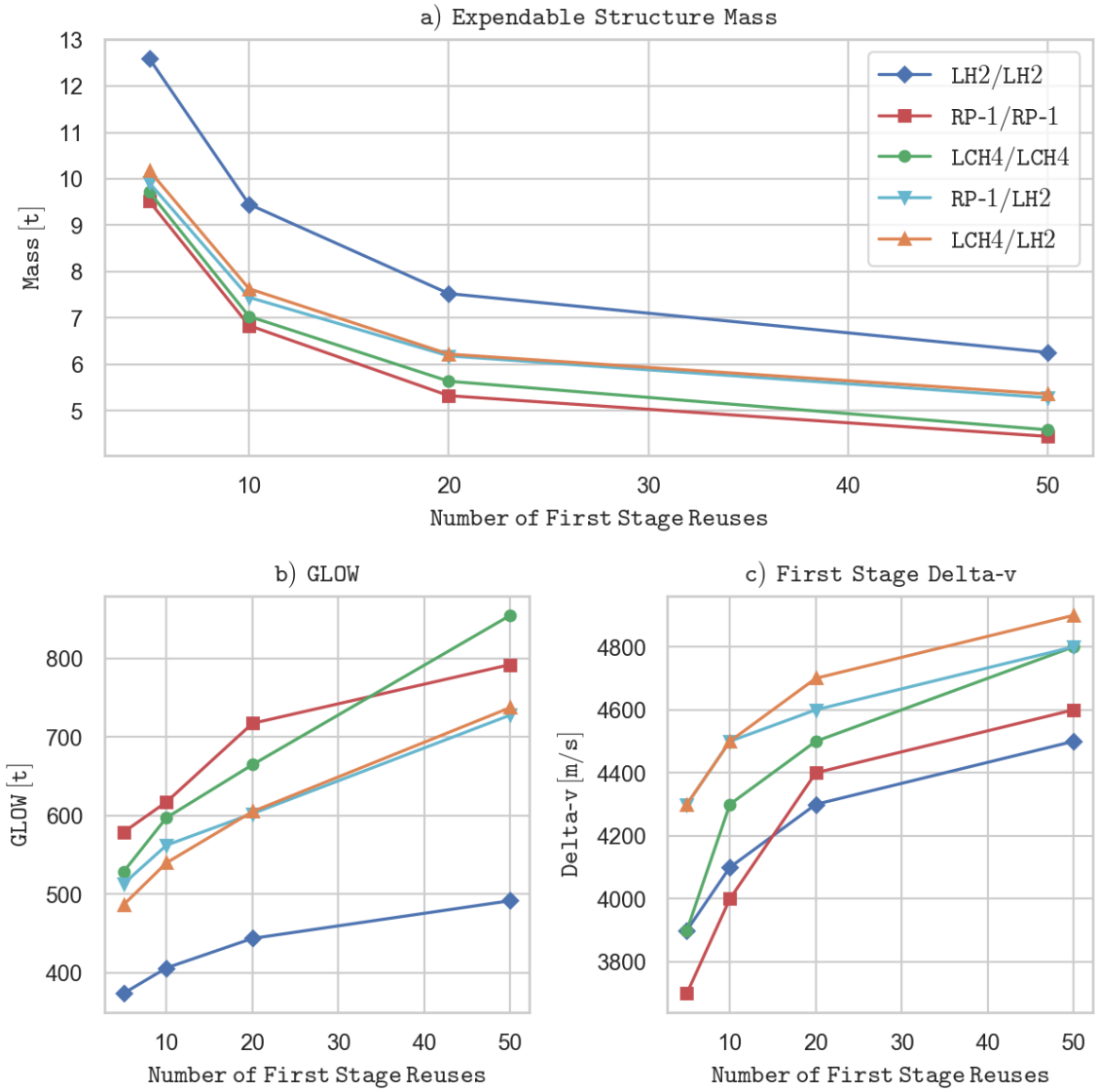

Figure 6.14: Expendable structure mass, GLOW and first stage delta-v comparison

Regarding the expendable structure mass, all propellant combinations show a similar trend. The LH2 launch vehicle has the highest and the RP-1 launch vehicle the lowest expendable structure mass for all reuse scenarios. While the LCH4 launch vehicle has a slightly higher expendable mass than the RP-1 launch vehicle, the hybrid rockets present values closely above the hydrocarbon rockets for fewer reuses and in between the hydrocarbon rockets and the LH2 launch vehicle for a larger number of reuses. This shift occurs because LH2 upper stages feature greater structure masses and the influence of the upper stage on the expendable mass increases with the number of first stage reuses. Increasing the number of reuses from 5 to 10, 20 or 50 yields a decrease in expendable mass of 25-28%, 38-44% and 47-53%, respectively. Comparing the delta-v allocation of the optimized launch vehicles, a tendency to higher first stage delta-v's with increasing number of reuses is observ-

able. If the first stage is reused more often, it becomes profitable to build larger first stages and smaller upper stages, although this entails heavier overall rockets, as depicted by the GLOW comparison. Whereas with 4300 m/s the optimized hybrid launch vehicles already feature a relatively large first stage delta-v for five reuses, the LH2, RP-1 and LCH4 launch vehicles have a lower first stage delta-v of 3700 and 3900 m/s for this scenario. The RP-1 and LCH4 rocket show a steeper increase of first stage delta-v, while the LH2 launch vehicle presents the same trend as the LCH4/LH2 launch vehicle. For 50 reuses, the LCH4/LH2 launch vehicle has the highest first stage delta-v of 4900 m/s, closely followed by the RP-1/LH2 and LCH4 rockets with 4800 m/s. This also affects the GLOW of these vehicles, which is disproportionately increased in comparison with the LH2 and RP-1 launch vehicles featuring the lowest first stage delta-v of 4500 and 4600 m/s, respectively.

Comparing the results of using the expendable mass as optimization objective with those of the total structure mass indicates that in terms of reusability it may be economically reasonable to apply delta-v allocations that result in heavier overall launch vehicles on the one hand but maximize the reusable portion of the rocket on the other hand. A direct comparison of GLOW values with the results of the optimization objective GLOW cannot be made, because for those the requirement of the same combustion chamber in both stages led to slightly heavier launch vehicles as the propulsion systems could only be adapted with respect to the nozzle area expansion ratio.

Chapter 7

Conclusion

7.1 Summary

Rocket reusability promises significant cost reductions in the space launch market. Landing the first stage of a launch vehicle after stage separation allows multiple uses of the rocket's most expensive parts, i.e. the propulsion system and the structures. The staging of the rocket has a large influence on the overall performance, the gross lift-off weight (GLOW), and the portion of the vehicle that is reused. The shift in launch vehicle design methodology from high-performance and expendable to low-cost and reusable also rekindled the discussion about the optimum propellant combination. Next to the widely used hydrogen and kerosene, methane became a contestant for future liquid rocket engines. However, no currently operational vehicle uses methane, making a comparison difficult.

In order to compare the three propellant combinations LOX/LH2, LOX/RP-1 and LOX/LCH4 on a launch system level, it was necessary to identify the optimum rocket parameters. Therefore, a multidisciplinary system design optimization approach was applied to develop an optimization program that is able to optimize a launch vehicle with reusable, vertical landing first stage for a given mission, i.e. payload mass and target orbit. Due to the implementation of various optimization objectives, the potential applications are manifold. At first, the GLOW was chosen as the parameter to be minimized, as a ligther rocket implies less costs.

Because of little information being available regarding the delta-v requirements for retropropulsive landings, SpaceX's Falcon 9 was analyzed by means of reverse engineering methods to develop a method of propellant mass calculation. As the required propellant mass and its allocation onto the stages are subject to the staging configuration and an optimum cannot be derived with traditional methods in case of reusable first stages, the delta-v allocation of the launch vehicle was added as a variable next to the other rocket parameters. In order to model the engines and subsequently evaluate the entire launch vehicle for a given set of parameters, NASA's

CEA program and detailed mass estimations were implemented. A regression analysis and comparison of performance data from generated and existing engines was necessary to account for the influence of the combustion chamber pressure on the shifting point position between shifting equilibrium and frozen equilibrium flow in the nozzle. Furthermore, the implementation of a trajectory simulation was required to obtain more accurate values for the mean I_{sp} of the first stage engines during ascent. The validation of the launch vehicle model in the optimization program with Falcon 9 as reference vehicle proved the assumptions and estimations to be reasonable. A difference in GLOW of 3.6% for the GTO mission and only 0.9% for the LEO mission were achieved for the same delta-v budgets.

Although sensible boundaries were implemented for all rocket parameters, the enormous amount of possible combinations made the use of genetic algorithms (GAs) necessary. If none of the rocket parameters are fixed for a particular investigation, a maximum of roughly $1.7 \cdot 10^{17}$ different combinations of the variables and their boundaries exist. With a tested capacity of around 30 parameter set evaluations per second, it would take 180 million years to test every possible combination. Here, the method of GAs to generate a whole population of random solutions and to manipulate it according to natural selection and genetics promised a more successful approach. During the hyperparameter tuning which was conducted to obtain the optimum settings of the GA, its capabilities were impressively demonstrated. With the GA, in less than 600 s a better launch vehicle was found than in more than 50000 s of random search. On the other hand, the disadvantage of GAs was revealed, as they do not guarantee to find the best individual solution. Nevertheless, the results proved that the GA in the optimization program is capable of both, the rapid testing of configurations and the accurate identification of optimum parameter sets.

The application of the optimization program to investigate the influence of staging configuration and propellant combination on launch vehicle performance showed that the GLOW depends strongly on the first stage delta-v. The higher the velocity at stage separation, the more propellant mass is required for the landing maneuvers. As expected, the LH2 launch vehicles achieved the lowest GLOWs. However, with a roughly 45% (LCH4) and 60% (RP-1) higher GLOW, the hydrocarbon rockets stayed in a reasonable range and further displayed advantages in the launch vehicle size and structure mass. Applying the assumptions of the RETALT study led to a very good accordance of the results, whereas a comparison with other current launch vehicle research studies indicated conservative assumptions for methane in particular by their authors. The subsequent sensitivity analyses illustrated the influence of the total delta-v budget, I_{sp} and structural efficiency on the overall launch vehicle performance. For appropriate delta-v allocations, the deviations in GLOW stayed within a reasonable range, thus indicating the robustness of the optimized launch vehicle solutions.

The application of the total structure mass and the expendable structure mass as alternative optimization objectives was the first step towards cost optimized launch vehicles and showed the influence of the number of first stage reuses on the launch

vehicle design. The higher the number of reuses, the larger is the first stage and the GLOW of the optimized launch vehicles. Furthermore, the results revealed that hybrid rockets, using hydrogen in the upper stage and hydrocarbon fuel in the first stage, combine the advantages of both sides. They are smaller in size and structure mass than the hydrogen vehicle and feature smaller GLOWs than the hydrocarbon rockets.

Overall, the optimization program proved to be a powerful tool for launch vehicle design and development. Its manifold use cases and application possibilities allow the investigation of the impact of various design choices on the reusable launch vehicle as well as the comparison of different configurations. The genetic algorithm further enables launch vehicle optimization with regard to any possible launch vehicle characteristic.

7.2 Outlook

Based on the work of this thesis, a few suggestions regarding the direction of future research can be given, the most important being the implementation of cost functions into the optimization program. Only when the subsystems of the rocket are realistically represented on a cost level, can the launch vehicles be optimized with regard to costs. Especially the propulsion systems need to be differentiated to be able to investigate the impact of the propellant choice on the costs of a launch vehicle.

Furthermore, the aerodynamic drag of rockets needs to be researched. A more detailed consideration of drag in the optimization program and trajectory simulation would enable the determination of the delta-v losses during ascent and more importantly an accurate estimation of the drag during descent and the resulting velocity compensation. This would also affect the launch vehicle geometry choice in the optimization program.

As the mass estimations have a large impact on how realistic the optimized launch vehicles are, more accurate models can further improve the performance of the optimizer. Particularly the engine mass estimation would benefit from higher detail, differentiation between hydrocarbon propellants, as well as incorporation of combustion chamber pressure and nozzle area expansion ratio into the model. Also, structural analyses would aid with the dimensioning of the propellant tank reinforcement and the landing gear structures.

In this thesis, launch vehicles were optimized either for a GTO or a LEO mission and it was subsequently analyzed if they were capable of accomplishing the other as well. As launch vehicles are ideally suitable for a variety of missions, a simultaneous optimization with regard to several different missions could be implemented. An analysis of the launch market could deliver a measure for emphasizing missions that

are expected to be performed more often. Incorporating (reusable) liquid propellant rocket boosters into the optimization program could allow an extension of the payload capability range of the investigated launch vehicles and hence enable the optimization of an entire family of launch vehicles, similar to Ariane 6.

The hyperparameter tuning that was conducted in the scope of this work revealed convergence on a local optimum to be the weakness of genetic algorithms. Therefore, possible solutions to decrease computation time and increase solution accuracy of the algorithm need to be examined.

Finally, the implementation of a graphical user interface would simplify the use of the optimization program and enable people to use it who are not familiar with its setup and structure.

Appendix A

Visible Landing Gear of Falcon 9

Figure A.1: Visible landing gear of Falcon 9 during landing maneuver [13]

Appendix B

Specific Impulse Comparison of Existing and Calculated Engines

Propellant Combination	Engine	Engine Cycle	ROF (* estimate)	p_cc [bar]	Expansion Ratio	Thrust (vac) [kN]	Thrust (sl) [kN]	Isp (vac) [s]	Isp (sl) [s]	Without Correction Formula Isp (vac) CEA Shifting EQ [s]	Isp (sl) CEA Shifting EQ [s]	Isp (vac) CEA Frozen EQ [s]	Isp (sl) CEA Frozen EQ [s]
LOX/LH2	Vulcain 1	GG	5,6	100	45,1	1140	815	440		436,2	332	425,6	321,4
	Vulcain 2	GG	7,2	115	58,2	1359	960	431	318	432	321	410,6	299,6
	HM7B	GG	5,69	36,6	83,1	64,8		446		458		441	
	RS-68	GG	6,8	103	21,5	3372	2949	409	359	414,8	368	399,5	353
	J-2	GG	5,9	52,6	27,5	1033		421		434	312	420,4	298,5
	Vinci	EX	5,8	60,8	243	180		465		479,7		461,5	
	J-2X	GG	6,2	95,1	92	1308		448		448	227	431	211
	RL-10A-3	EX	5	32,75	57	65,6		444		460,5		449,5	
	RL-10B-2	EX	5,88	44,12	280	110,1		465,5		481		459,9	
LOX/RP1	F-1	GG	2,64	67,7	16	7776	6770	305	265	321,9	280,3	307	265,6
	Merlin 1D	GG	2,34*	97	16	914	845	310	282	312	283,4	303	274
	Merlin 1D Vac	GG	2,34*	97	165	934		348		344,7		329,8	
	MC-1 (Fastrac)	GG	2,34	43,6	30	284,4		314		335,7	212	322	198

Propellant Combination	Engine	Engine Cycle	ROF (* estimate)	p_cc [bar]	Expansion Ratio	Thrust (vac) [kN]	Thrust (sl) [kN]	Isp (vac) [s]	Isp (sl) [s]	With Correction Formula Isp (vac) CEA Shifting EQ [s]	Isp (sl) CEA Shifting EQ [s]	Isp (vac) CEA Frozen EQ [s]	Isp (sl) CEA Frozen EQ [s]
LOX/LH2	Vulcain 1	GG	5,6	100	45,1	1140	815	440		431,7	328,5	439	331,5
	Vulcain 2	GG	7,2	115	58,2	1359	960	431	318	431,3	320,5	427,3	311,8
	HM7B	GG	5,69	36,6	83,1	64,8		446		437,7		437,7	
	RS-68	GG	6,8	103	21,5	3372	2949	409	359	411	365	412,8	364,7
	J-2	GG	5,9	52,6	27,5	1033		421		418,8	301	421,4	299
	Vinci	EX	5,8	60,8	243	180		465		464,7		464,9	
	J-2X	GG	6,2	95,1	92	1308		448		442,4	224,7	443,6	216,8
	RL-10A-3	EX	5	32,75	57	65,6		444		439		445	
	RL-10B-2	EX	5,88	44,12	280	110,1		465,5		461,7		458,6	
LOX/RP1	F-1	GG	2,64	67,7	16	7776	6770	305	265	312,9	272,5	310,7	268,7
	Merlin 1D	GG	2,34*	97	16	914	845	310	282	308,3	280	311,9	282,4
	Merlin 1D Vac	GG	2,34*	97	165	934		348		340,5		339,6	
	MC-1 (Fastrac)	GG	2,34	43,6	30	284,4		314		322		321	

Figure B.1: Comparison of the I_{sp} of existing engines with calculated engines with and without correction formula

Appendix C

Rocket Parameters

C.1 Boundary Values

Parameter	**Boundary Values First Stage**	**Boundary Values Upper Stage**
Stage Radius (r)	$1.5 - 4\ m$	$1.5 - 4\ m$ min. $0.75 \cdot$ first stage r max. $1.00 \cdot$ first stage r
Nozzle Throat Diameter	$0.1 - 1\ m$	$0.1 - 1\ m$
Combustion Chamber Pressure	$50 - 200\ bar$	$20 - 200\ bar$
Nozzle Area Expansion Ratio	$10 - 90$	$80 - 200$
Mixture Ratio	LOX/LH2: $4.0 - 8.0$ LOX/RP-1: $1.5 - 3.5$ LOX/LCH4: $2.0 - 4.0$	

Table C.1: Parameter boundary values in the optimization program

C.2 Constraints

Parameter	**Constraints First Stage**	**Constraints Upper Stage**
Minimum Number of Engines	5	1
Maximum Number of Engines	15	1
Minimum Acceleration	1.3 g	0.95 g
Maximum L/D Ratio	20	

Table C.2: Parameter constraints in the optimization program

Appendix D

Optimized Launch Vehicle Data

D.1 5000 kg Payload - 12000 m/s Delta-v

Payload 5000 kg / Delta-V 12000 m/s	LOX/LH2							
DeltaV Allocation First Stage / Upper Stage:	5000/7000	4500/7500	4000/8000	3500/8500	3000/9000	2500/9500	2000/10000
GLOW [kg]	919787	514993,1	391922,3	346158	332082,6	343285,5	382791,4
Payloadbay Mass [kg]	7627,5	7497,5	7440,3	7419,4	7409,5	7409,2	7415,8
Wet Mass Upper Stage [kg]	57358,6	56663,8	67700,7	82765,9	106075,2	135372,2	179508,7
Structure Mass Upper Stage [kg]	7126,2	5736,5	6363,4	7329,5	9014,3	10858,3	13655
Propellant Mass Upper Stage [kg]	50232,4	50927,3	61337,3	75436,4	97060,9	124513,9	165853,6
Wet Mass First Stage [kg]	854800,9	450831,8	316781,2	255972,7	218597,9	200504	195867
Structure Mass First Stage [kg]	80022	46986	35357,9	30372,3	27321,7	28483,2	32459,1
Propellant Mass First Stage [kg]	774779	403845,7	281423,4	225600,3	191276,3	172020,8	163407,9
Propellant Mass Landing First Stage [kg]	114146,8	53487	31354,6	20376	12837,7	8414,9	7545,8
Total Structure Mass [kg]	87148,2	52722,6	41721,3	37701,8	36336	39341,5	46114,1
Total Propellant Mass [kg]	825011,4	454773	342760,6	301036,8	288337,2	296534,8	329261,5
Total Launch Vehicle Length [m]	112,1	98,1	87,5	85,7	87	87,9	88
Propellant Upper Stage [-]	1	1	1	1	1	1	1
Propellant First Stage [-]	1	1	1	1	1	1	1
ROF (BK) Upper Stage [-]	7,1	7	7,1	7,1	7,2	7,2	7,3
ROF (BK) First Stage [-]	7,1	7	7,1	7,1	7,2	7,2	7,3
Combustion Chamber Pressure Upper Stage [bar]	120	120	120	105	115	110	110
Combustion Chamber Pressure First Stage [bar]	120	120	120	105	115	110	110
Expansion Ratio Upper Stage [-]	200	200	200	200	200	200	200
Expansion Ratio First Stage [-]	30	30	35	30	30	25	25
Radius Upper Stage [m]	2,3	1,9	1,8	1,8	1,9	2	2,2
Radius First Stage [m]	3,1	2,5	2,4	2,3	2,2	2,2	2,3
Structural Coefficient Upper Stage [-]	0,124	0,101	0,094	0,089	0,085	0,080	0,076
Structural Coefficient First Stage [-]	0,094	0,104	0,112	0,119	0,125	0,142	0,166
Upper Stage Length [m]	12,2	15,7	20	23,7	27,2	31,1	34
Upper Stage Total Tank Mass [kg]	2600,7	2700,5	3201,5	3806,3	4676,9	5718,9	7103,4
Number of Engines Upper Stage [-]	1	1	1	1	1	1	1
Mass Upper Stage Engine [kg]	1750,8	1057,6	1164,4	1333	1690,9	1994,8	2547,5
Mass Upper Stage Propulsion System [kg]	1916,3	1169,6	1284,4	1465,8	1851,6	2179,8	2777,9
Vacuum Thrust Upper Stage Engine [N]	1129374,7	633685,1	707819,9	826670,9	1085330,5	1310722,8	1731934,2
Total Vacuum Thrust Upper Stage [N]	1129374,7	633685,1	707819,9	826670,9	1085330,5	1310722,8	1731934,2
Vacuum Isp Upper Stage Engine [s]	451,2	451,5	451,2	451,7	451,8	451,6	451,1
First Stage Length [m]	87,9	70,5	55,8	50,2	47,9	45	42
First Stage Total Tank Mass [kg]	27468,2	16104,7	11534,7	9405,3	8198,8	7401,5	6915,9
Number of Engines First Stage [-]	13	13	9	7	5	5	5
Mass First Stage Engine [kg]	1633,9	988,4	1095,2	1244	1576,5	1842	2349,3
Mass First Stage Propulsion System [kg]	22747,1	13714,8	10540,1	9327,7	8466,2	9898,6	12641,7
Vacuum Thrust First Stage Engine [N]	1043612,3	586171,8	659636	763639,9	1001780,6	1196765,8	1579418,2
Total Vacuum Thrust First Stage [N]	13566959,4	7620233,2	5936723,8	5345479,5	5008902,9	5983828,8	7897091,2
Vacuum Isp First Stage Engine [s]	416,9	417,7	420,5	417,2	417	412,3	411,4
Sea Level Thrust First Stage Engine [N]	906408,7	508994,8	559313,8	648971,3	864577	1052448,3	1389172,6
Total Sea Level Thrust First Stage [N]	11783312,9	6616932	5033824,2	4542799,2	4322885,1	5262241,4	6945862,8
Sea Level Isp First Stage Engine [s]	362,1	362,7	356,5	354,6	359,9	362,6	361,9
Fairing Mass [kg]	1733,6	1757,7	1765,8	1765,8	1757,7	1750,1	1737,7
First Stage Mean Isp [s]	402,34	402,21	401,1	397,01	396,73	393,62	389,89
Delta-v with 15600 kg Payload First Stage [m/s]	4880,4	4325,2	3810,8	3326,2	2855,2	2390,7	1926,2
Delta-v with 15600 kg Payload Upper Stage [m/s]	4969,8	5217,3	5719,1	6275,5	6911,1	7551,1	8242,9
Total Delta-v with 15600 kg Payload [m/s]	9850,2	9542,5	9529,9	9601,7	9766,3	9941,7	10169,1

Figure D.1: Optimization program output - 5000 kg payload, 12000 m/s delta-v, LOX/LH2

Payload 5000 kg / Delta-V 12000 m/s	LOX/RP-1							
DeltaV Allocation First Stage / Upper Stage:	5000/7000	4500/7500	4000/8000	3500/8500	3000/9000	2500/9500	2000/10000	
GLOW [kg]	1455629,2	885192,4	653480,4	569209,4	533926,7	542756,5		
Payloadbay Mass [kg]	7495,9	7395,7	7366,1	7342,9	7318,4	7316,9		
Wet Mass Upper Stage [kg]	80824,4	85328	94928,8	118680,5	149280,4	194855,5		
Structure Mass Upper Stage [kg]	5362,9	4656,9	4328,9	5020,1	5906	7027,8		
Propellant Mass Upper Stage [kg]	75461,6	80671,1	90599,8	113660,4	143374,4	187827,7		
Wet Mass First Stage [kg]	1367308,9	792468,7	551185,5	443186	377327,9	340584,1		
Structure Mass First Stage [kg]	58366,5	39448,3	30752,9	26161,3	23199,4	22695,9		
Propellant Mass First Stage [kg]	1308942,4	753020,4	520432,5	417024,7	354128,5	317888,2		
Propellant Mass Landing First Stage [kg]	128698,8	67220,8	39801,8	24821	15178,9	9073,3		
Total Structure Mass [kg]	63729,3	44105,2	35081,8	31181,4	29105,4	29723,7		
Total Propellant Mass [kg]	1384404	833691,5	611032,4	530685,1	497502,9	505715,9		
Total Launch Vehicle Length [m]	90,1	74,2	70,9	68,7	63,3	64,1		
Propellant Upper Stage [-]	2	2	2	2	2	2		
Propellant First Stage [-]	2	2	2	2	2	2		
ROF (BK) Upper Stage [-]	2,7	2,8	2,9	2,9	3	3		
ROF (BK) First Stage [-]	2,7	2,8	2,9	2,9	3	3		
Combustion Chamber Pressure Upper Stage [bar]	115	115	110	105	110	110		
Combustion Chamber Pressure First Stage [bar]	115	115	110	105	110	110		
Expansion Ratio Upper Stage [-]	170	200	200	190	200	165		
Expansion Ratio First Stage [-]	20	25	25	25	25	30		
Radius Upper Stage [m]	2,1	1,9	1,7	1,8	2	2,1		
Radius First Stage [m]	2,8	2,5	2,2	2,1	2,2	2,2		
Structural Coefficient Upper Stage [-]	0,066	0,055	0,046	0,042	0,040	0,036		
Structural Coefficient First Stage [-]	0,043	0,050	0,056	0,059	0,061	0,067		
Upper Stage Length [m]	8,7	9,9	12,6	14	14,5	16,8		
Upper Stage Total Tank Mass [kg]	1343,8	1428,3	1625,2	1906	2194,5	2679,8		
Number of Engines Upper Stage [-]	1	1	1	1	1	1		
Mass Upper Stage Engine [kg]	1571,3	1280	1078,5	1215,6	1362,2	1551,1		
Mass Upper Stage Propulsion System [kg]	1821,7	1462	1226,2	1385,7	1561	1796		
Vacuum Thrust Upper Stage Engine [N]	1917817,7	1283153	965120,3	1172337,3	1438831,6	1865887,3		
Total Vacuum Thrust Upper Stage [N]	1917817,7	1283153	965120,3	1172337,3	1438831,6	1865887,3		
Vacuum Isp Upper Stage Engine [s]	347,6	350,8	352,1	352	352,5	350		
First Stage Length [m]	69,4	52,5	46,6	43	36,9	35,3		
First Stage Total Tank Mass [kg]	14191,7	8772,3	6482	5415,4	4560,7	4144,1		
Number of Engines First Stage [-]	12	11	11	8	6	5		
Mass First Stage Engine [kg]	1498,4	1212,4	1009,2	1146,6	1288	1489,4		
Mass First Stage Propulsion System [kg]	20269,8	14764,4	12181,4	10133,2	8611,1	8414,9		
Vacuum Thrust First Stage Engine [N]	1736076,5	1167046	873949,8	1063298,1	1297629,4	1714870,2		
Total Vacuum Thrust First Stage [N]	20832918,2	12837506,3	9613447,4	8506385,1	7785776,7	8574351		
Vacuum Isp First Stage Engine [s]	314,6	319	318,9	319,2	317,9	321,7		
Sea Level Thrust First Stage Engine [N]	1573464,9	1032859,7	769225,6	929834	1142423,8	1471609,1		
Total Sea Level Thrust First Stage [N]	18881578,4	11361456,2	8461481,1	7438671,9	6854542,9	7358045,7		
Sea Level Isp First Stage Engine [s]	285,2	282,4	280,7	279,2	279,9	276,1		
Fairing Mass [kg]	1743,3	1757,7	1774,1	1765,8	1750,1	1743,3		
First Stage Mean Isp [s]	306,06	307,78	306,53	305,42	303,55	302,78		
Delta-v with 15600 kg Payload First Stage [m/s]	4902,9	4373,6	3861,7	3374,6	2895,6	2421,8		
Delta-v with 15600 kg Payload Upper Stage [m/s]	5043,8	5367,4	5757,2	6312,3	6889,1	7507,7		
Total Delta-v with 15600 kg Payload [m/s]	9946,6	9741,0	9618,9	9686,9	9784,7	9929,5		

Figure D.2: Optimization program output - 5000 kg payload, 12000 m/s delta-v, LOX/RP-1

Payload 5000 kg / Delta-V 12000 m/s	LOX/LCH4						
DeltaV Allocation First Stage / Upper Stage:	5000/7000	4500/7500	4000/8000	3500/8500	3000/9000	2500/9500	2000/10000
GLOW [kg]	1232758,8	776587,4	589125,3	512604,4	485377,3	492896,6	
Payloadbay Mass [kg]	7485,6	7420,8	7389	7369,1	7338,9	7330,4	
Wet Mass Upper Stage [kg]	75685,4	81185,7	88847,4	110551,1	139244,8	180871,1	
Structure Mass Upper Stage [kg]	5812	5094,8	4616,8	5360,7	6341,6	7730,6	
Propellant Mass Upper Stage [kg]	69873,4	76090,9	84230,6	105190,4	132903,3	173140,5	
Wet Mass First Stage [kg]	1149587,7	687980,9	492888,9	394684,2	338793,6	304695,1	
Structure Mass First Stage [kg]	55461,2	38239,7	31046,4	26726,7	23897,9	23774,9	
Propellant Mass First Stage [kg]	1094126,5	649741,3	461842,5	367957,5	314895,7	280920,2	
Propellant Mass Landing First Stage [kg]	113151	60447,4	37692	23747,8	14776,3	8988,9	
Total Structure Mass [kg]	61273,2	43334,4	35663,2	32087,4	30239,5	31505,5	
Total Propellant Mass [kg]	1163999,9	725832,2	546073,1	473147,9	447799	454060,7	
Total Launch Vehicle Length [m]	90,3	80	77,2	72,8	68,7	66,5	
Propellant Upper Stage [-]	3	3	3	3	3	3	
Propellant First Stage [-]	3	3	3	3	3	3	
ROF (BK) Upper Stage [-]	3,7	3,6	3,6	3,7	3,7	3,7	
ROF (BK) First Stage [-]	3,7	3,6	3,6	3,7	3,7	3,7	
Combustion Chamber Pressure Upper Stage [bar]	115	115	110	115	105	115	
Combustion Chamber Pressure First Stage [bar]	115	115	110	115	105	115	
Expansion Ratio Upper Stage [-]	180	190	200	200	200	200	
Expansion Ratio First Stage [-]	25	30	25	30	30	30	
Radius Upper Stage [m]	2,2	1,9	1,7	1,7	2	2,2	
Radius First Stage [m]	2,9	2,5	2,2	2,2	2,2	2,3	
Structural Coefficient Upper Stage [-]	0,077	0,063	0,052	0,048	0,046	0,043	
Structural Coefficient First Stage [-]	0,048	0,056	0,063	0,068	0,071	0,078	
Upper Stage Length [m]	9	11,4	14,5	17,5	16,5	17,9	
Upper Stage Total Tank Mass [kg]	1563,6	1707	1942,9	2344,4	2601,9	3135,8	
Number of Engines Upper Stage [-]	1	1	1	1	1	1	
Mass Upper Stage Engine [kg]	1585,9	1336,3	1014,7	1173,4	1324,8	1542	
Mass Upper Stage Propulsion System [kg]	1840,5	1529,6	1153,4	1336,2	1515,8	1784,3	
Vacuum Thrust Upper Stage Engine [N]	1956258,5	1388052,5	880900	1104516,6	1366067,5	1842778,6	
Total Vacuum Thrust Upper Stage [N]	1956258,5	1388052,5	880900	1104516,6	1366067,5	1842778,6	
Vacuum Isp Upper Stage Engine [s]	365,6	366	366,9	367	367,5	367	
First Stage Length [m]	69,3	56,8	50,9	43,5	40,3	36,6	
First Stage Total Tank Mass [kg]	15263,9	9908,2	7532,1	6087,2	5261,9	4719,6	
Number of Engines First Stage [-]	10	9	11	8	6	5	
Mass First Stage Engine [kg]	1514,8	1276	947,3	1110,7	1260,9	1476,9	
Mass First Stage Propulsion System [kg]	17106,1	12765,9	11411,3	9800,3	8417,4	8337	
Vacuum Thrust First Stage Engine [N]	1775655	1276039,4	799250,1	1010425,2	1249364,6	1685796,3	
Total Vacuum Thrust First Stage [N]	17756549,9	11484354,5	8791751	8083402	7496187,6	8428981,5	
Vacuum Isp First Stage Engine [s]	331,9	336,5	332,9	335,7	336,1	335,7	
Sea Level Thrust First Stage Engine [N]	1572390,4	1102391,1	703434,4	873221,7	1063620,4	1456885,5	
Total Sea Level Thrust First Stage [N]	15723904,3	9921520	7737778,1	6985773,4	6381722,4	7284427,3	
Sea Level Isp First Stage Engine [s]	293,9	290,7	293	290,1	286,1	290,1	
Fairing Mass [kg]	1737,7	1757,7	1774,1	1774,1	1750,1	1737,7	
First Stage Mean Isp [s]	320,83	322,5	320,27	320,47	317,5	317,62	
Delta-v with 15600 kg Payload First Stage [m/s]	4891,2	4361,5	3852,3	3365,6	2888,5	2416,0	
Delta-v with 15600 kg Payload Upper Stage [m/s]	5039,1	5376,9	5746,5	6300,8	6885,4	7518,4	
Total Delta-v with 15600 kg Payload [m/s]	9930,3	9738,5	9598,8	9666,4	9773,8	9934,4	

Figure D.3: Optimization program output - 5000 kg payload, 12000 m/s delta-v, LOX/LCH4

D.2 15600 kg Payload - 9500 m/s Delta-v

Payload 15600 kg / Delta-V 9500 m/s	LOX/LH2						
DeltaV Allocation First Stage / Upper Stage:	5000/4500	4500/5000	4000/5500	3500/6000	3000/6500	2500/7000	2000/7500
GLOW [kg]	948114,7	564512,8	418725,8	356805,7	322274,3	312165,4	313661,1
Payloadbay Mass [kg]	18833,7	18679,5	18633	18602,8	18588,2	18571,5	18564,9
Wet Mass Upper Stage [kg]	48872,7	53439,1	62810,5	76783,4	91675,9	110971,7	134432,2
Structure Mass Upper Stage [kg]	6833,2	5911,5	6242,5	7339,6	8290,6	9591,4	11080,1
Propellant Mass Upper Stage [kg]	42039,4	47527,6	56567,9	69443,9	83385,3	101380,3	123352,1
Wet Mass First Stage [kg]	880408,3	492394,2	337282,3	261419,5	212010,2	182622,2	160663,9
Structure Mass First Stage [kg]	83256,1	50614,8	37484,2	30657,4	26570,5	26650,2	27242,5
Propellant Mass First Stage [kg]	797152,2	441779,4	299798,1	230762	185439,7	155971,9	133421,4
Propellant Mass Landing First Stage [kg]	117887,6	57668	33114,2	20340,5	12459,7	7819,7	6293,3
Total Structure Mass [kg]	90089,3	56526,3	43726,7	37997	34861,2	36241,6	38322,7
Total Propellant Mass [kg]	839191,7	489307	356366	300205,9	268825	257352,3	256773,4
Total Launch Vehicle Length [m]	119,9	94	90,5	86,6	86	82,9	83,9
Propellant Upper Stage [-]	1	1	1	1	1	1	1
Propellant First Stage [-]	1	1	1	1	1	1	1
ROF (BK) Upper Stage [-]	6,8	6,8	6,8	6,9	6,8	6,9	7
ROF (BK) First Stage [-]	6,8	6,8	6,8	6,9	6,8	6,9	7
Combustion Chamber Pressure Upper Stage [bar]	115	115	115	120	110	110	110
Combustion Chamber Pressure First Stage [bar]	115	115	115	120	110	110	110
Expansion Ratio Upper Stage [-]	190	200	200	200	200	200	200
Expansion Ratio First Stage [-]	30	25	30	30	25	25	25
Radius Upper Stage [m]	2,3	2	1,8	1,8	1,8	1,9	2
Radius First Stage [m]	3	2,7	2,4	2,3	2,2	2,2	2,1
Structural Coefficient Upper Stage [-]	0,140	0,111	0,099	0,096	0,090	0,086	0,082
Structural Coefficient First Stage [-]	0,095	0,103	0,111	0,117	0,125	0,146	0,170
Upper Stage Length [m]	11	13,9	18,9	22,6	26,6	28,8	31,3
Upper Stage Total Tank Mass [kg]	2307,4	2551,6	3036,3	3629,2	4282,5	4958,9	5757,2
Number of Engines Upper Stage [-]	1	1	1	1	1	1	1
Mass Upper Stage Engine [kg]	1797,9	1219,1	1219,1	1497,1	1608,8	1854,9	2117
Mass Upper Stage Propulsion System [kg]	1967	1343,2	1343,2	1642,6	1763	2028,7	2311,9
Vacuum Thrust Upper Stage Engine [N]	1164093,2	746123,6	746123,6	944238,9	1025272,9	1206370,7	1402662,2
Total Vacuum Thrust Upper Stage [N]	1164093,2	746123,6	746123,6	944238,9	1025272,9	1206370,7	1402662,2
Vacuum Isp Upper Stage Engine [s]	452,3	453	453	451,8	452,8	452,5	452,3
First Stage Length [m]	96,9	68,3	59,9	52,3	47,6	42,3	40,8
First Stage Total Tank Mass [kg]	29131,4	17254	12488	9882,5	8188,5	6924,5	6057,5
Number of Engines First Stage [-]	13	12	9	6	5	5	5
Mass First Stage Engine [kg]	1684,3	1130,9	1141	1399,8	1491,8	1718,1	1958,8
Mass First Stage Propulsion System [kg]	23454,2	14500	10984	9008,2	8009,7	9230,2	10529,7
Vacuum Thrust First Stage Engine [N]	1080501,1	684462,5	691520,7	874336,5	940444,3	1105326,3	1283787,4
Total Vacuum Thrust First Stage [N]	14046514,1	8213549,8	6223686,3	5246019,2	4702221,5	5526631,4	6418937,2
Vacuum Isp First Stage Engine [s]	419,9	415,6	419,9	418,3	415,3	414,6	413,9
Sea Level Thrust First Stage Engine [N]	931625,7	605062,3	596240,4	759047,4	826415,7	971501	1128581,8
Total Sea Level Thrust First Stage [N]	12111133,8	7260747,1	5366163,9	4554284,5	4132078,3	4857505,1	5642909
Sea Level Isp First Stage Engine [s]	362	367,4	362	363,2	365	364,4	363,9
Fairing Mass [kg]	1733,6	1750,1	1765,8	1765,8	1765,8	1757,7	1750,1
First Stage Mean Isp [s]	404,4	402,12	402,48	400,39	397,38	395,93	392,27
Delta-v with 5000 kg Payload First Stage [m/s]	5121,6	4673,6	4194,8	3686,6	3165,5	2632,1	2097,8
Delta-v with 5000 kg Payload Upper Stage [m/s]	6475,2	7219,7	7770,9	8188,9	8633,6	9032,7	9425,2
Total Delta-v with 5000 kg Payload [m/s]	11596,9	11893,4	11965,7	11875,5	11799,1	11664,8	11523,0

Figure D.4: Optimization program output - 15600 kg payload, 9500 m/s delta-v, LOX/LH2

Payload 15600 kg / Delta-V 9500 m/s	LOX/RP-1							
DeltaV Allocation First Stage / Upper Stage:	5000/4500	4500/5000	4000/5500	3500/6000	3000/6500	2500/7000	2000/7500	
GLOW [kg]	1422421,6	852712,1	664406,9	558047,8	504282,9	477014,5	485064,8	
Payloadbay Mass [kg]	18646,3	18571,7	18539,3	18513,9	18487,7	18476,4	18472	
Wet Mass Upper Stage [kg]	66588	78497	89408,2	107141,8	129105,7	158451,6	195745,2	
Structure Mass Upper Stage [kg]	5638,7	5082,9	4672,8	4947	5534,9	6318,7	7254,9	
Propellant Mass Upper Stage [kg]	60949,3	73414,2	84735,3	102194,7	123570,9	152132,9	188490,2	
Wet Mass First Stage [kg]	1337187,4	755643,4	556459,4	432392,1	356689,5	300086,4	270847,7	
Structure Mass First Stage [kg]	58869,2	35188,9	29484,6	25154,9	22309,1	20842,4	22935,4	
Propellant Mass First Stage [kg]	1278318,2	720454,5	526974,9	407237,2	334380,4	279244	247912,3	
Propellant Mass Landing First Stage [kg]	128311,4	59851,4	38201,5	23703	14567,7	8310,4	7232,2	
Total Structure Mass [kg]	64507,9	40271,8	34157,4	30101,9	27844	27161,1	30190,3	
Total Propellant Mass [kg]	1339267,5	793868,6	611710,2	509432	457951,2	431376,9	436402,5	
Total Launch Vehicle Length [m]	79,4	75,5	70,7	64,6	62,5	60,6	53	
Propellant Upper Stage [-]	2	2	2	2	2	2	2	
Propellant First Stage [-]	2	2	2	2	2	2	2	
ROF (BK) Upper Stage [-]	2,8	2,8	2,9	2,9	2,9	2,9	2,9	
ROF (BK) First Stage [-]	2,8	2,8	2,9	2,9	2,9	2,9	2,9	
Combustion Chamber Pressure Upper Stage [bar]	115	115	110	115	105	110	110	
Combustion Chamber Pressure First Stage [bar]	115	115	110	115	105	110	110	
Expansion Ratio Upper Stage [-]	195	140	175	190	200	195	175	
Expansion Ratio First Stage [-]	25	25	25	30	25	30	15	
Radius Upper Stage [m]	2,4	1,9	1,8	1,8	2	2,1	2,2	
Radius First Stage [m]	3,1	2,4	2,2	2,2	2,1	2,1	2,7	
Structural Coefficient Upper Stage [-]	0,085	0,065	0,052	0,046	0,043	0,040	0,037	
Structural Coefficient First Stage [-]	0,044	0,047	0,053	0,058	0,063	0,069	0,085	
Upper Stage Length [m]	7,8	9,3	11	12,8	12,9	14,2	15,8	
Upper Stage Total Tank Mass [kg]	1160,7	1332,3	1504,4	1748,5	1948,1	2257,4	2660,2	
Number of Engines Upper Stage [-]	1	1	1	1	1	1	1	
Mass Upper Stage Engine [kg]	1580,6	1572,1	1302,3	1283,8	1322,7	1457,1	1593,8	
Mass Upper Stage Propulsion System [kg]	1833,6	1822,8	1488,7	1466,6	1513,3	1677,7	1850,7	
Vacuum Thrust Upper Stage Engine [N]	1942126,8	1919971,7	1323778,5	1290097,6	1362074	1640518,1	1977496,4	
Total Vacuum Thrust Upper Stage [N]	1942126,8	1919971,7	1323778,5	1290097,6	1362074	1640518,1	1977496,4	
Vacuum Isp Upper Stage Engine [s]	350,5	346,5	350,5	351,1	352,6	351,8	350,5	
First Stage Length [m]	59,4	54,4	47,9	40	37,7	34,5	25,2	
First Stage Total Tank Mass [kg]	13481,6	8529,9	6557,3	5182	4429,7	3774,4	3367,4	
Number of Engines First Stage [-]	12	7	8	7	6	5	5	
Mass First Stage Engine [kg]	1511,6	1511,6	1234,8	1222,7	1251,6	1394,1	1498,3	
Mass First Stage Propulsion System [kg]	20469,7	11958,9	10960,8	9495,7	8351,1	7825	8470,6	
Vacuum Thrust First Stage Engine [N]	1767833	1767833	1204365,5	1183963,8	1233174,2	1503997,5	1735830,4	
Total Vacuum Thrust First Stage [N]	21213996,4	12374831,2	9634924,4	8287746,3	7399045	7519987,5	8679151,9	
Vacuum Isp First Stage Engine [s]	319	319	318,9	322,2	319,2	322,6	307,7	
Sea Level Thrust First Stage Engine [N]	1564568,5	1564568,5	1060048,1	1022940,1	1078387,3	1290193,8	1606479,2	
Total Sea Level Thrust First Stage [N]	18774821,7	10951979,3	8480384,5	7160580,8	6470324,1	6450969,2	8032395,8	
Sea Level Isp First Stage Engine [s]	282,4	282,4	280,7	278,4	279,2	276,7	284,7	
Fairing Mass [kg]	1731,7	1757,7	1765,8	1765,8	1750,1	1743,3	1737,7	
First Stage Mean Isp [s]	308,38	307,79	306,42	306,89	304,07	303,65	297,38	
Delta-v with 5000 kg Payload First Stage [m/s]	5102,7	4641,2	4146,0	3637,9	3119,3	2595,4	2068,3	
Delta-v with 5000 kg Payload Upper Stage [m/s]	6353,1	7003,1	7648,5	8167,2	8632,4	9056,3	9465,3	
Total Delta-v with 5000 kg Payload [m/s]	11455,7	11644,2	11794,6	11805,1	11751,7	11651,7	11533,6	

Figure D.5: Optimization program output - 15600 kg payload, 9500 m/s delta-v, LOX/RP-1

Payload 15600 kg / Delta-V 9500 m/s	LOX/LCH4						
DeltaV Allocation First Stage / Upper Stage:	5000/4500	4500/5000	4000/5500	3500/6000	3000/6500	2500/7000	2000/7500
GLOW [kg]	1202995,8	776150,7	599252,2	507896,5	459640,8	435930,1	437170,1
Payloadbay Mass [kg]	18644,7	18586,2	18557,1	18534,6	18513,7	18493	18482,8
Wet Mass Upper Stage [kg]	61992,9	73286,1	84774,4	100076,1	120799,5	147158,4	180958,1
Structure Mass Upper Stage [kg]	5547,5	5400,8	5182,7	5264,9	5857,6	6734,4	7907
Propellant Mass Upper Stage [kg]	56445,4	67885,2	79591,7	94811,3	114941,8	140424	173051,1
Wet Mass First Stage [kg]	1122358,3	684278,5	495920,6	389285,8	320327,7	270278,7	237729,1
Structure Mass First Stage [kg]	55091,6	37076	29670,2	25659,7	22873,6	21165,2	22419,5
Propellant Mass First Stage [kg]	1067266,7	647202,5	466250,5	363626,1	297454,1	249113,5	215309,6
Propellant Mass Landing First Stage [kg]	111592,9	58455,5	35795,8	22761,1	14052	8037,8	6639,1
Total Structure Mass [kg]	60639,1	42476,8	34852,9	30924,6	28731,2	27899,6	30326,5
Total Propellant Mass [kg]	1123712	715087,7	545842,2	458437,4	412395,9	389537,5	388360,7
Total Launch Vehicle Length [m]	88,9	75,9	76,9	70,2	68,3	65	60,2
Propellant Upper Stage [-]	3	3	3	3	3	3	3
Propellant First Stage [-]	3	3	3	3	3	3	3
ROF (BK) Upper Stage [-]	3,5	3,6	3,6	3,6	3,7	3,7	3,7
ROF (BK) First Stage [-]	3,5	3,6	3,6	3,6	3,7	3,7	3,7
Combustion Chamber Pressure Upper Stage [bar]	115	115	115	115	115	110	110
Combustion Chamber Pressure First Stage [bar]	115	115	115	115	115	110	110
Expansion Ratio Upper Stage [-]	185	165	195	200	200	200	200
Expansion Ratio First Stage [-]	25	30	30	30	30	30	25
Radius Upper Stage [m]	2,2	2	1,9	1,8	1,9	2,1	2,3
Radius First Stage [m]	2,9	2,6	2,2	2,2	2,1	2,1	2,3
Structural Coefficient Upper Stage [-]	0,089	0,074	0,061	0,053	0,048	0,046	0,044
Structural Coefficient First Stage [-]	0,049	0,054	0,060	0,066	0,071	0,078	0,094
Upper Stage Length [m]	8,3	9,8	11,8	14,7	15,9	16,1	16,8
Upper Stage Total Tank Mass [kg]	1359	1545,4	1768,1	2087	2374,4	2663,5	3120,9
Number of Engines Upper Stage [-]	1	1	1	1	1	1	1
Mass Upper Stage Engine [kg]	1578,4	1533,2	1336,9	1227,5	1287,3	1410,7	1554,2
Mass Upper Stage Propulsion System [kg]	1830,9	1773,2	1530,4	1399,7	1470,7	1620,3	1799,9
Vacuum Thrust Upper Stage Engine [N]	1936496,2	1820833,1	1389272,2	1192089,7	1296273	1538814,7	1873657,8
Total Vacuum Thrust Upper Stage [N]	1936496,2	1820833,1	1389272,2	1192089,7	1296273	1538814,7	1873657,8
Vacuum Isp Upper Stage Engine [s]	365	364,2	366,3	366,6	367	367,3	367,3
First Stage Length [m]	68,6	54,2	53,2	43,7	40,5	37	31,4
First Stage Total Tank Mass [kg]	15069,7	9749,4	7615	6051,8	5135,3	4367,1	3743,6
Number of Engines First Stage [-]	10	7	7	7	6	5	5
Mass First Stage Engine [kg]	1511,5	1475,3	1276	1166,7	1223,8	1346,3	1480,5
Mass First Stage Propulsion System [kg]	17063,9	11640,4	9938,7	9035,8	8153,4	7534,1	8359,4
Vacuum Thrust First Stage Engine [N]	1767549,9	1682131,5	1276039,4	1093998,1	1185846,3	1407554	1694114,3
Total Vacuum Thrust First Stage [N]	17675499	11774920,4	8932275,8	7657986,8	7115077,8	7037769,9	8470571,6
Vacuum Isp First Stage Engine [s]	333,2	336,5	336,5	336,5	335,7	335,9	332,1
Sea Level Thrust First Stage Engine [N]	1564285,3	1453220,7	1102391,1	945122,7	1024822,7	1207766,3	1491396,8
Total Sea Level Thrust First Stage [N]	15642853,4	10172544,6	7716737,8	6615858,9	6148935,9	6038831,7	7456983,8
Sea Level Isp First Stage Engine [s]	294,8	290,7	290,7	290,7	290,1	288,2	292,3
Fairing Mass [kg]	1737,7	1750,1	1757,7	1765,8	1757,7	1743,3	1733,7
First Stage Mean Isp [s]	322,15	322,7	321,79	320,76	318,98	316,46	314,22
Delta-v with 5000 kg Payload First Stage [m/s]	5115,7	4647,3	4156,3	3647,1	3127,6	2602,4	2074,5
Delta-v with 5000 kg Payload Upper Stage [m/s]	6414,0	7018,9	7630,5	8180,1	8648,9	9070,8	9461,2
Total Delta-v with 5000 kg Payload [m/s]	11529,6	11666,2	11786,7	11827,3	11776,5	11673,3	11535,7

Figure D.6: Optimization program output - 15600 kg payload, 9500 m/s delta-v, LOX/LCH4

D.3 7500 kg Payload - 12000 m/s Delta-v

Payload 7500 kg / Delta-V 12000 m/s	LOX/LH2						
DeltaV Allocation First Stage / Upper Stage:	5000/7000	4500/7500	4000/8000	3500/8500	3000/9000	2500/9500	2000/10000
GLOW [kg]	1139917,6	662161,3	519587,2	460362,8	439867,5	459627,9	507509,6
Payloadbay Mass [kg]	10355,1	10184,3	10129,7	10112	10097,6	10099,7	10113,1
Wet Mass Upper Stage [kg]	75331	76762,3	92720,1	112565,8	141912,5	182915	240164,1
Structure Mass Upper Stage [kg]	8674,2	7301,6	8223,5	9392,6	11353,4	14107	17655,4
Propellant Mass Upper Stage [kg]	66656,8	69460,7	84496,6	103173,1	130559,1	168808	222508,7
Wet Mass First Stage [kg]	1054231,5	575214,7	416737,4	337685	287857,4	266613,2	257232,5
Structure Mass First Stage [kg]	98393,4	58645,3	45246,9	39008	34405,6	37606,9	41827,4
Propellant Mass First Stage [kg]	955838	516569,4	371490,6	298677	253451,8	229006,3	215405,1
Propellant Mass Landing First Stage [kg]	139241,8	66575,8	40092,4	26092,7	16272,6	11021,6	9664,9
Total Structure Mass [kg]	107067,6	65946,9	53470,3	48400,6	45759,1	51713,9	59482,8
Total Propellant Mass [kg]	1022494,9	586030,1	455987,2	401850,2	384010,9	397814,3	437913,8
Total Launch Vehicle Length [m]	122,9	103	97,3	96,5	94,6	95,6	95,4
Propellant Upper Stage [-]	1	1	1	1	1	1	1
Propellant First Stage [-]	1	1	1	1	1	1	1
ROF (BK) Upper Stage [-]	6,9	6,9	7	7,2	7,2	7,1	7,2
ROF (BK) First Stage [-]	6,9	6,9	7	7,2	7,2	7,1	7,2
Combustion Chamber Pressure Upper Stage [bar]	120	115	120	110	110	115	115
Combustion Chamber Pressure First Stage [bar]	120	115	120	110	110	115	115
Expansion Ratio Upper Stage [-]	200	200	200	200	200	200	200
Expansion Ratio First Stage [-]	35	30	30	30	25	30	25
Radius Upper Stage [m]	2,5	2,1	2	1,9	2	2,2	2,5
Radius First Stage [m]	3,3	2,8	2,6	2,5	2,5	2,5	2,5
Structural Coefficient Upper Stage [-]	0,12	0,1	0,09	0,08	0,08	0,08	0,07
Structural Coefficient First Stage [-]	0,09	0,1	0,11	0,12	0,12	0,14	0,16
Upper Stage Length [m]	13,7	17,6	22,4	28,6	32,5	35,2	36
Upper Stage Total Tank Mass [kg]	3284	3442,6	4124,1	4924,9	5973,7	7360,5	9054,5
Number of Engines Upper Stage [-]	1	1	1	1	1	1	1
Mass Upper Stage Engine [kg]	2005,6	1330,3	1500,4	1743,2	2126,2	2643,3	3279,5
Mass Upper Stage Propulsion System [kg]	2191,4	1462,9	1646,1	1908	2321,8	2881,7	3572
Vacuum Thrust Upper Stage Engine [N]	1318813	824746,1	946616	1123733,6	1409611,4	1806276,6	2308211,6
Total Vacuum Thrust Upper Stage [N]	1318813	824746,1	946616	1123733,6	1409611,4	1806276,6	2308211,6
Vacuum Isp Upper Stage Engine [s]	451,8	452,8	451,5	451,6	451,6	452,2	451,8
First Stage Length [m]	97	73,4	63	56,1	50,3	48,4	47,3
First Stage Total Tank Mass [kg]	33399,3	19589,7	14670	11830,7	10160,3	9366,6	8790,9
Number of Engines First Stage [-]	14	13	9	7	5	5	5
Mass First Stage Engine [kg]	1888,5	1243,9	1401,6	1625	1963,2	2465,9	3027,7
Mass First Stage Propulsion System [kg]	28340,4	17284,7	13508,1	12201,4	10553,3	13272,7	16318,3
Vacuum Thrust First Stage Engine [N]	1231306,8	763605,4	875639,3	1037111,1	1287056,7	1668933,5	2107874,7
Total Vacuum Thrust First Stage [N]	17238295,3	9926870,1	7880754	7259777,8	6435283,6	8344667,7	10539373,5
Vacuum Isp First Stage Engine [s]	421,8	419,2	417,7	416,8	412,3	417,8	412,6
Sea Level Thrust First Stage Engine [N]	1043445,9	658558,9	760350,2	888636,3	1131851,1	1440022,7	1864711,5
Total Sea Level Thrust First Stage [N]	14608242,4	8561265,8	6843151,9	6220454,4	5659255,5	7200113,6	9323557,6
Sea Level Isp First Stage Engine [s]	357,4	361,5	362,7	357,1	362,6	360,5	365
Structural Index Upper Stage	0,173	0,144	0,128	0,116	0,107	0,099	0,091
Structural Index First Stage	0,103	0,114	0,122	0,131	0,136	0,164	0,194
Landing Propellant Mass / First Stage Wet Mass	0,132	0,116	0,096	0,077	0,057	0,041	0,038

Figure D.7: Optimization program output - 7500 kg payload, 12000 m/s delta-v, LOX/LH2

Payload 7500 kg / Delta-V 12000 m/s	LOX/RP-1						
DeltaV Allocation First Stage / Upper Stage:	5000/7000	4500/7500	4000/8000	3500/8500	3000/9000	2500/9500	2000/10000
GLOW [kg]		1127132,6	869083	758769			
Payloadbay Mass [kg]		10063,8	10025,5	10002,4			
Wet Mass Upper Stage [kg]		117824,7	132787,7	163155,2			
Structure Mass Upper Stage [kg]		5846,2	5646,8	6271,7			
Propellant Mass Upper Stage [kg]		111978,6	127141	156883,5			
Wet Mass First Stage [kg]		999244,1	726269,8	585611,4			
Structure Mass First Stage [kg]		46674,3	38000,7	33159,9			
Propellant Mass First Stage [kg]		952569,8	688269	552451,5			
Propellant Mass Landing First Stage [kg]		79437,2	49146,5	31199,9			
Total Structure Mass [kg]		52520,5	43647,5	39431,6			
Total Propellant Mass [kg]		1064548,3	815410	709335			
Total Launch Vehicle Length [m]		77,6	74,6	68,3			
Propellant Upper Stage [-]		2	2	2			
Propellant First Stage [-]		2	2	2			
ROF (BK) Upper Stage [-]		2,8	2,9	2,9			
ROF (BK) First Stage [-]		2,8	2,9	2,9			
Combustion Chamber Pressure Upper Stage [bar]		115	110	115			
Combustion Chamber Pressure First Stage [bar]		115	110	115			
Expansion Ratio Upper Stage [-]		180	200	190			
Expansion Ratio First Stage [-]		25	25	30			
Radius Upper Stage [m]		2,1	2	2			
Radius First Stage [m]		2,8	2,5	2,6			
Structural Coefficient Upper Stage [-]		0,05	0,04	0,04			
Structural Coefficient First Stage [-]		0,05	0,05	0,06			
Upper Stage Length [m]		11,2	13,2	15,6			
Upper Stage Total Tank Mass [kg]		1781,4	1993,9	2368			
Number of Engines Upper Stage [-]		1	1	1			
Mass Upper Stage Engine [kg]		1532	1357,9	1441,2			
Mass Upper Stage Propulsion System [kg]		1771,6	1555,8	1657,9			
Vacuum Thrust Upper Stage Engine [N]		1817756,7	1430348,4	1604988,3			
Total Vacuum Thrust Upper Stage [N]		1817756,7	1430348,4	1604988,3			
Vacuum Isp Upper Stage Engine [s]		349,6	352,1	351,1			
First Stage Length [m]		54,5	49,6	40,8			
First Stage Total Tank Mass [kg]		10551,9	8057,6	6550,7			
Number of Engines First Stage [-]		10	10	8			
Mass First Stage Engine [kg]		1465,3	1286,7	1379,1			
Mass First Stage Propulsion System [kg]		16485	14306,8	12346,4			
Vacuum Thrust First Stage Engine [N]		1659069,9	1295229,9	1472949			
Total Vacuum Thrust First Stage [N]		16590698,7	12952298,9	11783591,9			
Vacuum Isp First Stage Engine [s]		319	318,9	322,2			
Sea Level Thrust First Stage Engine [N]		1468310,8	1140024,3	1272622,2			
Total Sea Level Thrust First Stage [N]		14683108,4	11400242,6	10180977,9			
Sea Level Isp First Stage Engine [s]		282,4	280,7	278,4			
Structural Index Upper Stage		0,075	0,064	0,056			
Structural Index First Stage		0,049	0,055	0,060			
Landing Propellant Mass / First Stage Wet Mass		0,079	0,068	0,053			

Figure D.8: Optimization program output - 7500 kg payload, 12000 m/s delta-v, LOX/RP-1

Payload 7500 kg / Delta-V 12000 m/s	LOX/LCH4						
DeltaV Allocation First Stage / Upper Stage:	5000/7000	4500/7500	4000/8000	3500/8500	3000/9000	2500/9500	2000/10000
GLOW [kg]	1574463,6	988782	768398,3	679396,3	658119,7		
Payloadbay Mass [kg]	10216,5	10105,4	10057,9	10030,5	10005,8		
Wet Mass Upper Stage [kg]	96215,4	106788,7	124424,4	152677,9	192015,9		
Structure Mass Upper Stage [kg]	6398,3	5906,4	6024,9	6838	8168		
Propellant Mass Upper Stage [kg]	89817,1	100882,4	118399,5	145839,9	183847,9		
Wet Mass First Stage [kg]	1468031,7	871887,9	633915,9	516687,9	456098		
Structure Mass First Stage [kg]	69573,2	46403,1	37146,2	31890,6	30804		
Propellant Mass First Stage [kg]	1398458,5	825484,8	596769,8	484797,3	425294		
Propellant Mass Landing First Stage [kg]	142918,1	73827,7	44805,2	28370,6	18976		
Total Structure Mass [kg]	75971,5	52309,5	43171,1	38728,5	38972,1		
Total Propellant Mass [kg]	1488275,6	926367,1	715169,3	630637,2	609141,9		
Total Launch Vehicle Length [m]	102,5	90,2	81,5	78,6	70,9		
Propellant Upper Stage [-]	3	3	3	3	3		
Propellant First Stage [-]	3	3	3	3	3		
ROF (BK) Upper Stage [-]	3,6	3,6	3,6	3,7	3,8		
ROF (BK) First Stage [-]	3,6	3,6	3,6	3,7	3,8		
Combustion Chamber Pressure Upper Stage [bar]	115	115	115	115	115		
Combustion Chamber Pressure First Stage [bar]	115	115	115	115	115		
Expansion Ratio Upper Stage [-]	185	190	195	190	200		
Expansion Ratio First Stage [-]	20	25	30	30	30		
Radius Upper Stage [m]	2,3	2	1,9	2	2,3		
Radius First Stage [m]	3	2,6	2,5	2,4	2,6		
Structural Coefficient Upper Stage [-]	0,07	0,06	0,05	0,04	0,04		
Structural Coefficient First Stage [-]	0,05	0,05	0,06	0,06	0,07		
Upper Stage Length [m]	10,2	13,3	16,4	18	17,6		
Upper Stage Total Tank Mass [kg]	1904,8	2092,7	2445,7	2825,1	3271,9		
Number of Engines Upper Stage [-]	1	1	1	1	1		
Mass Upper Stage Engine [kg]	1582,8	1439,5	1336,9	1443,4	1591,9		
Mass Upper Stage Propulsion System [kg]	1836,4	1655,9	1530,4	1660,6	1848,2		
Vacuum Thrust Upper Stage Engine [N]	1947939,5	1601306,1	1389272,2	1609773,6	1972308,5		
Total Vacuum Thrust Upper Stage [N]	1947939,5	1601306,1	1389272,2	1609773,6	1972308,5		
Vacuum Isp Upper Stage Engine [s]	365,7	366	366,3	366,3	367		
First Stage Length [m]	80,2	65	53,3	48,8	41,3		
First Stage Total Tank Mass [kg]	19105	12222,6	9157,5	7622,9	6607,9		
Number of Engines First Stage [-]	13	10	9	7	6		
Mass First Stage Engine [kg]	1502,7	1370,5	1276	1380,2	1524,3		
Mass First Stage Propulsion System [kg]	22025,8	15317,7	12765,9	10818,4	10352,6		
Vacuum Thrust First Stage Engine [N]	1746362,9	1455567,8	1276039,4	1475291	1798681,1		
Total Vacuum Thrust First Stage [N]	22702717,5	14555678,3	11484354,5	10327037,2	10792086,5		
Vacuum Isp First Stage Engine [s]	327,8	332,7	336,5	335,7	334,7		
Sea Level Thrust First Stage Engine [N]	1583751,2	1288628,9	1102391,1	1274964,3	1554763,6		
Total Sea Level Thrust First Stage [N]	20588766,1	12886288,6	9921520	8924750	9328581,6		
Sea Level Isp First Stage Engine [s]	297,3	294,5	290,7	290,1	289,3		
Structural Index Upper Stage	0,101	0,084	0,072	0,064	0,058		
Structural Index First Stage	0,050	0,056	0,062	0,066	0,072		
Landing Propellant Mass / First Stage Wet Mass	0,097	0,085	0,071	0,055	0,042		

Figure D.9: Optimization program output - 7500 kg payload, 12000 m/s delta-v, LOX/LCH4

D.4 7500 kg Payload - 11500 m/s Delta-v

Payload 7500 kg / Delta-V 11500 m/s	LOX/LH2						
DeltaV Allocation First Stage / Upper Stage:	5000/6500	4500/7000	4000/7500	3500/8000	3000/8500	2500/9000	2000/9500
GLOW [kg]	990483,1	570556	436731,2	378511,1	357550,9	361263,3	392833,8
Payloadbay Mass [kg]	10296,7	10150,3	10089,4	10070,8	10056,2	10050,9	10056,8
Wet Mass Upper Stage [kg]	61170,9	63021,1	74322,3	90026,6	112051,2	140542,3	181890,9
Structure Mass Upper Stage [kg]	7503,2	6354,5	6910,1	7868,9	9366,4	11161,4	13943
Propellant Mass Upper Stage [kg]	53667,7	56666,6	67412,2	82157,7	102684,9	129380,9	167947,9
Wet Mass First Stage [kg]	919015,5	497384,6	352319,6	278413,6	235443,5	210670,1	200886,1
Structure Mass First Stage [kg]	86206,6	50598,5	38755,1	32803,6	28400,3	29766,7	33540,3
Propellant Mass First Stage [kg]	832808,9	446786,1	313564,5	245610	207043,2	180903,4	167345,9
Propellant Mass Landing First Stage [kg]	122505,3	57892,1	34501,4	21873	13525,7	8788,8	7770,7
Total Structure Mass [kg]	93709,8	56953,1	45665,1	40672,6	37766,6	40928,1	47483,2
Total Propellant Mass [kg]	886476,6	503452,6	380976,7	327767,7	309728,1	310284,3	335293,8
Total Launch Vehicle Length [m]	119,2	100,1	89,3	87,8	87,8	87,5	89,3
Propellant Upper Stage [-]	1	1	1	1	1	1	1
Propellant First Stage [-]	1	1	1	1	1	1	1
ROF (BK) Upper Stage [-]	6,9	7	7	7,2	7,2	7,4	7,3
ROF (BK) First Stage [-]	6,9	7	7	7,2	7,2	7,4	7,3
Combustion Chamber Pressure Upper Stage [bar]	120	115	110	115	110	115	115
Combustion Chamber Pressure First Stage [bar]	120	115	110	115	110	115	115
Expansion Ratio Upper Stage [-]	195	200	200	200	200	200	200
Expansion Ratio First Stage [-]	30	25	30	30	20	30	25
Radius Upper Stage [m]	2,4	2	1,9	1,8	1,9	2	2,2
Radius First Stage [m]	3,1	2,6	2,5	2,4	2,3	2,3	2,3
Structural Coefficient Upper Stage [-]	0,12	0,1	0,09	0,09	0,08	0,08	0,08
Structural Coefficient First Stage [-]	0,09	0,1	0,11	0,12	0,12	0,14	0,17
Upper Stage Length [m]	12,4	15,9	19,8	25,6	28,5	31,9	34,5
Upper Stage Total Tank Mass [kg]	2775	2909,7	3412,4	4114,7	4903,6	5860,9	7215,6
Number of Engines Upper Stage [-]	1	1	1	1	1	1	1
Mass Upper Stage Engine [kg]	1742	1224,5	1279,9	1452,3	1743,2	2086,9	2654,4
Mass Upper Stage Propulsion System [kg]	1906,8	1349,1	1408,6	1594,3	1908	2279,4	2893,8
Vacuum Thrust Upper Stage Engine [N]	1122897,8	749943,4	788997,5	911979,1	1123733,6	1379985,7	1814931,9
Total Vacuum Thrust Upper Stage [N]	1122897,8	749943,4	788997,5	911979,1	1123733,6	1379985,7	1814931,9
Vacuum Isp Upper Stage Engine [s]	451,4	452,5	452,3	451,8	451,6	451	451,4
First Stage Length [m]	94,7	72,3	57,6	50,4	47,4	43,8	42,8
First Stage Total Tank Mass [kg]	29904,8	17390,7	12577	10038,5	8654,2	7562,1	7095,9
Number of Engines First Stage [-]	14	12	9	7	5	5	5
Mass First Stage Engine [kg]	1629,7	1133,8	1195,7	1354,2	1590,1	1941,5	2448,2
Mass First Stage Propulsion System [kg]	24429,9	14536,7	11513,1	10158,5	8539,8	10436,1	13177
Vacuum Thrust First Stage Engine [N]	1040532,7	686442,4	729729	841774	1011706,1	1270838,1	1655321
Total Vacuum Thrust First Stage [N]	14567458,4	8237308,2	6567561	5892417,8	5058530,7	6354190,7	8276604,9
Vacuum Isp First Stage Engine [s]	418,3	414,2	418,3	417	406,5	415,3	411,7
Sea Level Thrust First Stage Engine [N]	903329,2	607042,1	624965,2	726484,8	912723	1097189,9	1464562
Total Sea Level Thrust First Stage [N]	12646608,3	7284505,6	5624686,8	5085393,9	4563614,8	5485949,3	7322809,8
Sea Level Isp First Stage Engine [s]	363,2	366,3	358,2	359,9	366,8	358,5	364,3
Structural Index Upper Stage	0,192	0,159	0,141	0,127	0,116	0,106	0,098
Structural Index First Stage	0,104	0,113	0,124	0,134	0,137	0,165	0,200
Landing Propellant Mass / First Stage Wet Mass	0,133	0,116	0,098	0,079	0,057	0,042	0,039

Figure D.10: Optimization program output - 7500 kg payload, 11500 m/s delta-v, LOX/LH2

Payload 7500 kg / Delta-V 11500 m/s	LOX/RP-1						
DeltaV Allocation First Stage / Upper Stage:	5000/6500	4500/7000	4000/7500	3500/8000	3000/8500	2500/9000	2000/9500
GLOW [kg]	1587042,7	958367,8	725431,5	628360,1	580965,1		
Payloadbay Mass [kg]	10144,5	10040,1	10014,9	9980,1	9967,8		
Wet Mass Upper Stage [kg]	87162,8	96588,6	108344,7	130475,5	162700,6		
Structure Mass Upper Stage [kg]	5939,6	5309,6	4960	5436,3	6264,6		
Propellant Mass Upper Stage [kg]	81223,2	91279	103384,7	125039,2	156436		
Wet Mass First Stage [kg]	1489735,5	851739,1	607071,8	487904,6	408296,8		
Structure Mass First Stage [kg]	63178,7	40463,9	32080,9	28826,3	24904,8		
Propellant Mass First Stage [kg]	1426556,8	811275,2	574990,9	459078,3	383392		
Propellant Mass Landing First Stage [kg]	139480,4	68852,9	41515,9	27161,2	16135,4		
Total Structure Mass [kg]	69118,3	45773,5	37040,9	34262,6	31169,4		
Total Propellant Mass [kg]	1507780	902554,3	678375,6	584117,5	539828		
Total Launch Vehicle Length [m]	91,4	75,4	75,9	65	66,9		
Propellant Upper Stage [-]	2	2	2	2	2		
Propellant First Stage [-]	2	2	2	2	2		
ROF (BK) Upper Stage [-]	2,8	2,8	2,9	2,9	2,9		
ROF (BK) First Stage [-]	2,8	2,8	2,9	2,9	2,9		
Combustion Chamber Pressure Upper Stage [bar]	115	115	115	110	115		
Combustion Chamber Pressure First Stage [bar]	115	115	115	110	115		
Expansion Ratio Upper Stage [-]	180	175	190	195	190		
Expansion Ratio First Stage [-]	20	25	25	30	30		
Radius Upper Stage [m]	2,4	2	1,8	1,9	2		
Radius First Stage [m]	2,9	2,6	2,2	2,4	2,2		
Structural Coefficient Upper Stage [-]	0,07	0,05	0,05	0,04	0,04		
Structural Coefficient First Stage [-]	0,04	0,05	0,05	0,06	0,06		
Upper Stage Length [m]	8,6	10,2	12,9	14	15,6		
Upper Stage Total Tank Mass [kg]	1405,6	1547,3	1765,1	2011	2362,4		
Number of Engines Upper Stage [-]	1	1	1	1	1		
Mass Upper Stage Engine [kg]	1578,6	1483,4	1283,8	1305	1441,2		
Mass Upper Stage Propulsion System [kg]	1831,1	1710,4	1466,6	1492	1657,9		
Vacuum Thrust Upper Stage Engine [N]	1936922,9	1700755	1290097,6	1328819,7	1604988,3		
Total Vacuum Thrust Upper Stage [N]	1936922,9	1700755	1290097,6	1328819,7	1604988,3		
Vacuum Isp Upper Stage Engine [s]	349,6	349,2	351,1	351,8	351,1		
First Stage Length [m]	70,7	53,3	51,2	39,2	39,4		
First Stage Total Tank Mass [kg]	15189,7	9288,4	7114,8	5643,1	4907,3		
Number of Engines First Stage [-]	13	9	9	8	6		
Mass First Stage Engine [kg]	1501	1417,7	1214,5	1243	1379,1		
Mass First Stage Propulsion System [kg]	21998,9	14310,2	12110,1	11038	9270,7		
Vacuum Thrust First Stage Engine [N]	1742438,5	1553759,5	1170502,3	1218238	1472949		
Total Vacuum Thrust First Stage [N]	22651700,6	13983835,5	10534520,7	9745903,8	8837693,9		
Vacuum Isp First Stage Engine [s]	314,5	319	318,5	322,6	322,2		
Sea Level Thrust First Stage Engine [N]	1579826,9	1375109	1036315,9	1045057	1272622,2		
Total Sea Level Thrust First Stage [N]	20537749,2	12375981,1	9326843,4	8360456	7635733,4		
Sea Level Isp First Stage Engine [s]	285,1	282,4	282	276,7	278,4		
Structural Index Upper Stage	0,106	0,086	0,072	0,063	0,056		
Structural Index First Stage	0,044	0,050	0,056	0,063	0,065		
Landing Propellant Mass / First Stage Wet Mass	0,094	0,081	0,068	0,056	0,040		

Figure D.11: Optimization program output - 7500 kg payload, 11500 m/s delta-v, LOX/RP-1

Payload 7500 kg / Delta-V 11500 m/s	LOX/LCH4						
DeltaV Allocation First Stage / Upper Stage:	5000/6500	4500/7000	4000/7500	3500/8000	3000/8500	2500/9000	2000/9500
GLOW [kg]	1322330	853226,7	648032	560472,9	524138,9	527984,6	
Payloadbay Mass [kg]	10120,9	10078,9	10046,6	10012,9	9987,2	9979,1	
Wet Mass Upper Stage [kg]	79823,4	88793,8	98641,7	122229,7	150080,1	191528,5	
Structure Mass Upper Stage [kg]	6042,9	5374,6	5033,3	5836,1	6696,4	7913,7	
Propellant Mass Upper Stage [kg]	73780,5	83419,2	93608,4	116393,5	143383,7	183614,8	
Wet Mass First Stage [kg]	1232385,7	754354	539343,7	428230,3	364071,6	326477,1	
Structure Mass First Stage [kg]	60140,3	40809,1	32837	27300,8	25343,8	24701,9	
Propellant Mass First Stage [kg]	1172245,4	713544,9	506506,7	400929,5	338727,7	301775,2	
Propellant Mass Landing First Stage [kg]	121775,2	64933,5	39880,7	24285	15568,6	9401,7	
Total Structure Mass [kg]	66183,3	46183,7	37870,3	33136,9	32040,3	32615,6	
Total Propellant Mass [kg]	1246025,9	796964,1	600115,1	517323,1	482111,5	485389,9	
Total Launch Vehicle Length [m]	91,7	85,4	83,1	76,1	72	67,8	
Propellant Upper Stage [-]	3	3	3	3	3	3	
Propellant First Stage [-]	3	3	3	3	3	3	
ROF (BK) Upper Stage [-]	3,5	3,5	3,6	3,7	3,7	3,8	
ROF (BK) First Stage [-]	3,5	3,5	3,6	3,7	3,7	3,8	
Combustion Chamber Pressure Upper Stage [bar]	115	110	110	115	115	115	
Combustion Chamber Pressure First Stage [bar]	115	110	110	115	115	115	
Expansion Ratio Upper Stage [-]	200	170	200	190	200	170	
Expansion Ratio First Stage [-]	25	25	25	30	30	25	
Radius Upper Stage [m]	2,3	1,9	1,7	1,8	2	2,1	
Radius First Stage [m]	3	2,5	2,2	2,2	2,2	2,4	
Structural Coefficient Upper Stage [-]	0,08	0,06	0,05	0,05	0,04	0,04	
Structural Coefficient First Stage [-]	0,05	0,05	0,06	0,06	0,07	0,08	
Upper Stage Length [m]	9,1	12,3	15,9	17,5	17,7	20,2	
Upper Stage Total Tank Mass [kg]	1624,6	1840	2125,5	2473	2784,6	3331,8	
Number of Engines Upper Stage [-]	1	1	1	1	1	1	
Mass Upper Stage Engine [kg]	1580,3	1398,6	1136,6	1286	1393,8	1587,4	
Mass Upper Stage Propulsion System [kg]	1833,3	1605,4	1293,3	1469,2	1599,6	1842,5	
Vacuum Thrust Upper Stage Engine [N]	1941443,6	1513342,5	1048343,8	1293944,1	1503369,9	1960369,2	
Total Vacuum Thrust Upper Stage [N]	1941443,6	1513342,5	1048343,8	1293944,1	1503369,9	1960369,2	
Vacuum Isp Upper Stage Engine [s]	365,9	364,3	366,9	366,3	367	364,7	
First Stage Length [m]	70,6	61,2	55,5	46,9	42,4	35,6	
First Stage Total Tank Mass [kg]	16278,2	10847,3	8210,9	6586,7	5644,4	4961,4	
Number of Engines First Stage [-]	11	9	10	7	6	5	
Mass First Stage Engine [kg]	1511,5	1334,8	1068,3	1223,8	1329,7	1515,7	
Mass First Stage Propulsion System [kg]	18765,9	13400,2	11751,9	9505	8911,3	8580,1	
Vacuum Thrust First Stage Engine [N]	1767549,9	1385053,5	951173,7	1185846,3	1375301	1777659,3	
Total Vacuum Thrust First Stage [N]	19443048,9	12465481,1	9511736,6	8300924,1	8251806,2	8888296,3	
Vacuum Isp First Stage Engine [s]	333,2	333,4	332,9	335,7	335,7	330,8	
Sea Level Thrust First Stage Engine [N]	1564285,3	1218563,7	837145	1024822,7	1188551,7	1574394,7	
Total Sea Level Thrust First Stage [N]	17207138,7	10967073,7	8371450,4	7173758,6	7131310,3	7871973,5	
Sea Level Isp First Stage Engine [s]	294,8	293,3	293	290,1	290,1	292,9	
Structural Index Upper Stage	0,117	0,095	0,081	0,072	0,064	0,057	
Structural Index First Stage	0,051	0,057	0,065	0,068	0,075	0,082	
Landing Propellant Mass / First Stage Wet Mass	0,099	0,086	0,074	0,057	0,043	0,029	

Figure D.12: Optimization program output - 7500 kg payload, 11500 m/s delta-v, LOX/LCH4

Bibliography

[1] ESA. Types of Orbits. (https://www.esa.int/Enabling_Support/Space_Transportation/Types_of_orbits), Last Accessed: 2020-05-23.

[2] T. Bruno (President and CEO of United Launch Alliance). First Stage Costs. (https://twitter.com/torybruno/status/561933155951595520), Last Accessed: 2020-05-23.

[3] M. Oschwald. Raumfahrtantriebe I, Manuskript zur Vorlesung. 2017.

[4] R. A. Braeunig. Rocket and Space Technology. *Rocket Propulsion*, (http://www.braeunig.us/space/index.htm), Last Accessed: 2020-05-23.

[5] NASA. Chemical Equilibrium with Applications. (https://cearun.grc.nasa.gov/), Last Accessed: 2020-05-23.

[6] U. Walter. Astronautics: The Physics of Space Flight. *Springer*, 3rd Edition(https://doi.org/10.1007/978-3-319-74373-8):47–64, 2019.

[7] H. Curtis. Orbital Mechanics for Engineering Students. Butterworth-Heinemann, 2005.

[8] SpaceX. Falcon 9 Trajectory. (https://www.spacex.com/sites/spacex/files/16892430560_f87dff78c0_o_1.jpg), Last Accessed: 2020-05-23.

[9] F. Castellini. Multidisciplinary Design Optimization for Expendable Launch Vehicles. *PhD Thesis, Univerity of Milan*, 2012.

[10] D.A. Coley. An Introduction to Genetic Algorithms for Scientists and Engineers. 1999.

[11] Tutorials Point. Genetic Algorithms Tutorial. (https://www.tutorialspoint.com/genetic_algorithms/genetic_algorithms_parent_selection.htm), Last Accessed: 2020-05-23.

[12] Steffen Christall. Linking of Liquid Bipropellant Rocket Engine Design Methodology with Launch Vehicle Optimization. *Master Thesis*, 2017.

[13] SpaceX. CRS-8 First Stage Landing. (https://www.flickr.com/photos/spacex/25787998624/), Last Accessed: 2020-05-23.

[14] W. Ley, K. Wittmann, and W. Hallmann. Handbuch der Raumfahrttechnik. 5th Edition, Hanser, January 2019.

[15] G.P. Sutton and O. Biblarz. Rocket Propulsion Elements. 7th Edition, John Wiley & Sons, 2001.

[16] SpaceX. Falcon User's Guide. January 2019.

[17] SpaceX. Falcon 9 Launch Vehicle. (https://www.spacex.com/falcon9), Last Accessed: 2020-05-23.

[18] Space Launch Report. SpaceX Falcon 9 v1.2 Data Sheet. (https://www.spacelaunchreport.com/falcon9ft.html), Last Accessed: 2020-05-23.

[19] S. Stappert, J. Wilken, M. Sippel, and E. Dumont. Assessment of a European Reusable VTVL Booster Stage. 2018.

[20] S. Stappert, J. Wilken, L. Bussler, and M. Sippel. A Systematic Comparison of Reusable First Stage Return Options. *8th european conference for aeronautics and space sciences (eucass)*, 2019.

[21] L. Bussle, J. Wilken, S. Stapper, M. Sippel, I. Dietlein, and E. Dumont. Assessment of VTVL and VTHL Reusable First Stages. *HiSST: International Conference on High-Speed Vehicle Science Technology*, November 2018.

[22] S. Stappert, J. Wilken, L. Bussler, M. Sippel, S. Karl, J. Klevanski, C. Hantz, L.E Briese, and K. Schnepper. European Next Reusable Ariane (ENTRAIN): A Multidisciplinary Study on a VTVL and a VTHL Booster Stage. *70th International Astronautical Congress (IAC)*, (IAC-19-D2.4.2), 2019.

[23] A Marwege, A. Gülhan, J. Klevanski, J. Riehmer, D. Kirchheck, S. Karl, D. Bonetti, J. Vos, M. Jevons, A. Krammer, and J. Carvalho. Retro Propulsion Assisted Landing Technologies (RETALT): Current Status and Outlook of the EU Funded Project on Reusable Launch Vehicles. *70th International Astronautical Congress (IAC)*, (IAC-19.D2.4.5x49370), 2019.

[24] Arianespace. Ariane 5 User's Manual. Issue 5, Revision 0, July 2008.

[25] H. Burkhardt, M. Sippel, A. Herbertz, and J. Klevanski. Kerosene vs Methane: A Propellant Tradeoff for Reusable Liquid Booster Stages. *Journal of Spacecraft and Rockets*, 41(5), September 2004.

[26] D. Preclik, G. Hagemann, O. Knab, L. Brummer, C. Mäding, and D. Wiedmann. LOX/Hydrocarbon Propellant Trade Considerations for Future Reusable Liquid Booster Engines. *Joint Propulsion Conference*, July 2005.

[27] G. Waxenegger-Wilfing, K. Dresia, J.C. Deeken, and M. Oschwald. Heat Transfer Prediction for Methane in Regenerative Cooling Channels with Neural Networks. July 2019.

[28] B.J. McBride and S. Gordon. Computer Program for Calculation of Complex Chemical Equilibrium Compositions and Applications. *NASA Reference Publication 1311*, June 1996.

[29] L.E. Bollinger, M. Goldsmith, and A.W. Lemmon. Liquid Rocket and Propellants. *Progress in Astronautics and Rocketry-Volume 2*, 1960.

[30] M. Oschwald and R. Stark. Performance Losses in the Nozzle. Lecture Slides from Space Propulsion I, RWTH Aachen University. May 2018.

[31] V.J. Sarli, W.G. Bruwell, and R. Hofland. Evaluation of the Bray Sudden-Freezing Criterion for Predicting Nonequilibrium Performance in Multireaction Rocket Nozzle Expansions. *AIAA Propulsion Joint Specialist Conference*, June 1965.

[32] SpaceX. Koreasat-5A Webcast. (https://www.youtube.com/watch?v=CNRTNxZSPhE), Last Accessed: 2020-05-23.

[33] P. Rachov. Comparison of Liquid Propellant Rocket Engine Feed Systems. *Technical report, University of Buenos Aires*, December 2010.

[34] Systemanalytische Untersuchung einer Brennkammer in faserkeramischer Bauweise von Raketenantrieben. *PhD Thesis, RWTH Aachen University*, 2008.

[35] D.L. Akin. Mass Estimating Relations. Lecture slides from Principles of Space Systems Design. *University of Maryland*, 2009.

[36] G. Schmidt. Technik der Flüssigkeits-Raketentriebwerke. 1999.

[37] Alcoa Mill Products, Inc. Alloy 2090-T83 Sheet.

[38] O. Kreis. Stufungsoptimierung für ein Trägersystem mit LOX/Methan Antrieb. *Technical Report DLR-LA-RAS-RP-010, Institut für Raumfahrtantriebe, Deutsches Zentrum für Luft- und Raumfahrt e. V., Lampoldshausen, Germany*, 2015.

[39] SpaceX. Landing Legs. (https://www.spacex.com/news/2013/03/26/landing-leg), Last Accessed: 2020-05-23.

[40] E. Musk (Founder and CEO of SpaceX). Size and Weight of Landing Legs. (https://twitter.com/elonmusk/status/330054002148515841), Last Accessed: 2020-05-23.

[41] SpaceX. Grid Fins. (https://www.spacex.com/news/2015/08/31/grid-fins), Last Accessed: 2020-05-23.

[42] SpaceX. The Why and How of Landing Rockets. (https://www.spacex.com/news/2015/06/24/why-and-how-landing-rockets), Last Accessed: 2020-05-23.

[43] Spaceflight101. Falcon 9 v1.1 F9R Launch Vehicle Overview. (http://spaceflight101.com/spacerockets/falcon-9-v1-1-f9r/), Last Accessed: 2020-05-23.

[44] T. Bäck. Evolutionary Algorithms in Theory and Practice. *Oxford University Pres, Inc.*, 1996.

[45] K. Sastry, D. Goldberg, and G. Kendall. Genetic Algorithms. (doi.org/10.1007/0.387.28356.0.4), 2005.

[46] F.M. De Rinville, F.A. Fortin, M.A. Gardner, M. Parizeau, and C. Gagné. DEAP: A Python Framework for Evolutionary Algorithms. *GECCO'12*, July 2012.

[47] D.K. Huzel and D.H. Huang. Modern Engineering For Design of Liquid-Propellant Rocket Engines. *Progress in Astronautics and Aeronautics, AIAA*, 147, 1992.

[48] Dr. M. Mathews and S.J. Leszkiewicz. Efficient Spacecraft Formationkeeping with Consideration of Ballistic Coefficient Control. *NASA-Goddard Space Flight Center, Code 554*, 1988.

[49] SpaceX. Reusability is the Key to Making Human Life Multiplanetary. (https://www.spacex.com/reusability-key-making-human-life-multi-planetary), Last Accessed: 2020-05-23.

[50] J. Wilken and S. Stappert. Investigation of a European Reusable VTVL First Stage. *8th european conference for aeronautics and space sciences (eucass)*, 2019.